Royal Netherlands
Meteorological Institute
Ministry of Infrastructure and the Environment

The influence of the effective ozone temperature on OMDOAO3

Albert Oude Nijhuis

De Bilt, 2012 | Trainee report

The influence of the effective ozone temperature on OMDOAO3: Validation of the fitted temperature and improvements for the operational method.

Thesis submitted in partial fulfillment of the requirements for the degree of Master of Science in *Meteorology, Physical Oceanography and Climate* at the University of Utrecht.

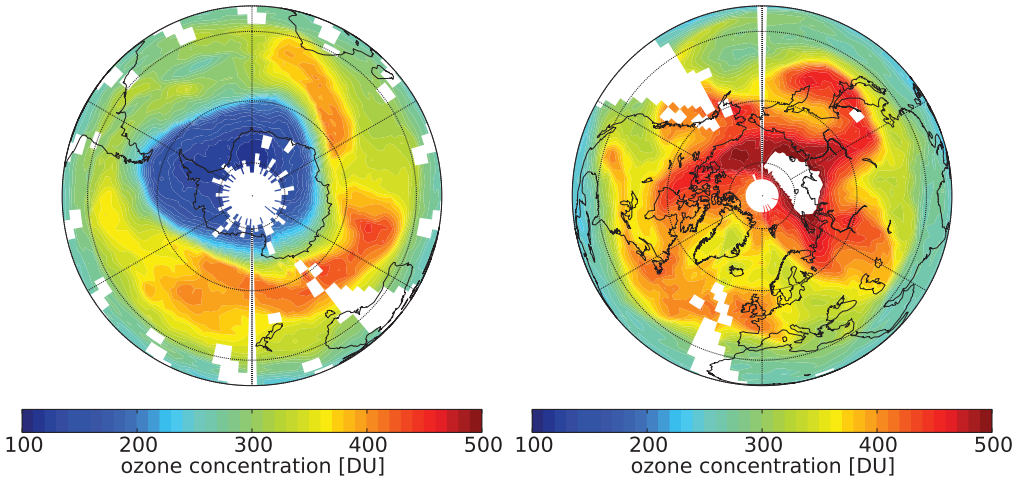

(a) SH spring, 2005-09-26

(b) NH spring, 2005-03-26

The ozone hole. Polar images of ozone where the differential optical absorption spectroscopy (DOAS) technique is applied to OMI measurements. Left: The ozone hole in the Antarctic region in spring 2005. Right: The same season in 2005 for the Arctic region, where the ozone hole did not exist.

Author:
Albert OUDE NIJHUIS

Supervisors:
Dr. Pepijn VEEFKIND (KNMI)
Dr. Maarten SNEEP (KNMI)
Dr. Johan DE HAAN (KNMI)
Dr. Geert-Jan ROELOFS (IMAU)

The influence of the effective ozone temperature on OMDOAO3: Validation of the fitted temperature and improvements for the operational method.

version 1.2.2

Author:
Albert OUDE NIJHUIS

Supervisors:
Dr. Pepijn VEEFKIND (KNMI)
Dr. Maarten SNEEP (KNMI)
Dr. Johan DE HAAN (KNMI)
Dr. Geert-Jan ROELOFS (IMAU)

Abstract

For monitoring the ozone layer as well as to detect changes in global ozone amounts due to climate change, multi-year trends in ozone need to be established with very high accuracy. The long-term ozone record is a combination of in-situ balloon soundings, ground-based and satellite remote sensing. Although it is well known that the ozone absorption cross-sections - which are a critical input to remote sensing retrievals - are temperature dependent, most of the remote sensing algorithms disregard this effect. As a consequence a temperature trend may cause a false ozone trend. Satellite retrievals using spectrometers can derive the ozone temperature from the spectra itself, and providing total ozone values that are potentially independent of the temperature. However, the validation of these retrieved temperatures is limited. In this study the validation results of the spectrally fitted effective temperature with the differential optical absorption spectroscopy (DOAS) technique are shown. Temperature sensitivities of the Ozone Monitoring Instrument (OMI) ozone products and ground-based ozone observations are estimated. Improvements for the DOAS technique are investigated. Simulations show that such improvements can reduce the temperature sensitivity by a factor of five, which improves the DOAS method and enhances the accuracy for ozone trend determination.

Universiteit Utrecht

Contents

Introduction

Ozone, chemically formula O_3, named after the Greek verb ozein ($o\zeta\varepsilon\iota\nu$, "to smell"), is a trace gas in the atmosphere, which predominantly is located in the stratosphere (10-50 km). Its presence there, which is commonly known as the "ozone layer", causes a stratospheric temperature inversion and results in a maximum temperature at the stratopause. The ozone layer extends over the entire globe with some variation in altitude and thickness. In addition to its radiative properties, ozone reacts with many other trace gas species, some of which are anthropogenic in origin. The geographical and vertical distributions of ozone in the atmosphere are determined by a complex interaction of atmospheric dynamics and photochemistry. [2] A schematic tropical ozone profile is shown in figure 1.

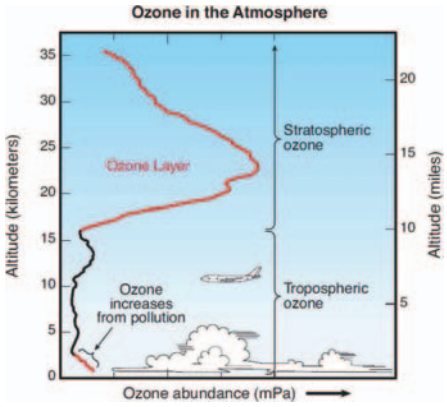

Figure 1: Ozone in the atmosphere. Ozone is present throughout the troposphere and stratosphere. This profile shows schematically how ozone changes with altitude in the tropics. Most ozone resides in the stratospheric "ozone layer". The vertical extent or thickness of this layers varies from region to region and with season over the globe. Increases in ozone occur near the surface as a result of pollution from human activities. Figure taken over from *Twenty questions about the ozone layer: 2010 update*[1].

Stratospheric ozone is formed naturally by a two step chemical reaction involving solar ultraviolet radiation and oxygen molecules. First two oxygen atoms are formed via the destruction of an oxygen molecule, and in the next step ozone is formed via the combination of an oxygen atom and an oxygen molecule. See figure 2. These reactions occur continuously whenever solar ultraviolet radiation is present in the stratosphere. As a result, the largest ozone production occurs in the tropical stratosphere. The production of stratospheric ozone is balanced by its destruction in chemical reactions. Ozone reacts continuously with sunlight and a wide variety of natural and human produced chemicals in the stratosphere. Important reactive gases that destroy ozone are hydrogen and nitrogen oxides and those containing chlorine and bromine. Ozone abundances in the stratosphere and troposphere are determined by the balance between chemical processes that produce and destroy ozone. The balance is determined by the amounts of reactive gases and how the rate or effectiveness of the various reactions varies with sunlight intensity, location in the atmosphere, and other factors. The balance of production and loss reactions combined with atmospheric air motions determines the global distribution of ozone on timescales of days to many months. Global ozone has decreased during the past several decades because the amounts of reactive gases containing chlorine and bromine have increased in the stratosphere due to human activities. [1]

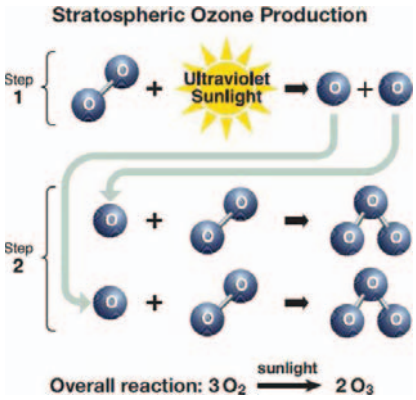

Figure 2: Stratospheric ozone production. Ozone is naturally produced in the stratosphere by a two step reactive process. In the first step, solar ultraviolet radiation (sun light) breaks apart an oxygen molecule to form two separate oxygen atoms. In the second step, each atom then undergoes a binding collision with another oxygen molecule to form an ozone molecule. In the overall process, three oxygen molecules plus sun light react to form two ozone molecules. Figure taken over from *Twenty questions about the ozone layer: 2010 update*[1].

Ozone in the stratosphere absorbs a large part of the Sun's biologically harmful ultraviolet radiation. This is seen as beneficial because (increased) exposure of UV-B radiation at the surface increases the risk of skin cancer, cataracts, and a suppressed immune system. Excessive UV-B radiation also can damage terrestrial plant life, single-cell organisms and aquatic ecosystems. UV-A, which is not absorbed significantly by ozone, causes premature aging of the skin. In contrast, ozone formed at the Earth's surface in excess of natural amounts is considered "bad" ozone because it is harmful to humans, plants, and animals. Natural ozone near the surface and in the lower atmosphere plays an important beneficial role in chemically removing pollutants from the atmosphere. [1]

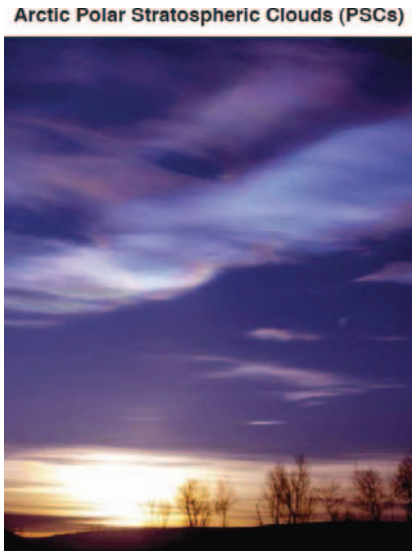

Figure 3: Polar stratospheric clouds. This photograph of an Arctic polar stratospheric cloud (PSC) was taken from the ground at Kiruna, Sweden (67°N), on 27 January 2000. PSCs form in the ozone layer during winters in the Arctic and Antarctic stratospheres wherever low temperatures occur. The particles grow from the condensation of water and nitric acid (HNO_3). The clouds often can be seen with the human eye when the Sun is near the horizon. Reactions on PSCs cause the highly reactive chlorine gas ClO to be formed, which is very effective in the chemical destruction of ozone. Figure taken over from *Twenty questions about the ozone layer: 2010 update*[1].

In the mid-1970s, it was discovered that gases containing chlorine and bromine atoms released by human activities could causes stratospheric ozone depletion. These gases, referred to as halogen source gases, and as ozone-depleting substances (ODS), chemically release their chlorine and bromine atoms after they reach the stratosphere. The severe depletion of the Antarctic ozone layer, known as the "ozone hole", occurs because of the special atmospheric and chemical conditions that exist there and nowhere else on the globe. The very low winter temperatures in the Antarctic stratosphere cause polar stratospheric clouds (PSCs) to form, see figure 3. Special reactions that occur on PSCs, combined with the relative isolation of polar stratospheric air, allow chlorine and bromine reactions to produce the ozone hole in Antarctic springtime. International efforts have been successful in protecting the ozone layer through controls on ODS production and consumption. Substantial recovery of the ozone layer from the effects of anthropogenic ozone-depleting substances (ODS) is expected near the middle of the 21st century, assuming global compliance with the Montreal Protocol. [1]

The severe depletion of the Antarctic ozone layer was first reported in the mid-1980s. Antarctic ozone depletion is seasonal, occurring primarily in late winter and early spring (August-November). Peak depletion occurs in early October when ozone is often completely destroyed over a range of altitudes, thereby reducing total ozone by as much as two-thirds at some locations. This severe depletion creates the "ozone hole" apparent in images of An tactic total ozone made using satellite observations. See figure 4. In most years the maximum area of the ozone hole far exceeds the size of the Antarctic continent. [1]

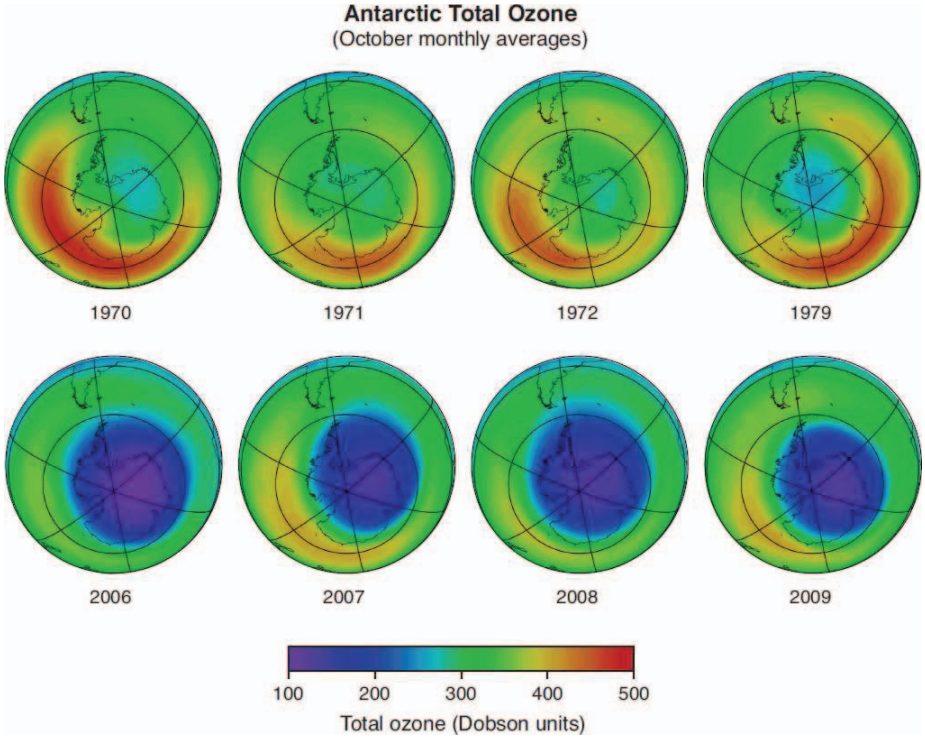

Figure 4: Antarctic total ozone. Long-term changes in Antarctic total ozone are demonstrated with this series of total ozone maps derived from satellite observations. Each map is an average during October, the month of maximum ozone depletion over Antarctica. In the 1970s, no ozone hole was observed as defined by a significant region with total ozone values less than 220 DU (dark blue and purple colors). Starting in the 1980s, the ozone hole began to appear and increased in size (not shown here). The maps from the 2000s show the large extent (about 25 million square kilometers) of the most recent ozone holes. The largest total-ozone values at high southern latitudes are still found in a crescent-shaped region outside the ozone hole in October. The maps show that these maximum values and their extent have significantly diminished since the 1970s. Figure taken over from *Twenty questions about the ozone layer: 2010 update*[1].

Depletion of the global ozone layer began gradually in the 1980s and reached a maximum of about 5% in the early 1990s (compared to 1964-1980 average). The depletion has lessened since then and now is about 3.5% averaged over the globe (2006-2009 compared with 1964-1980 average). The average depletion exceeds the natural year-to-year variations of global total ozone. The ozone loss is very small near the equator and increases with latitude toward the poles. The larger polar depletion is attributed to the late winter/early spring ozone destruction that occurs there each year. See figure 5. [1]

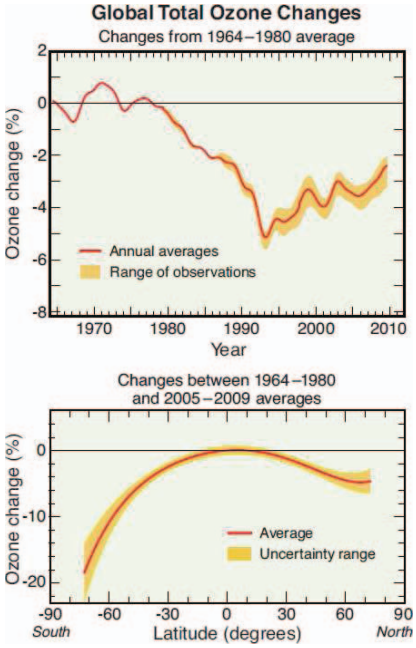

Figure 5: Global total ozone changes. Satellite observations show depletion of global total ozone beginning in the 1980s. The top panel compares annual averages of global ozone with the average from the period 1964 to 1980 before the ozone hole appeared. Seasonal and solar effects have been removed from the observational data set. On average, global ozone decreased each year between 1980 and 1990. The depletion worsened for a few years after 1991 due to the effect of volcanic aerosol from the Mt. Pinatubo eruption. Average global ozone for 2005-2009 is about 3.5% below the 1964-to-1980 average. The bottom panel shows how the 2005-2009 depletion varies with latitude over the globe. The largest decreases have occurred at high latitudes in both hemispheres because of the large winter/spring depletion in polar regions. The losses in the Southern Hemisphere are greater than those in the Northern Hemisphere because of the Antarctic ozone hole. Long-term changes in the tropics are much smaller because reactive halogen gases are less abundant in the tropical lower stratosphere than at mid or high latitudes and ozone production rates are greater. Figure taken over from *Twenty questions about the ozone layer: 2010 update*[1].

Recent observations show the development of an Arctic ozone hole. In a study of [3, G. Manney et al., 2011] , unprecedented Arctic ozone loss is observed. See figure 6. In this figure it can be seen that ozone mixing ratios in the Arctic region decreased to extreme low values that normally only occur in the Antarctic region. The authors also found that the winter mean volume of air in which PSC may form is closely correlated with the potential for ozone loss. The winter mean volume is determined with a simple relation for temperature, $T < T_{\text{act}}$, with $T_{\text{act}} \approx 196$ K being the activation temperature at which PSCs start to form, and chlorine, a catalyst for ozone destruction, is activated.

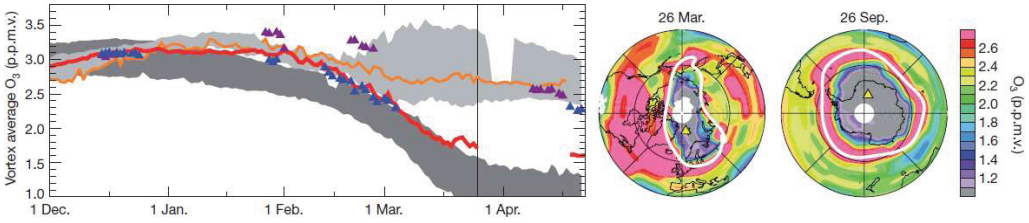

Figure 6: Left: Vortex-averaged time series at 485K potential temperature (∼20 km,∼50 hPa) for ozone. Averaging for the time series is done within the white contour shown on the maps. Antarctic dates are shifted by six months to show the equivalent season. Blue (purple) triangles are values from the AURA MLS, for time series, 1995-96 (1996-97). Shading is for Aura MLS measurements from 2005-10. Light (dark) gray shading shows the range of Arctic (Antarctic) values for 1979-2010. Red (orange) shows the 2010-11 (2004-05) Arctic winter. The vertical line shows the date of the maps in 2011 (2010) in the Arctic (Antarctic) in the middle (right). Figure taken over from *Unprecedented Arctic ozone loss in 2011*[3].

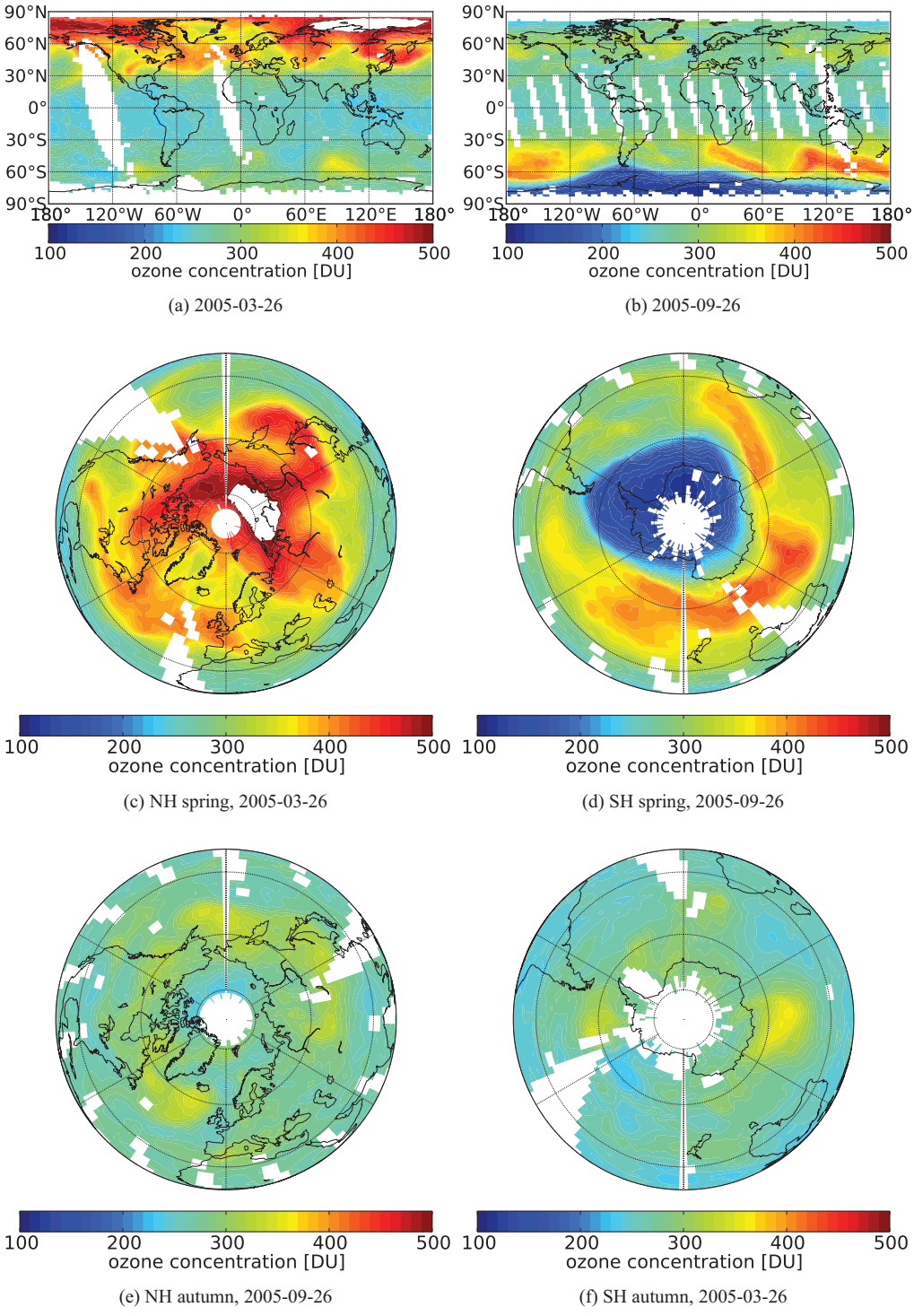

(a) 2005-03-26

(b) 2005-09-26

(c) NH spring, 2005-03-26

(d) SH spring, 2005-09-26

(e) NH autumn, 2005-09-26

(f) SH autumn, 2005-03-26

Figure 7: Typical measurements in spring and autumn from the OMI satellite obtained with the differential optical absorption spectroscopy (DOAS) technique. Data has been gridded on a $3^\circ \times 2^\circ$ (longitude $\times$ latitude) grid to reduce noise.

For monitoring the ozone layer as well as to detect changes in global ozone amounts due to climate change, multi-year trends in ozone need to be established with very high accuracy. The long-term ozone record is a combination of in-situ balloon soundings, ground-based and satellite remote sensing. For example, see figure 7, where typical measurements from the OMI satellite are shown. Although it is well known that the ozone absorption cross-sections - which are a critical input to remote sensing retrievals - are temperature dependent, most of the remote sensing algorithms disregards this effect. As a consequence a temperature trend may cause a false ozone trend. An essential first step is to determine which ozone products are sensitive to variations in effective ozone temperature.

In a study of [4, R. J. van der A et al., 2010] , the temperature sensitivity for different satellite instruments has been estimated, varying from -0.10 to +0.13 %/K, based on direct sun observations of the Brewer instrument, which are assumed to be insensitive to temperature variations.[1] Such sensitivities are large compared to a threshold value of 0.01 %/K, which is a temperature sensitivity for which ozone trends can be determined with a 1% accuracy (see section 1), and therefore errors in the calculated ozone trends, determined with satellite products, can be expected on the order of 10%. Satellite retrievals using spectrometers may derive the ozone temperature from the spectra itself, and providing total ozone values potentially independent of the temperature. [5] However, the validation of these retrieved temperatures is limited.

[1] In the article[4], a temperature correction is mentioned based on a regression scheme, varying between 0.34 to -0.44 DU/K for satellite products. In this study the assumption has been made that Brewer direct sun observation are insensitive for variations in effective ozone temperature. The temperature correction has been converted to a temperature sensitivity of the satellite products, by assuming a standard ozone column amount of 350 DU. For example for a temperature correction of 0.34 DU/K, the temperature sensitivity is obtained as: $\alpha = -100 \cdot 0.34/350 = -0.10$ %/K.

Objectives and outline

The objectives of this study are: 1. To validate the OMDOAO3 fitted effective temperature; 2. to estimate the temperature sensitivity of OMI ozone products and 3. to improve the DOAS concept such that an ozone trend can accurately be determined with DOAS obtained vertical ozone column amounts.

In the first section OMI ozone products, ground-based measurements and balloon borne ozone sondes are introduced. Ozone products that can be used for validating the OMI ozone products, and to determine their temperature sensitivities are identified.

In the second section, definitions for effective ozone temperature are derived, given the Lambert-Beer law, and the concept of temperature spread is introduced. These definitions are helpful in understanding potential differences between ozone column amounts and effective temperatures from different products. Differences between vertical and slant ozone effective temperature are discussed in detail.

In the third section, the OMI ozone products are compared. For each product the ozone column amount is used, and an effective temperature is either available or calculated. The OMDOAO3 fitted ozone effective temperatures are compared with 1.) OMO3PR ozone effective temperatures, based on a retrieved ozone profile and temperature profile from a medium-range weather forecasting model (ECMWF) and 2. OMTO3 effective temperature, based on temperature and ozone profiles from the TOMS v8 climatology. Temperature sensitivity are estimated for the OMI ozone products. In section 4, ground-based measurements are used to validate the OMI ozone products. The ozone column amounts are compared, and temperature sensitivities are estimated for the OMI ozone products.

In the last section, the DOAS method is investigated in more detail. The implementation of ozone optical depth, and a wavelength dependent air mass factor are considered. Simulations are done for which the results are summarized.

1. Ozone products

The essential purpose of this section is to identify ozone products that can be used to validate the OMDOAO3 effective temperature, and estimate the temperature sensitivities of OMI ozone products. First a historical overview of ozone products is given. Secondly the ozone absorption cross sections, which are a critical input for ozone retrievals, are introduced. Then the concept of determining the temperature sensitivity is introduced and finally all the relevant ozone products are discussed in detail and their temperature sensitivities are estimated with theory. See figure 8 for an overview of ozone measurements. Because of time constraints, and/or data availability, this study is limited to the most widely used ozone retrieval methods. There are however also other satellite ozone products, alternative ground-based measurement techniques and rocket soundings. A complete overview of ozone retrievals can be found in e.g. *WMO GUIDE TO METEOROLOGICAL INSTRUMENTS AND METHODS OF OBSERVATION* [2].

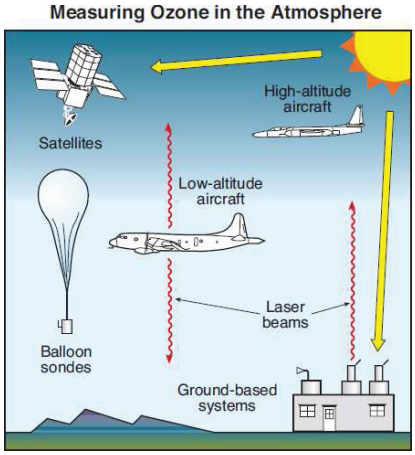

Figure 8: Ozone measurements. Ozone is measured throughout the atmosphere with instruments on the ground, aircraft, high-altitude balloons, and satellites. Some instruments measure ozone locally in sampled air and others measure ozone remotely some distance away from the instrument. Instruments use optical techniques, with the Sun and lasers as light sources; detect the microwave emissions from ozone; or use chemical reactions that are unique to ozone. At many locations over the globe, regular measurements are made to monitor total ozone amounts and their variations over time. Figure taken over from *Twenty questions about the ozone layer: 2010 update*[1].

1.1. Historical overview

A schematic overview of the progress in ozone observations can be seen in figure 10. In the 1880s Marie Alfred Cornu, Sir Walther Noel Hartley and Sir William Huggins discovered that ozone acts as a strong absorber in the atmosphere for UV solar radiation between 200 and 300 nm. The electronic bands of the ozone absorption spectrum were discovered, see figure 9, and fulfilled the requirements of the atmospheric absorber. In the 1900s Leon Teisserenc de Bort and Richard Assmann discovered the temperature inversion at the stratopause ($\sim$10-20 km), which is consistent with the assumption that an absorbing layer - the ozone layer - exists at altitudes between 10 and 50 km. [6]

In 1925 G. Dobson developed a new stable spectrophotometer for the quantification of the vertical column density of ozone. Nowadays, the vertical column density of ozone, is still expressed in Dobson units (DU), which is defined as the thickness of the atmospheric vertical ozone column density, under standard conditions for temperature and pressure (STP), measured in 10^{-5} m. Dobson spectrophotometers use a simple spectroscopic method: the direct or scattered solar intensity is measured in different narrow (1 nm) spectral intervals of which some are located inside and some outside the Huggins absorption bands, see figure 9. From the ratio of

the radiation at different wavelengths the thickness of the ozone layer is determined. The impact of absorption and scattering by aerosols or SO_2 on the ozone retrieval can be accounted for by combining different wavelength pairs, for which the influence of ozone and such interfering effects are different. Dobson spectrometers became widely used, and a global network of more than 100 instruments was established in 1957. These instruments provide data over a long time span, and is an important basis for the investigation of the long term evolution of the atmospheric ozone layer. In 1973 Alan Brewer developed a similar instrument, but with slightly other wavelengths, such that next to ozone also SO_2 and NO_2 could be determined. Similar to the Dobson instruments, a network of Brewer spectrometers was established which is still in operation. [6]

In 1976 U. Platt and D. Perner introduced the DOAS (Differential Optical Absorption Spectroscopy) method, which was first applied to tropospheric observations using artificial light sources. The key concept of DOAS is the simultaneous fit of several trace gas absorption spectra to the measured atmospheric spectrum using only the high frequency part. This concept is an elegant way to deal with possible spectral interference between absorption structures of different trace gases and the effects of atmospheric scattering. [6]

After early conceptual studies and prototype measurements, long-term spectroscopic UV/VIS observations from space started in 1970 on board the US research satellite Nimubs 4. First they measured Solar Backscatter Ultraviolet (SBUV) only in the nadir direction, i.e. pointing downward and measuring the solar light reflected from the ground or scattered from the atmosphere. From the SBUV data it is possible to retrieve information on the atmospheric ozone concentration (profile), because the penetration depth strongly depends on the ozone absorption cross section, and thus on wavelength. Later, TOMS was launched in 1979 on Nimbus 7, that observed backscattered light in distinct wavelength channels, but at longer wavelengths, such that it became possible to measure the vertical column density of ozone from space. The TOMS instrument on board Nimbus 7 has yielded the longest continuous global data set on the ozone layer (1979-1992), covering in particular the formation and evolution of the ozone hole. Since then, several other TOMS instruments were launched on other satellites. [6]

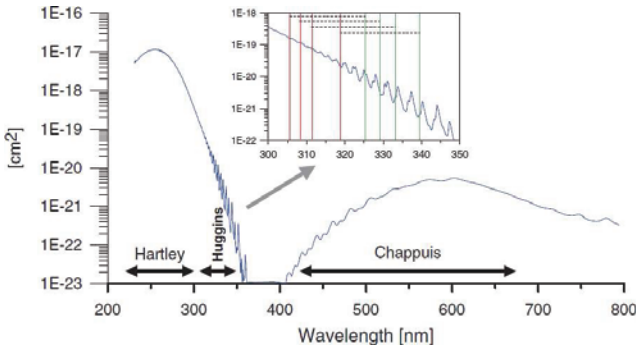

Figure 9: The ozone absorption cross-sections (Bogumil et al. 2003). The highly structured O3 Huggins Bands are displayed in the panel with an expanded wavelength scale. Also shown in the panel are the wavelength pairs used by Dobson spectrometers. Figure taken over from *The Remote Sensing of Tropospheric Composition from Space* [6].

A new quality of the observed spectral information became available in 1995 with the launch of the first DOAS-type instrument, the Global Ozone Monitoring Experiment (GOME) on the European research satellite ERS-2. Similar to SBUV and TOMS, GOME is a nadir viewing instrument but it contiguously measures a large spectral range (237-793 nm, having a spectral resolution between 0.2 and 0.4 nm). Its standard ground pixel size is 320 x 40 km^2 (East-West $\times$ North-South) enabling global coverage to be achieved each 3 days. By applying the DOAS method on the new high spec-

tral resolution data, it has been possible to analyze the atmospheric absorptions of a large variety of weak atmospheric absorbers such as NO_2, BrO, SO_2, OCLO, HCHO, CHOCHO, IO and O_2-O_2. In March 2002 the Scanning Imaging Absorption SpectroMeter for Atmospheric CartograpHY (SCIAMACHY) was launched on board the European research satellite ENVISAT. Compared to GOME, its spectra cover a wider wavelength range (213-2380 nm), facilitating measurements of several greenhouse gases (CO_2, CH_4 and N_2O), and the pollutant CO. In addition to nadir viewing, SCIAMACHY also makes observations in limb and solar and lunar occultation geometry, which yield profiles of stratospheric and mesospheric trace constituents. In 2004, the Ozone Monitoring Instrument (OMI) was launched, which is located on the AURA satellite, see figure 11. Charge-coupled device (CCD) pixels are used for OMI which makes daily global coverage and a high spatial resolution possible. Compared to GOME and SCIAMACHY, it has a limited spectral range (270-500 nm), but a higher spatial resolution (up to 13 x 24 km^2) in nadir viewing mode. Together with its daily global coverage, it provides unprecedented detail of the spatial-temporal variability of tropospheric trace gases. For the next two decades, new GOME instruments, and TROPOMI, are scheduled for launch and thus extending the time series of GOME, SCIAMACHY, and OMI into the next decades. [6]

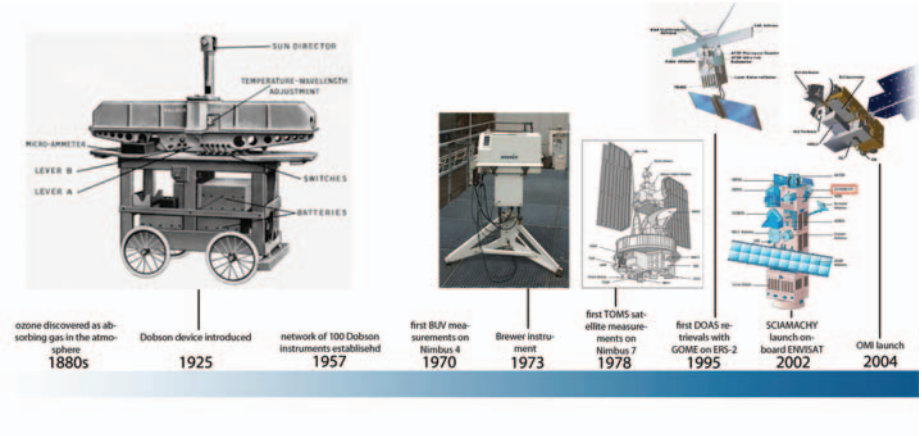

Figure 10: Illustration of the progress in ozone observations.

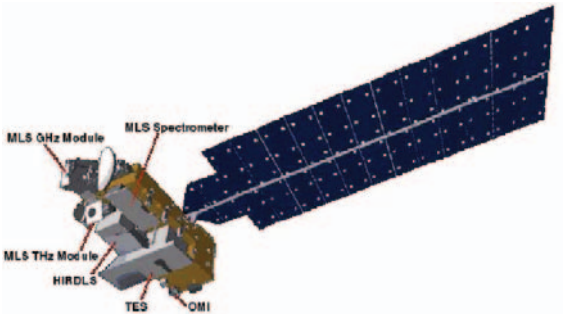

Figure 11: Picture of the AURA instrument, on which the ozone measurement instrument (OMI) is located. OMI produces high-resolution maps and uses ultraviolet and visible radiation. Next to OMI, there are several other instruments: 1. HIRDLS (High Resolution Limb Sounder), which measures infrared radiation from ozone, water vapor CFCs, methane and nitrogen compounds. The HIRDLS chopper shutdown on March 17, 2008 and has not produced science since. 2. MLS (Microwave Limb Sounder), which measures emissions from ozone, chlorine and other trace gases, and clarifies the role of water vapor in global warming. 3. TES (Tropospheric Emission Spectrometer), which measures tropospheric ozone in infrared wavelengths and also carbon monoxide, methane and nitrogen oxides. AURA instrument list taken over from `http://en.wikipedia.org/wiki/Aura_%28satellite%29`. Picture from `http://gmao.gsfc.nasa.gov/operations/candp/InstTeamCust.php`

1.2. Ozone absorption cross-sections

One of the critical input elements of remote sensing ozone retrievals (ground-based or satellite) are the ozone lab absorption cross-sections, for which there are quite some flavors: Bass & Paur (1984)[7], Brion (1998)[8], Voigt (1000 mbar, 2001)[9], Voigt (100 mbar, 2001)[9] and Serdyuchenko (2011)[10]. These cross-sections differ by their absolute value, and also by their temperature dependency. In comparison studies the cross-sections are mostly compared on an integral scale, e.g. for the Huggins band (320-360 nm), and do not differ more than a few percent [11, J. Orphal, 2003] . The integral comparison may give a good impression but differences on a high resolution can be as high as 10%. Ozone lab cross-sections sets, that are freely available, differ in resolution (0.05 nm for Bass & Paur, ~ 0.015 nm for Voigt or 0.01 nm for others), and temperatures (11 points for Serdyuchenko or 5/6 points for others) at which the cross-sections are available. The cross sections from [10, Serdyuchenko et al., 2011] are new and used experimentally in this study. These new cross-sections may have the potential of capturing the temperature dependency better, as the cross-sections are measured at 11 temperatures in the lab, instead of 5/6 temperatures for older sets of cross-sections. Once the ozone lab absorption cross-sections are chosen, they can be used after convoluting them with an instrumental slit function and a reference solar spectrum, and making a polynomial fit to the coefficients. A second-degree polynomial fit is mostly used for the ozone absorption cross-sections:

$$\sigma(\lambda, T) = a_0(\lambda) + a_1(\lambda)T + a_2(\lambda)T^2 \tag{1}$$

Here σ is the ozone absorption cross-section, λ wavelength, T temperature and a_i are the temperature expansion coefficients. In this study, a weighting function has been used for the polynomial fit for the temperature dependency of the cross sections. As a weighting function, a normal distribution is taken, with a mean value of -46.6 $^{\circ}C$ and a standard deviation of 35 $^{\circ}C$, which is plotted in figure 12b. This weighting function gives a higher weight to realistic effective ozone temperatures, and a lower weight to unrealistic ozone temperatures. This weighting has little influence when the errors in the measurement with respect to the fitted polynomial are low. When the errors get larger, preference is given to measurements that are relevant for the ozone retrieval. The convolution process of the absorption cross-sections, which is taking the instrumental slit function into account, is described the next subsection.

1.2.1. Principle of convoluting cross-sections

In this subsection, the difference between convoluted (or effective) and laboratory cross sections is explained. The ozone absorption cross sections are a key element for an ozone retrieval. The ozone absorption cross sections are a measure for how much radiation is attenuated along an ozone path, which is formulated by the Lambert-Beer law:

$$dI(\lambda) = -I(\lambda)\sigma(\lambda, T)n(l)dl$$

The Lambert-Beer law states that for an infinitesimal small non-scattering layer dl, the amount of absorption is proportional to the radiative intensity I, the absorption cross section σ and the ozone density n. Integration over an ozone path leads to:

$$I(\lambda) = I_0(\lambda)\exp - \int \sigma(\lambda, T)n(l)dl$$

where I_0 is the initial radiation and I is the attenuated radiation via absorption.

A spectrophotometer, either for a satellite or ground-based instrument, measures the radiances with a certain slit function or the so-called spectral response function. The slit function characterizes the relative intensities for different wavelengths at which the radiance is measured. Typical parameters for a slit function are the central wavelength and the full-width half maximum (FWHM). The consequence of a slit function width a certain bandwidth, is that the cross sections used for an ozone retrieval slightly deviate from the laboratory cross sections. These cross sections are referred to as the convoluted or effective cross sections. For the OMI instrument the effective ozone absorption cross sections are calculated with the high-resolution lab cross sections $\sigma_x(\lambda)$, instrumental slit functions $S(\lambda_0, \lambda)$ and a reference solar spectrum $F_0(\lambda)$. A typical reference slant column amount N_s has to be chosen. The effective cross section for wavelength λ_0 is then calculated as[12]:

$$\sigma_x^{\text{eff}}(\lambda_0) = -\frac{1}{N_s}\ln\left[\frac{\int S(\lambda_0, \lambda)F_0(\lambda)\exp\left(-N_s\sigma_x(\lambda)\right)d\lambda}{\int S(\lambda_0, \lambda)d\lambda \int F_0(\lambda)d\lambda}\right] \quad (2)$$

The derivation of this formula is outside the scope of this study. The only key thing to remember is that the convoluted cross sections deviate slightly from the laboratory cross sections. Next to spectral features of the solar spectrum, the instrumental slit function and the cross sections themselves another effect is important. The ring effect, i.e. rotational Raman scattering, can also be taken into account. For details on how to account for the ring effect, we refer to *Accounting for Raman scattering in DOAS*[12]. Slit functions for the OMI instrument and the Brewer instrument and a reference solar spectrum are shown in figure 12.

Note that the convolution process itself is not depending on temperature. This means that we can either do a polynomial fit of the temperature expansion coefficients of the ozone absorption cross sections before or after the convolution, see equation 1.

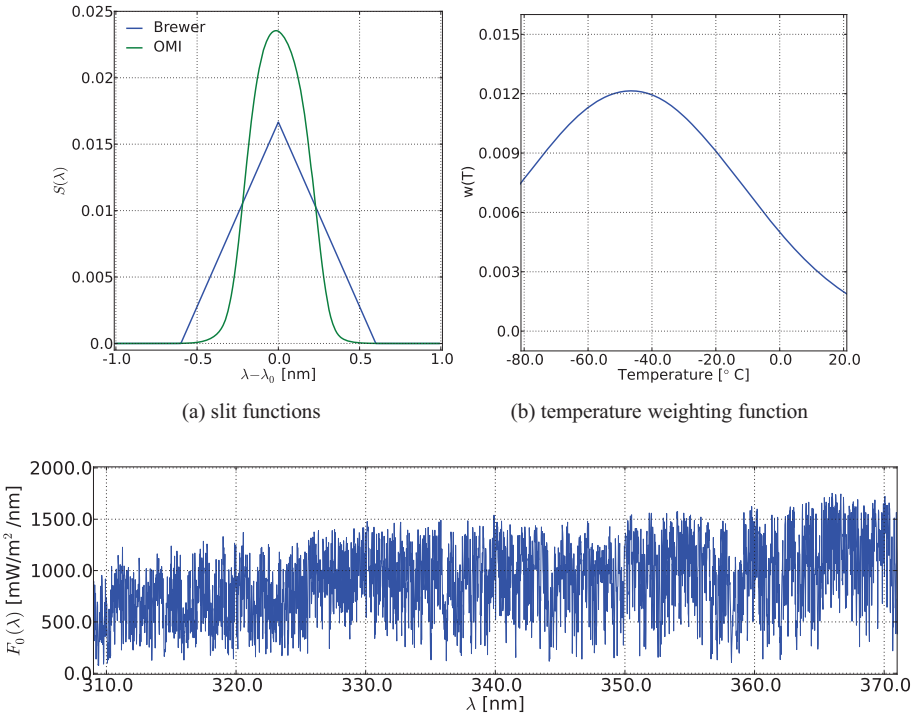

(a) slit functions

(b) temperature weighting function

(c) solar spectrum

Figure 12: (a) Slit functions for Brewer instrument[13] and OMI satellite [14, eq. 2 on p. 1231] (b) Temperature weighting function, that can be used when the cross-sections are fitted to a second-degree polynomial. (c) Reference solar spectrum from [15, M. Dobber et al., 2008] .

1.3. Temperature sensitivity

In this subsection the concept of temperature sensitivity is explained and a threshold value for temperature sensitivity is determined for an ozone retrieval that can accurately determine ozone trends. In the subsections hereafter, ozone products are discussed in detail and temperature sensitivities of these products are estimated.

The temperature sensitivity is defined as the relative error in the ozone column, N, that is produced (measured minus true), for a deviation in temperature, T, (true minus assumed in the measurement):

$$\text{“Temperature sensitivity”} = 100 \times \frac{(N_{\text{meas}} - N_{\text{true}})}{N_{\text{meas}} * (T_{\text{true}} - T_{\text{meas}})} \text{ [\%/K]}$$

The advantage of using the relative amount in the definition of temperature sensitivity, is that the use of either the slant or vertical ozone column amount becomes irrelevant. Alternatively we may define the temperature sensitivity as

$$\text{“Temperature sensitivity”} = 100 \times \frac{(N_{\text{meas}} - N_{\text{true}})}{N_{\text{meas}} * (T_{\text{true}} - T_0)} \text{ [\%/K]}$$

Here T_0 is a constant reference temperature. The essential change for the latter is that the ozone retrieval itself is depending on effective ozone temperature. Note that in many ozone retrievals a constant effective temperature is assumed, $T_{\text{meas}} = T_0$, and the two definitions are equal.

In the next subsections theoretical estimates of the temperature sensitivity will be deduced from the measurement principles and ozone absorption cross-sections. A theoretical estimate of the temperature sensitivity is meant as an indication whether the retrieval method is depending on temperature. A temperature correction, which is minus one times the temperature sensitivity, which in principle could be done, is not straightforward because the effective temperature itself is also dependent on geometry and clouds. A more elaborate explanation for definitions in effective temperature will be given in section 2. The temperature sensitivities from a theoretical calculation has therefore to be seen in a binary way: either the retrieval is dependent on temperature or it is not.

A threshold value for temperature sensitivity for being able to calculate an ozone trend accurately can be calculated simply. A list of typical trends in ozone effective temperatures and ozone column amounts is given in table 1. Here stratospheric temperature trends for climate (1979-2007), solar cycle and volcanic eruptions have been taken over from [16, Randel et al., 2009] , which is a good estimator for trends in ozone effective temperature, and for winter/spring depletion in polar regions it has been estimated from a medium-range weather forecasting model (ECMWF). Alternatively model simulations from the IPCC AR4 can be studied, see figure 13, which contain similar temperature changes. Trends in ozone have been taken over from *Twenty questions about the ozone layer: 2010 update*[1]. The relative change in ozone per change in temperature, $\mathrm{dO_3/O_3dT}$, varies between 1 and 5 %/K. Therefore we can state that a temperature sensitivity of 0.01 %/K is a reasonable threshold value. If the temperature sensitivity is equal or less than this threshold value then an ozone retrieval is able to capture the ozone trends, mentioned in table 1, with at least 1% accuracy. The next step is now to determine the temperature sensitivity of ozone products, and identify which ozone products can be used as a reference to determine the temperature sensitivity of OMI ozone products.

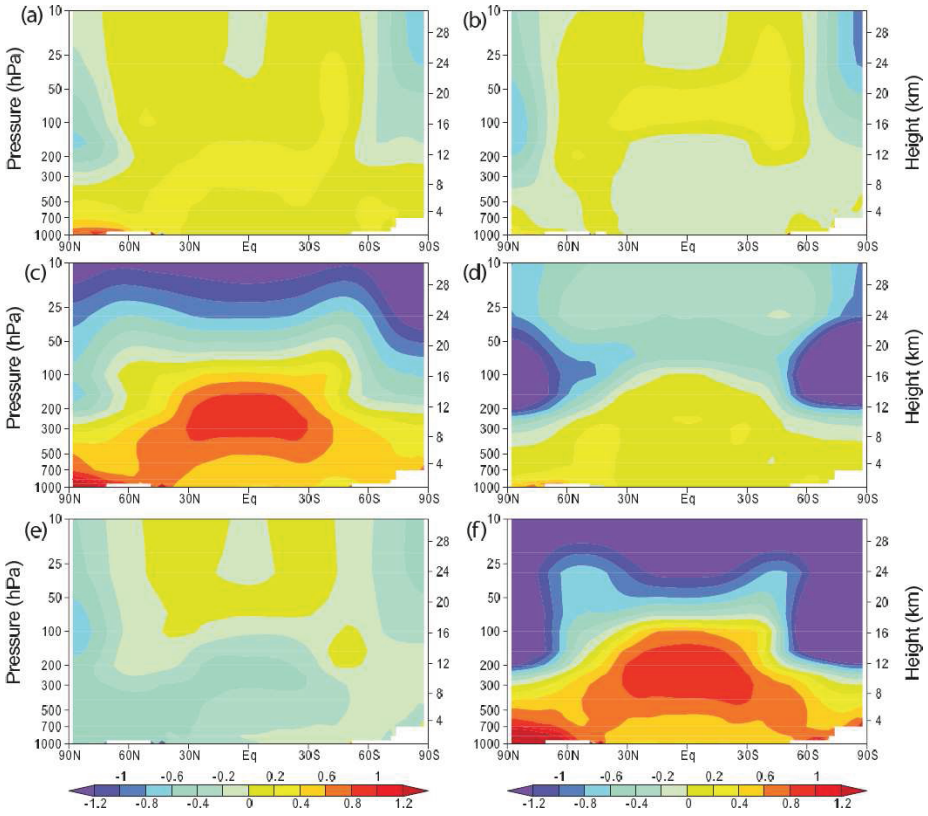

Figure 13: Zonal mean atmospheric temperature change from 1890 to 1999 (C per century) as simulated by the PCM model from (a) solar forcing, (b) volcanoes, (c) well-mixed greenhouse gases, (d) tropospheric and stratospheric ozone changes, (e) direct sulphate aerosol forcing and (f) the sum of all forcings. Plot is from 1,000 hPa to 10 hPa (shown on left scale) and from 0 km to 30 km (shown on right). Figure taken over from *IPCC AR4*[17].

	Ozone [%]	Temp. [K]	Time scale	dO_3/O_3dT [%/K]
Climate (2005-09 vs. 1964-80)	-3.5	-1.5	30 Years	2.33
Solar cycle	[1,2]	0.5	6 Years	[2,4]
Volcanic eruption	[-2,-4]	[+1,+2]	Years	[-1.0, -4]
Winter/spring depletion in Polar regions	[-30,-50]	[10, 15]	Months	[-2, -5]

Table 1: Range in observed changes in ozone column amounts and range in effective ozone temperatures with time scales on which they occur. The simultaneous change in relative ozone abundance and temperature give rough estimates for dO_3/O_3dT, on which a threshold value for temperature sensitivity can be estimated such that an ozone retrieval is insensitive to temperature variations. A temperature sensitivity of 0.01 %/K is a reasonable threshold value (see text). If the temperature sensitivity is equal or less than this threshold value then an ozone retrieval is able to capture the ozone trends with at least 1% accuracy.

1.4. Dobson spectrometer

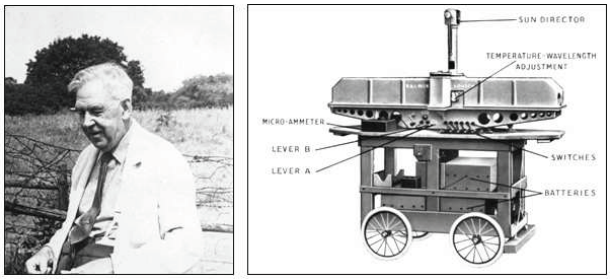

Figure 14: Left: G.M.B. Dobson (25-02-1889 - 11-03-1976) Right: The mobile Dobson spectrometer shown on a industrial drawing. Figure taken over from www.knmi.nl/cms/content/100061/twintig_vragen_en_antwoorden_over_de_ozonlaag Dobson instrument are still in operation, for example in Ukkel, Belgium.

In this subsection the Dobson instrument is introduced in detail, and the temperature sensitivity is estimated. The Dobson spectrophotometer is a large and manually controlled two-beam instrument based on the differential absorption method in the ultraviolet Huggins band where ozone exhibits strong absorption features, see figure 14.

Total ozone observations are made with the Dobson spectrometer by measuring the relative intensities of selected pairs of ultraviolet wavelengths, called the A, B*, C, C', and D wavelength pairs, emanating from the sun, moon or zenith sky. In passing through the atmosphere to the instrument, both wavelengths from a wavelength pair lose intensity because of scattering of the light by air molecules and dust particles. One of the two wavelengths is strongly attenuated while passing through the ozone layer whereas for the other wavelength the attenuation is relatively weak. The relative intensity of the A, or other wavelength pair as seen by the instrument therefore, varies with the amount of ozone present in the atmosphere. Thus, by measuring the relative intensities of suitably selected wavelength pairs with the Dobson instrument, it is possible to determine how much ozone is present in a vertical column of air extending from ground level to the top of the atmosphere in the neighborhood of the instrument.[18]

The AD double pair wavelength observations on direct sun with ground quart plate in the inlet window (AD-DSQP observations) are defined as the most reliable and are most used for the Dobson instrument. These observations have been recommended as standard by the International Ozone Commission (IOC). All other observations are reduced to the AD level before publication of the data.[18] An AD-DSQP measurement can be captured with the following simple equation:

$$N_v = \frac{\ln \frac{I_{305.0}}{I_{325.0}} - \ln \frac{I_{317.5}}{I_{339.9}} - B_1}{\Delta_{O_3} \cdot \mu} \tag{3}$$

Here N_v is the vertical ozone column amount, I_* the measured radiance at wavelength *, B_1 an extra terrestrial coefficient, which also accounts for scattering for the O_3 wavelength combination, Δ_{O_3} the differential O_3 absorption coefficient for the O_3 wavelength combination and μ the path-lengthening factor for an ozone layer of height 22 km. With different ozone absorption cross sections, the temperature sensitivity of the Dobson instrument can be estimated. New estimates for the temperature sensitivity are given in table 2 and the differential cross sections can be seen in figure 15. We can argue that the newest cross sections from Serdyuchenko[10] are most reliable because it has measurements at 11 temperatures, giving a temperature sensitivity of 0.125 ± 0.021 % / K. This temperature sensitivity is consistent within the error margin for

	Sensitivity [% / K]
	AD
Bass (1984) [7]	0.157 ± 0.013
Brion (1998) [8]	0.057 ± 0.039
Voigt (100 mbar, 2001) [9]	0.106 ± 0.024
Voigt (1000 mbar, 2001) [9]	0.104 ± 0.029
Serdyuchenko (2011)[10]	0.125 ± 0.021

Table 2: Calculated temperature sensitivity of the Dobson AD-DSQP measurements for different lab cross sections, evaluated at $T = -47°$C, which is an average effective ozone temperature. The uncertainty has been estimated by taking the difference from a 10 ° perturbation.

all other available cross sections, only the temperature sensitivity estimated with the Brion cross sections is on the low side. In figure 15, it can be seen that most probable reason for the lower sensitivity, estimated with the Brion cross sections, is that the Brion cross sections are lacking a lab measurement at a low temperature ($<$ -55 °C), which resulted in an anomalous fit. The estimated temperature sensitivity of 0.125 ± 0.021 % / K for the Dobson measurements is much higher than the threshold value 0.01 % / K, that is estimated for an ozone retrieval that is insensitive for temperature variations. It can therefore be concluded that the Dobson observations are sensitivity to temperature variations, and that the errors in ozone trends, based on the Dobson observations, can be expected on the order of 10%.

Theoretical derivation of the Dobson temperature sensitivity
We can write the measurement of ozone for the Dobson measurement in a reduced way as: [18, p. 7]

$$\begin{aligned} M_{\text{Dobson,AD}} &= (\sigma_{305.0} - \sigma_{325.0})N_s - (\sigma_{317.5} - \sigma_{339.9})N_s \\ &= \Delta_{O_3} N_s \\ \text{with } \Delta_{O_3} &= (\sigma_{305.0} - \sigma_{325.0}) - (\sigma_{317.5} - \sigma_{339.9}) \end{aligned} \tag{4}$$

Here M is a measurement, σ the ozone absorption cross section and N_s slant ozone column amount. The subscripts of the cross sections stand for the wavelengths. For a single measurement we can state that

$$M_{\text{Dobson,AD}} = \Delta_{O_3}(T) N_{s,t} = \Delta_{O_3}(T_0) N_{s,m}$$

where subscript m stands for measured, subscript t for true, T_0 is the climatological or constant temperature used in the measurement and T the real effective ozone temperature. Next we can estimate the temperature sensitivity:

$$\begin{aligned} N_{s,m} &= \frac{\Delta_{O_3}(T)}{\Delta_{O_3}(T_0)} N_{s,t} \\ \rightarrow \alpha = \frac{1}{N_{s,t}} \frac{\partial N_{s,m}}{\partial T} &= \frac{N_{s,t}}{N_{s,t}} \frac{1}{\Delta_{O_3}(T_0)} \frac{\partial \Delta_{O_3}}{\partial T} = \frac{1}{\Delta_{O_3}(T_0)} \left. \frac{\partial \Delta_{O_3}}{\partial T} \right|_{T_0} \end{aligned}$$

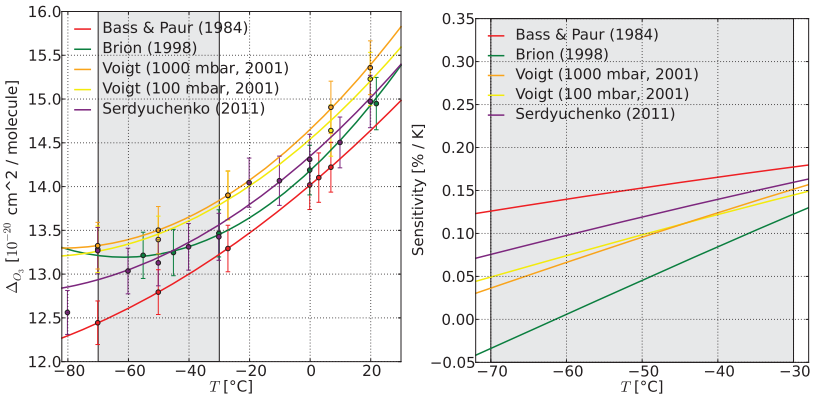

(a) Δ_{O_3} ozone cross sections (b) sensitivity

Figure 15: (a) Differential ozone absorption cross sections for AD-DSQP Dobson measurements (see text), which have been convoluted with the Brewer slit function and solar spectrum plotted as function of temperature for different lab-cross sections [7, 8, 9, 10]. The Brewer slit function has been used because the slit function that is used in a Dobson measurement is not clear from the documentation, but the effect on the cross-sections will be small. The original data points are shown before the fit was applied. Error bars denote the propagated errors, where a 1% error is assumed in the lab cross section, which is a typical value reported in literature for the error margin. (b) Temperature sensitivity derived from the differential absorption cross section. Realistic ozone effective temperatures are shaded.

1.5. Brewer direct sun observations

In this subsection the Brewer instrument is discussed in more detail and its temperature sensitivity is calculated. The Brewer grating spectrophotometer is in principle similar to the Dobson instrument, but it has an improved optical design and is fully automated. See figure 16. Direct sun measurements are the standard measurements to retrieve the ozone column amount with a differential absorption technique [13]. For direct sun measurements a linear combination is taken over the logarithm of measured irradiances for different wavelengths. The ozone column amount is determined from the wavelengths 310.1, 313.5, 316.8 and 320.1 nm. A direct sun Brewer measurement of the ozone column amount can be written as:

$$N_v = \frac{\ln \frac{I_{316.8}}{I_{310.1}} - 0.5 \cdot \ln \frac{I_{316.8}}{I_{313.5}} - 1.7 \cdot \ln \frac{I_{320.1}}{I_{316.8}} - B_1}{\Delta_{O_3} \cdot \mu}$$

Figure 16: Brewer instrument, located at on the rooftop of the KNMI building in De Bilt, the Netherlands.

Here N_v is the vertical ozone column amount, I_* the measured radiance at wavelength *, B_1 an extra terrestrial coefficients for the O_3 wavelength combination (instrument dependent), Δ_{O_3} the differential O_3 absorption coefficient for the O_3 wavelength combination (instrument dependent) and μ the path-lengthening factor for an ozone layer of height 22 km. The measured irradiances I_*, which for the Brewer instrument are count rates, are corrected for dead time, local temperature and (if applicable) Rayleigh scattering. The extraterrestrial constant B_1 is found by calibrating a Brewer instrument with a reference Brewer instrument. [13]

The Brewer temperature sensitivities, derived in several theoretical studies, varies both in magnitude and sign. In a study of [19, Kerr, J. B., 2002] , a calculated value of $0.094\%/\mathrm{K}$, is given; in a presentation of [20, Redondas et al., 2006] , a temperature sensitivity of $0.09\%/\mathrm{K}$ is shown for cross sections from Bass[7], and $-0.044\%/\mathrm{K}$ for lab cross-sections from Brion[8]. New estimates for the temperature sensitivity are calculated and listed in table 3. The differential cross sections are plotted in figure 17. It can be seen that the cross sections are inconsistent when the temperature sensitivity for the Brewer instrument is derived. We can argue that the newest cross sections from Serdyuchenko[10] are most reliable because it has measurements at 11 temperatures, giving a small temperature sensitivity of 0.014 ± 0.003 % / K. In a recent study of [19, Kerr, J. B., 2002] , for 1998-1999 Toronto data a temperature sensitivity of $-0.005\%/\mathrm{K}$ was found. Now we have achieved something new: both recent measurements from Toronto and a simple theoretical approach with the latest cross sections from Serdyuchenko give a small temperature sensitivity of the Brewer instrument that is one the order of $0.01\%/\mathrm{K}$. It can therefore be concluded that the Brewer direct sun observations are not sensitive to temperature variations, and that the errors in ozone trends, based on those measurements, can be determined with an accuracy of 1%.

	Sensitivity [% / K]
Bass (1984) [7]	0.118 ± 0.017
Brion (1998) [8]	-0.083 ± 0.033
Serdyuchenko (2011)[10]	0.022 ± 0.002

Table 3: Calculated temperature sensitivities for the Brewer instrument for different lab cross sections, evaluated at $T = -45°\mathrm{C}$. The uncertainty has been estimated by taking the difference from a 10 ° perturbation.

Theoretical derivation of the Brewer temperature sensitivity
We can write the measurement of ozone for the Brewer measurement in a simplified way as: [13, p. 113]:

$$\begin{aligned} M_{\text{Brewer}} &= (\sigma_{316.8} - \sigma_{310.1})N_s - 0.5(\sigma_{316.8} - \sigma_{313.5})N_s - 1.7(\sigma_{320.1} - \sigma_{316.8})N_s \\ &= \Delta_{O_3} N_s \\ \text{with } \Delta_{O_3} &= (\sigma_{316.8} - \sigma_{310.1}) - 0.5(\sigma_{316.8} - \sigma_{313.5}) - 1.7(\sigma_{320.1} - \sigma_{316.8}) \end{aligned} \tag{5}$$

Here M is a measurement, σ the ozone absorption cross section and N_s the slant ozone column amount. The subscripts of the cross sections stand for the wavelengths. For a single measurement we can state that

$$M_{\text{Brewer}} = \Delta_{O_3}(T) N_{s,t} = \Delta_{O_3}(T_0) N_{s,m}$$

where subscript m stands for measured, subscript t for true, T_0 is the (climatological) effective temperature used in the measurement and T the real effective temperature. Next we can estimated the sensitivity:

$$N_{s,m} = \frac{\Delta_{O_3}(T)}{\Delta_{O_3}(T_0)} N_{s,t}$$

$$\rightarrow \alpha = \frac{1}{N_{s,t}} \frac{\partial N_{s,m}}{\partial T} = \frac{N_{s,t}}{N_{s,t}} \frac{1}{\Delta_{O_3}(T_0)} \frac{\partial \Delta_{O_3}}{\partial T} = \frac{1}{\Delta_{O_3}(T_0)} \left. \frac{\partial \Delta_{O_3}}{\partial T} \right|_{T_0}$$

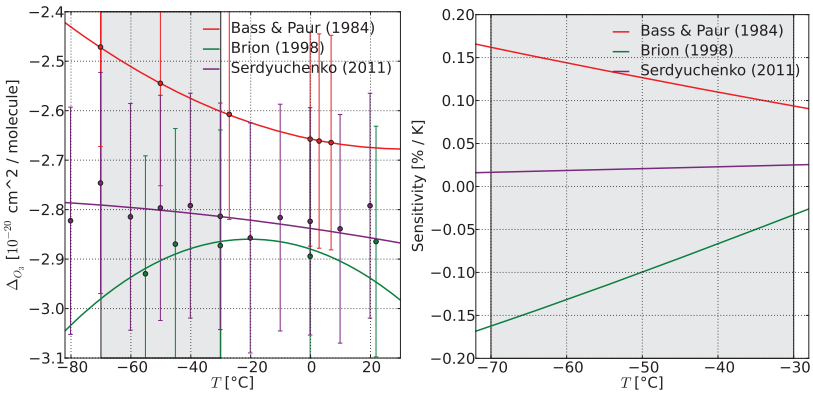

(a) Δ_{O_3} ozone cross sections (b) Sensitivity

Figure 17: (a) differential ozone absorption cross sections, which have been convoluted with the Brewer slit function and solar spectrum for the Brewer instrument plotted as function of temperature for different lab-cross sections [7, 8, 9, 10]. Error bars denote the propagated errors, where a 1% error is assumed in the lab X-section, which is a typical value reported in literature for the error margin. (b) temperature sensitivity derived from the differential absorption cross section. Realistic ozone effective temperatures are shaded.

1.5.1. Alternative retrieval methods with the Brewer instrument

A Brewer instrument is an advanced spectrophotometer, that is used for ground based measurement, where different measurement methods have been developed to retrieve the ozone column amount and other concentrations of atmospheric constituents such as aerosols and SO_2. The different measurement methods are 1. direct sun, 2. Umkehr (for profile retrievals), 3. Système d'Analyse par Observation Zénithale (SAOZ, for column retrievals) and 4. group-scan. The standard method for ozone column retrievals is the direct sun measurement, already discussed, but a recent study showed that it is possible to enhance the Brewer observations with a new method, the so-called group-scan method.

In a recent study of [19, Kerr, J. B., 2002] , 45 wavelengths are used with the Brewer instrument. The spectra observed with the group-scan method are analyzed by a modified version of the DOAS analysis technique. The main difference between a normal DOAS technique and the new technique is the treatment of variability in observing conditions from one of the nine groups of five wavelengths to another. This is done by assuming that the main source of variability is due to changes in the optical depth of aerosols or thin clouds and that the variability affects five wavelengths for each group equally. In their study they claim they have a precision on the order of $\pm 0.1\%$. The reference ET (=extraterrestrial) spectrum is determined with a zero air mass extrapolation or the so-called Langley method. Results of their measurements made at Toronto demonstrate that it is possible to obtain an effective temperature value for atmospheric ozone. These measurements suggest that the temperature dependence of ozone absorption has little effect on Brewer total ozone values and that the temperature dependence of the Dobson total ozone measurement likely explains most of the observed seasonal differences between Dobson and Brewer measurements.[19]

1.6. OMI Total Ozone Mapping Spectrometer (OMTO3)

In this subsection the OMTO3 algorithm is introduced in detail and its temperature sensitivity is estimated. A common technique for remote sensing of ozone is the use of a wavelength pair, where one wavelength is the "ozone-absorbing wavelength" and the other is the "non-ozone absorbing wavelength". The difference between measured radiances can, together with corrections for scattering, clouds and geometry, be directly related to the ozone column. Such a retrieval is the basis for the Dobson instruments, which already has been discussed. The TOMS algorithm is an improved version of such a retrieval, where the difference in sun-normalized reflectance for two wavelengths is used as input for an optimal estimation technique, instead of a direct analytic relation. The TOMS algorithm has a long heritage, where the first satellite instrument was launched in 1979 on Nimbus 7 where it became possible to measure the vertical column density of ozone from space. The TOMS instrument on board Nimbus 7 has yielded the longest continuous global data set on the ozone layer (1979-1992), covering in particular the formation and evolution of the ozone hole.

The OMI instrument also has a TOMS algorithm, was is called OMTO3. The OMTO3 algorithm uses two wavelengths: 317.5 and 331.2 nm (and 331.2 and 360 nm for high solar zenith angle conditions). In the optimal estimation technique, measured radiances are compared against radiances calculated from a priori, with a radiative transfer model, to estimate a change in ozone from a priori. The ozone column amount is estimated as: [21]

$$N_v = N_{v,0} - (\ln I - \ln I_0) \Big/ \left.\frac{\partial \ln I}{\partial N_v}\right|_{N_v = N_{v,0}} \tag{6}$$

Here N_v is the vertical ozone column amount and I the measured sun-normalized radiance at the top of the atmosphere. The subscript 0 is indicating that the variable is the climatological one, a-priori calculated. This climatology consist of 21 standard profiles for which the sun-normalized radiances at the top of the atmosphere are calculated and stored in a look-up table.

The cross-sections for OMTO3 and its temperature sensitivity are plotted in figure 18. Values for the temperature sensitivity are listed in table 4. If we derive the temperature sensitivity for the OMTO3 algorithm, we get a quite consistent picture from cross sections from Brion[8], Bass[7], Serdyuchenko[10] and Voigt[9], only the low pressure cross sections from Voigt[9] give different results. We can argue that the newest cross sections from Serdyuchenko[10] are most reliable because it has measurements at 11 temperatures, giving a temperature sensitivity of 0.175 ± 0.025 % / K. This temperature sensitivity is much higher than the threshold value of 0.01 % /K, that was estimated for a retrieval method that is insensitive to temperature variations. Errors in effective ozone temperature are made with the OMTO3 algorithm when there are differences with respect to the ozone effective temperature that is used in the radiative transfer model to calculate the sun-normalized radiances at the top of the atmosphere. OMTO3 uses the TOMS v8 climatology for ozone and temperature profiles, which depends on month and latitude for temperature profiles and on month, latitude and ozone column amount for ozone profiles. The use of different ozone profiles with the same temperature profiles is essentially inconsistent because a different ozone profile will result in a different temperature profile. The errors in effective ozone temperature for OMTO3 are therefore longitudinal variations in effective ozone temperature and changes in long-term stratospheric temperatures caused by climate change or volcanic eruptions. The latter changes in long-term stratospheric temperatures can have a significant effect on the ozone trend. Based on temperature sensitivity for OMTO3, the error in an ozone trend from OMTO3 can be estimated as $\sim$20%.

	Sensitivity [% / K]	
	standard	alternative
Bass (1984) [7]	0.173 ± 0.018	-
Brion (1998) [8]	0.163 ± 0.033	0.137 ± 0.044
Voigt (100 mbar, 2001) [9]	-0.038 ± 0.058	0.340 ± 0.010
Voigt (1000 mbar, 2001) [9]	0.164 ± 0.017	0.238 ± 0.012
Serdyuchenko (2011)[10]	0.175 ± 0.025	0.132 ± 0.065

Table 4: Calculated sensitivity for temperature of the OMTO3 algorithm for different lab cross sections, evaluated at $T = -47°$C, which is an average effective ozone temperature. The sensitivity is calculated for the standard wavelength pair (317.5 and 331.2 nm) and for the alternative wavelength pair (331.2 and 360 nm). The uncertainty has been estimated by taking the difference from a 10 ° perturbation. The Bass (1984) cross sections are available until 342.78 nm, and therefore no value is reported for the alternative wavelength pair for the Bass cross sections.

Theoretical derivation of the OMTO3 temperature sensitivity
The sun-normalized radiances can be written as:

$$I = \frac{I_1}{I_2} = \frac{\exp\left[-\sum_l m_{l,1}\sigma_{l,1}x_l\right]}{\exp\left[-\sum_l m_{l,2}\sigma_{l,2}x_l\right]} = \exp\left[-\sum_l (m_{l,1}\sigma_{l,1} - m_{l,2}\sigma_{l,2})x_l\right] \qquad (7)$$

where I_1 is referring to the "ozone absorbing" radiance (wavelength 1), and I_2 is referring to the "non-ozone absorbing" radiance (wavelength 2); $m_{l,*}$ is a layer resolved air mass-factor (at wavelength λ_*) and x_l is the ozone profile. The air mass factor converts an average scattered light path to a vertical light path. Therefore the air mass factor accounts for a cloud height dependency, cloud albedo, surface albedo, aerosols, solar geometry and viewing geometry.

For simplicity the air mass factors are assumed to be the same at the two different wavelengths, $m_{l,1} = m_{l,2}$. As a consequence the estimate for the temperature sensitivity may not be very accurate. However, the main goal here is to get an estimate for the temperature sensitivity of the OMTO3 vertical ozone column. For this purpose the simplification is justified. The temperature sensitivity can be compared with a threshold value or with the temperature sensitivity of other ozone retrieval algorithms.

Ozone absorption coefficients at 317.5 and 331.2 nm, that are convoluted with an OMI slit function, are used to do the derivation. Or alternatively for high solar zenith angles 331.2 and 360 nm. The sun-normalized radiance can be written as:

$$\begin{aligned} -\log I = \Delta_{O_3}(T)N_{s,t} &= \Delta_{O_3}(T_0)N_{s,m} \\ \text{with } \Delta_{O_3} &= \sigma_1 - \sigma_2 \end{aligned} \qquad (8)$$

where subscript m stands for measured, subscript t for true, T_0 is the (climatological) effective temperature used in the measurement and T the real effective temperature.

Next we can estimated the sensitivity:

$$N_{s,m} = \frac{\Delta_{O_3}(T)}{\Delta_{O_3}(T_0)} N_{s,t}$$

$$\rightarrow \alpha = \frac{1}{N_{s,t}} \frac{\partial N_{s,m}}{\partial T} = \frac{N_{s,t}}{N_{s,t}} \frac{1}{\Delta_{O_3}(T_0)} \frac{\partial \Delta_{O_3}}{\partial T} = \frac{1}{\Delta_{O_3}(T_0)} \left. \frac{\partial \Delta_{O_3}}{\partial T} \right|_{T_0}$$

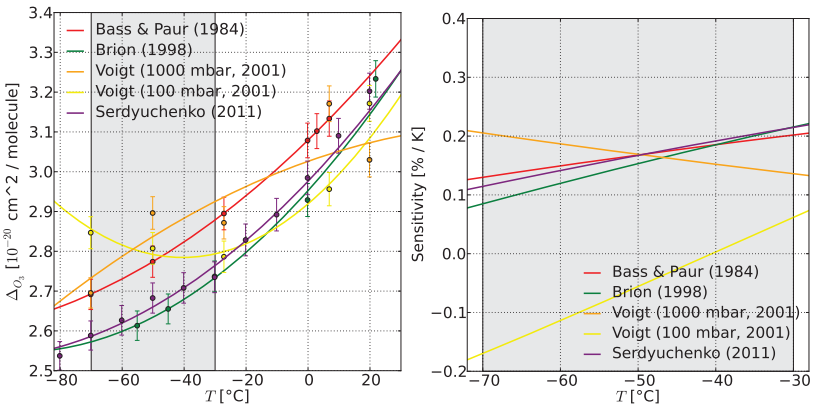

(a) Δ_{O_3} ozone cross sections

(b) sensitivity

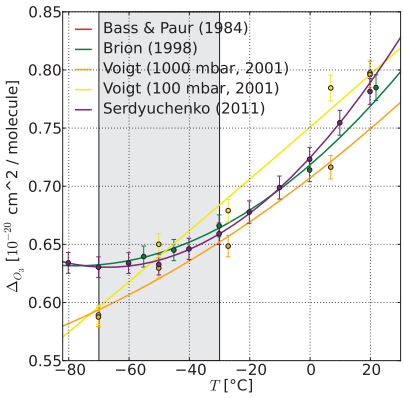

(c) Δ_{O_3} ozone cross sections (alt.)

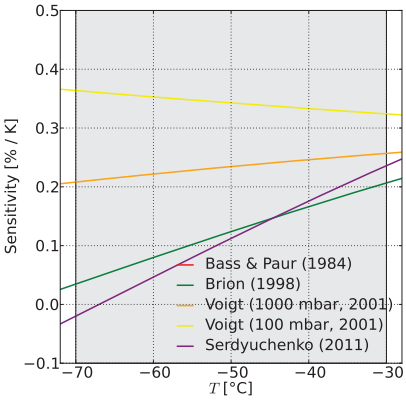

(d) sensitivity (alt.)

Figure 18: (a) differential ozone absorption cross sections for OMTO3, which have been convoluted with the OMI slit function and solar spectrum plotted as function of temperature for different lab-cross sections [7, 8, 9, 10]. Also the original data points are shown, before the fit was applied. Error bars denote the propagated errors, where a 1% error is assumed in the lab X-section, which is a typical value reported in literature for the error margin. (b) temperature sensitivity derived from the differential absorption cross section. Realistic ozone effective temperatures are shaded. (c) and (d) similar plots but then for the alternative wavelength pair 331.2 and 360 nm.

1.7. OMI Differential Optical Absorption Spectroscopy (OMDOAO3)

In this subsection the DOAS implementation for the OMI instrument, referred to as OMDOAO3, is discussed in detail, and the temperature sensitivity is estimated with a radiative transfer model. In the DOAS (Differential Optical Absorption Spectroscopy) implementation for OMI the ozone the vertical ozone column is determined in three steps. In the first step the actual DOAS fitting is performed, resulting in the so-called slant column density, which is the amount of ozone along an average photon path from the sun through the atmosphere to the satellite. In the second step the air mass factor is determined, which is needed to convert the slant column density into a vertical column. The air mass factor is calculated with the help of a radiative transfer model and ozone and temperature profile from the TOMS v8 Climatology. The air mass factor is determined by applying the DOAS fit to simulated OMI spectra, a method that is often referred to as the empirical air mass factor. In the last step a correction is performed for clouds. The cloud information, needed to derive accurate air mass factors and for corrections factors for cloudy and partly cloudy conditions, is obtained from the OMI cloud product which is derived from the O_2-O_2 collision complex absorption band around 477 nm.

We will focus mainly on the first step where the slant column amount is determined. In this part the convoluted cross-sections are used to obtain a slant column and an effective temperature. The current OMDOAO3 implementation uses a 5 nm wide fit window, that is centered around 334.1 nm. This window has been selected on the basis of the very low temperature sensitivity shown by this wavelength range. [22] The slant column density in a DOAS algorithm is calculated via a fit of equation 9 for about 30 wavelengths. [5, p. 1240]

$$\frac{I(\lambda)}{F(\lambda)} = P(\lambda)\exp\left[-N_s\sigma_{O3}(\lambda, T_{\text{eff}})\right] \tag{9}$$

where I is the measured radiance, F the measured extraterrestrial solar irradiance, P a low-order polynomial, N_s ozone slant column density, $\sigma_{O3}(\lambda, T_{\text{eff}})$ convoluted absorption cross section of ozone, λ the wavelength and T_{eff} the effective temperature. In the current algorithm, the ozone absorption cross sections are linearized at a reference temperature $T_0 = -73.15°C$ as:

$$\sigma_{O3}(\lambda, T_{\text{eff}}) = \sigma_{O3}(\lambda, T_0) + \alpha(\lambda)(T_{\text{eff}} - T_0) \text{ with } \alpha(\lambda) = \left.\frac{d\sigma_{O3}(\lambda)}{dT}\right|_{T=T_0}$$

By considering the slant optical depth, the definition for the effective ozone temperature follows:

$$\begin{aligned}\tau_s(\lambda) = \int n(z)m(\lambda,z)\left[\sigma(\lambda,T_0) + \alpha(\lambda)(T(z) - T_0)\right]dz = \\ N_s\left[\sigma(\lambda,T_0) + \alpha(\lambda)(\frac{\int n(z)m(\lambda,z)T(z)dz}{N_s} - T_0)\right]dz = \\ N_s\left[\sigma(\lambda,T_0) + \alpha(\lambda)(T_{\text{eff}} - T_0)\right]\end{aligned}$$

Here m is the altitude resolved air mass factor (amf), n number density of ozone, $T(z)$ temperature profile and T_0 a reference temperature. An s (slant) has been added as subscript to emphasize that the amf is included in the integral. The amf converts a slant and scattered light path to a vertical light path, which depends on cloud height, cloud albedo, surface albedo, aerosols, solar

geometry and viewing geometry. Hence the slant effective ozone temperature is defined as: [12, p. 13]

$$T_{\text{eff},s} - T_0 = \frac{\int m(z,\lambda)n(z)(T(z)-T_0)dz}{\int m(z,\lambda)n(z)dz} \tag{10}$$

In the DOAS fit,next to the ozone effective temperature T_{eff} and slant ozone column density N_s, a second degree polynomial $P(\lambda)$ is fitted:

$$P(\lambda) = c_0 + c_1(\lambda - \lambda_0) + c_1(\lambda - \lambda_0)^2$$

This polynomial acts as a high pass filter, to account for absorption that varies gradually with wavelength, which is caused by reflection by the surface and scattering by molecules, aerosols, and clouds. The high-pass filter also takes out gradually varying radiometric calibration errors and other instrumental multiplicative effects.

In the OMDOAO3 retrieval algorithm inelastic rotational Raman scattering is explicitly taken into account. Inelastic scattering is scattering where the wavelength changes with a scattering event. Inelastic rotational Raman scattering is the redistribution of the intensity of scattered photons over several nanometers. As the loss of intensity through Raman scattering is proportional to the local intensity, while the gain in intensity is proportional to the intensity at neighboring wavelength, the effect results in a filling-in of deep Fraunhofer lines in the scattered light spectrum. The amount of filling-in depends on the relative amounts of inelastic and elastic scattering and can be simulated with radiative transfer models. In the retrieval, it is accounted for by the inclusion of a pseudo-absorber, the so called Ring spectrum, which can be computed with a radiative transfer model.[6] In the OMDOAO3, it is implemented by adding another term with the fitting parameter, c_{Ring}, which is a measure for the amount of rotational Raman scattering :

$$\frac{I(\lambda)}{F(\lambda)} = P(\lambda)\exp\left[-N_s\sigma_{O3}(\lambda,T_{\text{eff}})\right] + c_{\text{Ring}}\frac{I_{\text{Ring}}(\lambda)}{F(\lambda)}\exp\left[-N_s\sigma'_{O3}(\lambda,T_{\text{eff}})\right] \tag{11}$$

Here I_{Ring} is the ring spectrum and $\sigma'_{O3}(\lambda,T_{\text{eff}})$ is the effective cross section for inelastic scattering. The effective cross section is a linear combination of the non-scrambled and scrambled cross-section.[12] An overview of ring effect studies can be found in [23, Kelly V. Chance and Robert J.D. Spurr, 1997] and the technical details of the implementation in the DOAS algorithm can be found in [12, J.F. de Haan, 2003] .

For the current DOAS implementation, the linearized Brion ozone absorption coefficients[8] are used. First the lab cross sections are fitted to a second degree polynomial and consequently convoluted with the OMI slit function. After that, the convoluted cross-sections are linearized at $T_0 = -73.15°C$. This convolution process can also be applied to different lab cross-sections, and the resulting convoluted cross-sections are shown in figures 19b and 21. In these plots also the linearized cross-sections are shown (Brion, lin), which is how they are currently used in the DOAS algorithm. Linearization of the cross-sections at a reference temperature, that is outside the range of realistic temperatures, may have an impact on the retrieved temperature and also induce a temperature-dependency in the ozone retrieval. In figure 21 the ozone absorption cross sections are shown for several wavelengths, and it can be seen that sometimes the linearization goes well but it may have a negative impact on the ozone retrieval for higher ozone temperatures where the linear approximation is less accurate. This point will be discussed in detail in section 5.

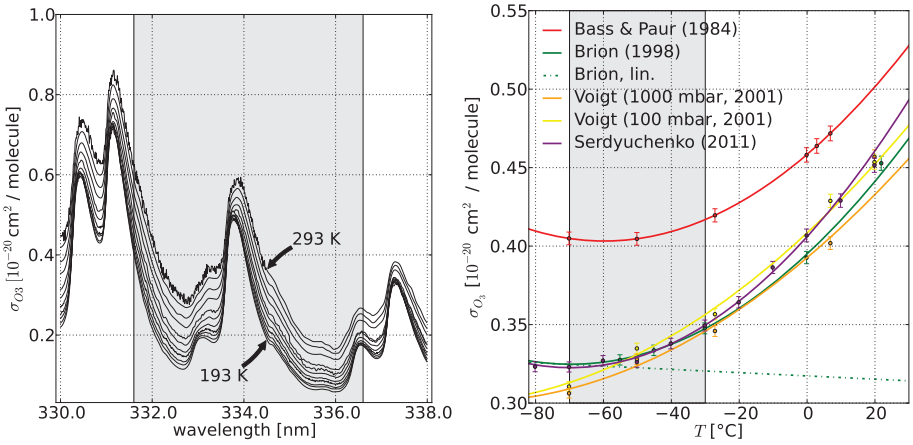

(a) lab X-sections

(b) 333.6 nm

Figure 19: Ozone absorption cross sections in the OMDOAO3 wavelength region: (a) lab-X-sections stacked for 11 different temperatures (193-293 K, step size 10 K) from Serdyuchenko [10] (b) second-degree polynomial fits for the convoluted cross-sections (with OMI slit function and solar spectrum), for different lab-cross sections [7, 8, 9, 10]. Original data points are shown with a 1% error bar, which is a typical value reported in literature for the error margin. The linearized cross-sections of Brion, that are used in the current implementation, are plotted (Brion, lin.). The current DOAS fit window and realistic ozone effective temperatures are shaded.

A theoretical estimate for the temperature sensitivity of OMDOAO3 can be made, by assuming that the slant column is fitted accurately. The temperature sensitivity is calculated from a change in slant column amount for a change in effective temperature. It turns out that the temperature sensitivity is -0.011 ± 0.002 % / K for wavelengths higher than 330 nm, and increases in magnitude to -0.025 ± 0.011 % / K for wavelengths between 320 and 330 nm, see figure 20. However, such a theoretical analysis is not complete, because a fit function acts on a wavelength band, instead of just one wavelength, and simplifications that are used for the fitting routine, may have an impact on the temperature sensitivity.

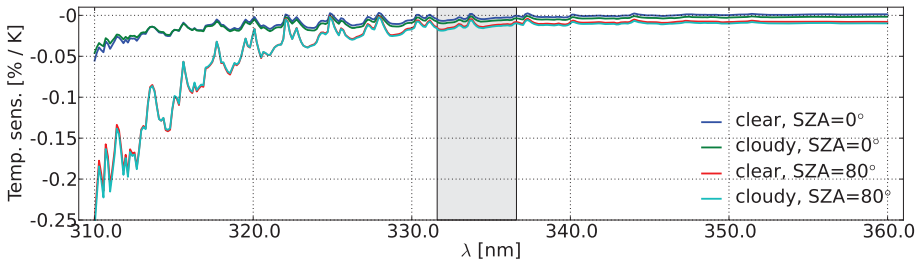

Figure 20: Spectrum of the temperature sensitivity. The temperature sensitivity has been calculated with a radiative transfer model, DISAMAR[24], where the change in slant column amount has been calculated for a change in effective temperature. The current DOAS fit window is shaded.

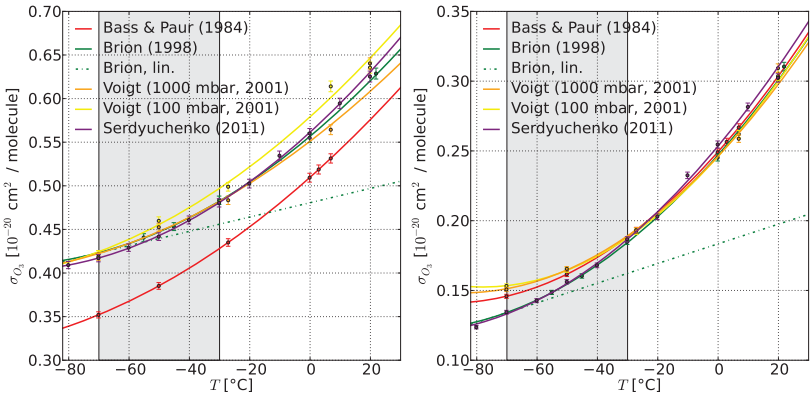

(a) 331.6 nm

(b) 332.6 nm

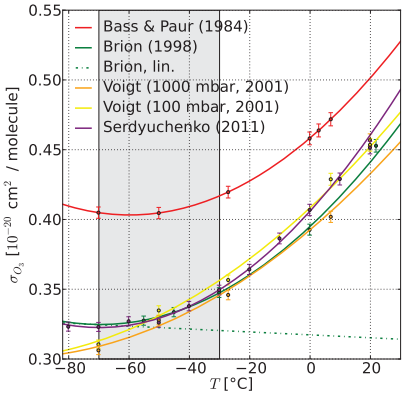

(c) 333.6 nm

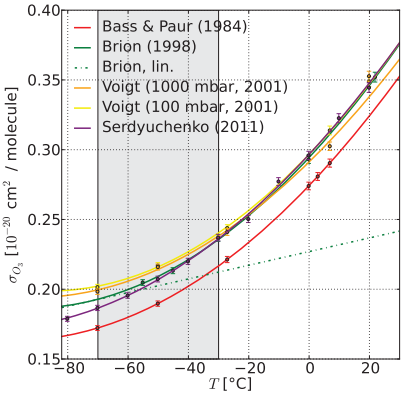

(d) 334.6 nm

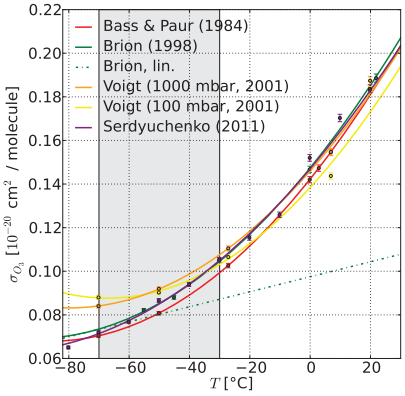

(e) 335.6 nm

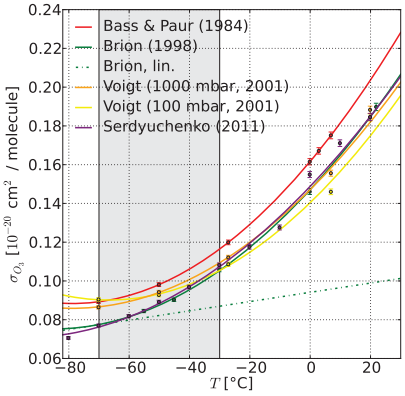

(f) 336.1 nm

Figure 21: Temperature dependency of ozone absorption cross sections in the OMDOAO3 wavelength region: second-degree polynomial fits for the convoluted cross-sections (with OMI slit function and solar spectrum), for different lab-cross sections [7, 8, 9, 10]. Original data points are shown with a 1% error bar, which is a typical value reported in literature for the error margin. The linearized cross-section of Brion, that are used in the current implementation, are plotted. Realistic ozone effective temperatures are shaded.

1.8. OMI Ozone Profile Product (OMO3PR)

In this subsection the OMI ozone profile product is introduced in more detail, and the temperature sensitivity is estimated. In this study accurate collocated ozone and temperature profiles are needed to calculate a reference ozone effective temperature that can be used to estimate the temperature sensitivity of OMI ozone products. It turns out that the OMI ozone profile product is an excellent candidate for this purpose.

The operational ozone profile algorithm is based on the physical mechanism of a 4 orders of magnitude increase in the ozone absorption cross sections from 330 nm to 270 nm. Envisage that light with a wavelength of 270 nm penetrates the atmosphere to an altitude of roughly 60 km while much of the incident light at 330 nm reaches the ground surface. Hence, a change in ozone in the troposphere affects the radiance spectrum at longer wavelengths while a change in ozone at the top of the atmosphere affects the radiance at all wavelengths. The retrieval algorithm is based on optimal estimation where the amount of ozone in each atmospheric layer is adjusted such that the difference between the modeled and measured sun-normalized radiance is minimal. This approach is common practice nowadays for the retrieval of nadir ozone profiles from UV/VIS spectra recorded by a number of satellite based platforms such as OMI, SCIAMACHY and GOME-2, differing mainly in the auxiliary information such as surface albedo and a-priori information, e.g. a-priori ozone profile.

The OMO3PR algorithm uses the newly developed LABOS radiative transfer model, a pseudo spherical correction for direct sun light and corrections for the initial assumption that the atmospheric layers are homogeneous. Ozone cross sections are used from Brion[8]. A quadratic polynomial in the temperature is used for each wavelength and the coefficients of the polynomial are obtained from fitting data measured at 218, 228, 243, and 295 K. Global ECMWF pressure and temperature profiles are used in the retrieval. The degrees of freedom of the signal (DOF or DFS: the number of independent pieces of information that is retrieved from the reflectance spectrum, taking into account the noise of the signal) of 6-7 is not large enough to determine the ozone amount for all of the 18 layers used here. In optimal estimation the retrieval is constrained by the measured data, weighted by the measurement error, and subject to the a-priori statistics of the atmosphere. As a result the retrieved profile will not differ too much from a climatological average, unless forced by the measured radiance. The ozone profile is given in terms of the layer-column of ozone in DU for an 18-layer atmosphere ranging from surface pressure to 0.3 hPa. [25]

[25, M. Kroon et al., 2011] have shown that the quality of OMI operational ozone profiles is sufficient for scientific explorations. The OMO3PR algorithm, MLS and TES, three very different types of remote sensing instruments with synergistic data products aboard the Aura platform, has proven to be extremely valuable for cross validation. Validation of OMI profiles against MLS show that OMI is in agreement with MLS within $\pm$10%. for most latitudes except for the Polar regions during the ozone hole seasons where differences up to $\pm$30% may occur. Figure 22 shows an example of comparisons with MLS for August 1th, 2007. The main conclusions of these comparisons are as expected from simulated results and that comparison of OMO3PR profiles with MLS agree very well for the pressure range up to 400 hPa. In the upper troposphere and lower stratosphere little profile information is contained in the UV spectrum and this part of the ozone profile may therefore be of less quality. [25]

The OMI vertical ozone profiles provides maps of the global ozone layer in three dimensions on a daily basis with a horizontal resolution of at least 65 km x 48 km and capturing the vertical ozone structures from the surface up to 65 km in 18 pressure layers, with a vertical resolution

of at least 6 km. These retrievals constitute a comprehensive data set to study the spatial and temporal distribution of ozone everywhere on the globe. [25]

From numbers in documentation of the algorithm, a temperature sensitivity for OMO3PR can be estimated as 0.2%/K. However, as in OMO3PR the temperature profile from a medium weather forecasting model (ECMWF) is used, it is unlikely that there will be systematic errors based on an error in the assumed temperature(s) for the profile retrieval. However, the ozone retrieval itself may be dependent on effective ozone temperature, which for example can be caused by an error in the temperature dependency of the ozone absorption cross sections that are used.

An advantage of the OMO3PR is that relatively easy an ozone effective temperature can be calculated, that is collocated with the other OMI products:

$$T_{\text{eff}} = \int n(z)T(z)dz \Big/ \int n(z)dz$$

Here $n(z)$ is the OMO3PR determined ozone profile and $T(z)$ the temperature profile from a medium range weather forecasting model (ECMWF). As the ozone profiles are validated against a variety of other instruments[25], we can state that this effective ozone temperatures is essentially a good estimator for the ozone effective temperature.

Estimation of the OMO3PR temperature sensitivity
In *Algorithm Theoretical Basis Document* [21], percentage errors in retrieved ozone are given for an error in modeled temperature. Typical values are $0.6 \pm 0.4\%$ per 5 K. A typical resulting value for the the temperature sensitivity is then $0.13 \pm 0.08\%/\mathrm{K}$. The uncertainty in this estimate is a result from the temperature dependence of the absorption cross sections with altitude.

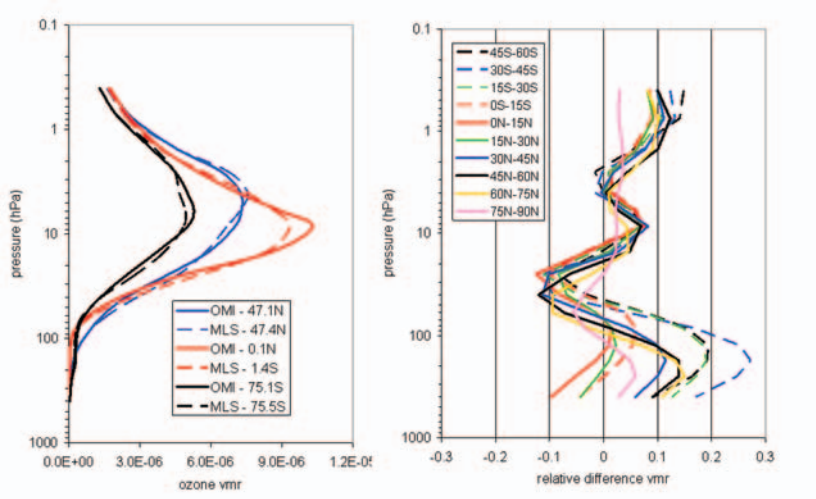

Figure 22: Left: Comparison of retrieved profiles from OMI (solid) and MLS (dashed) for three latitudes for OMI orbit 6754 in week 42 2005. The black curves pertain to a part of the ozone hole. The latitudes used are listed in the legend. Right: Average relative differences between ozone profile retrieved from OMI and MLS for week 30, 2005 (OMI orbits 5428 5529). Results are given for different latitude bands and solid lines are for the northern hemisphere while dashed lines are for the southern hemisphere. For each latitude band about 2000 co-locations were used, except for 45S-60S where 681 co-locations were used.

1.9. Balloon borne sondes

In this section balloon borne ozone sondes are discussed in detail and the use of such sondes for the validation of OMI ozone products is considered. The vertical profile of ozone is measured with ozone sondes, laser-radars (LIDARs), ground-based spectrometers and various satellite-born instruments. The longest records exist for balloon borne ozone sondes, which are ozone analyzers coupled to radiosondes. They operate regularly in all climatic regions and under severe weather conditions. They have been the backbone of ozone profiling since the 1960s.[2] The ozone sondes measures the concentration of ozone as function of height by sampling ambient air during its balloon-borne ascent to an altitude typically between 30 and 35 km. The vertical ozone column amount and effective ozone temperature can be determined with ozone sondes, by making some assumptions on the missing profile above the bursting height. The use of those resulting quantities for the validation of OMI ozone products is considered in this subsection.

All types of wet-chemical in situ sondes are based on the electrochemical oxidation of potassium iodide by ozone in an aqueous solution. The chemical reaction forms two electrons per ozone molecule captured in the solution. The resulting current is a quantitative measure for the number of ozone molecules pumped through the reaction chamber(s). The main components of the sonde are a reaction chamber, where ozone molecules react with the chemical solutions (bubbler), an air pump, a power supply and an electronic interface that convert the raw current signal and transfers it to the radiosonde. To protect the sensitive parts of the instrument from mechanical impact and low temperature, all components are mounted in a Styrofoam box. To transfer the ozone signal to the ground receiver, the ozone sonde has to be connected to a suitable meteorological radiosonde. [2] See figure 25 for a typical sonde launch at KNMI.

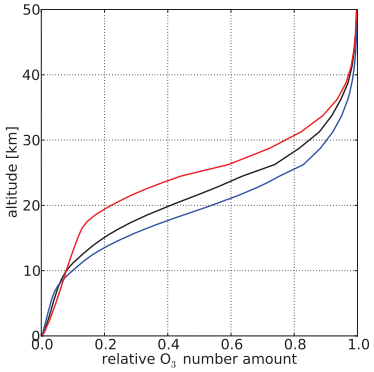

Figure 23: Relative cumulative ozone amount plotted against height for U.S. 1976 standard atmospheric profiles[26]: standard (black), subarctic winter (blue) and tropics (red).

Sondes have a typical bursting height of 30-35 km, which can be seen by measurements in 2005, see figure 24. Hence they measure approximately 90% of the ozone column amount, see figure 23. When we are interested in determining ozone column amounts or ozone effective temperature, there have to be made assumptions for the remaining 10% of the ozone and temperature profile. For example, we could assume a constant mixing ratio, but errors can be expected up to the order of $\sim$3% of the ozone column amount. Such large errors are unacceptable, if we compare it with other ozone measurements which claim to have errors of 1% or less.

For the study of trends, it is likely that such a comparison will not give scientific valuable results. This can be proven by a simple comparison of the ozone column amounts and ozone effective temperatures that are determined with ozone sondes from 2005. For the calculation for ozone column amount for the sonde, a constant mixing ratio from the bursting point till 40 km height is assumed, in combination with a standard profile for mixing ratios from the U.S. Standard Atmosphere 1976 for heights above 40 km. For the missing upper part, temperature

lapse rates from the U.S. standard atmosphere are used. In the experiment the bursting heights are binned and for the bins, differences in ozone column amount and effective temperature are calculated, where references values for ozone column amount and effective temperature are used from satellite products (OMDOAO3/OMO3PR). See figure 24 for the results. We can see that the results for the ozone sondes, are depending on the bursting height. Depending on the region (polar regions, mid latitudes or tropics), the effective temperature may vary several degrees as function of bursting height, and the ozone column amount up till $\sim$5% as function of bursting height. Hence it can be concluded that sondes are useful for ozone profile determination but are not valuable for the accurate determination of ozone effective temperature or ozone column amount with these assumptions . Therefore the ozone sondes are not used in this study for validation of OMI ozone products. There may however be a more advanced method to estimate the upper missing part above the bursting height that gives realistic values for the key ozone variables.

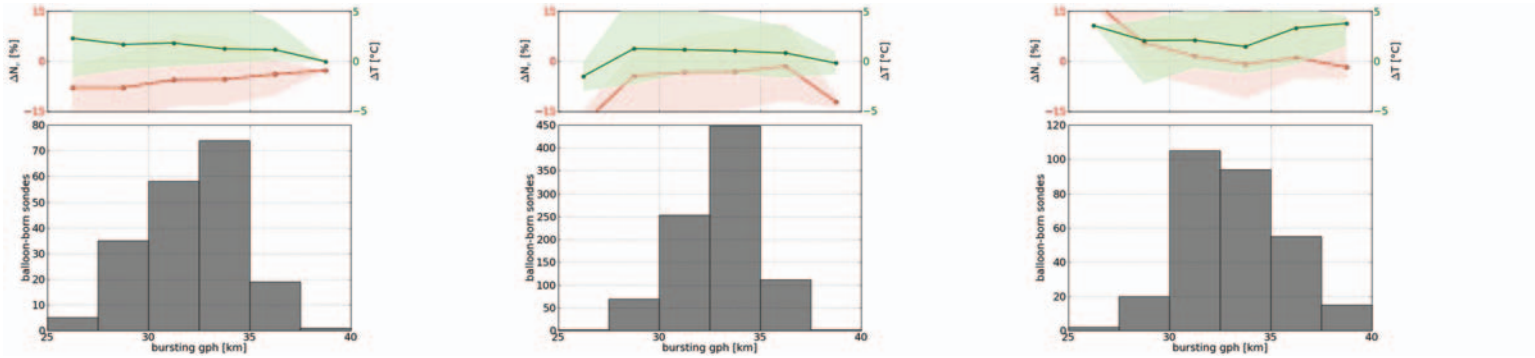

(a) Polar regions (b) Mid latitudes (c) Tropics

Figure 24: (a) - (c) Validation of the use of balloon borne sondes for different regions. Lower panel: distribution of balloon bursting height plotted with the frequency on the left axis. Upper panel: Difference in ozone column amount (red, sonde - OMDOAO3) and effective temperature (green, sonde - OMO3PR). For the determination of OMO3PR effective temperature, ozone profiles and temperatures profiles from OMO3PR (OMI ozone profile product) and ECMWF (temperature profile from a medium weather forecasting model) have been multiplied, see equation 17. The spread is shown for the differences, $\pm\sigma$, light colored shading. For polar regions 192 sondes were used from 6 locations; for mid latitudes 887 sondes were used from 18 locations; for tropics 291 sondes were used from 9 locations. Data has been used from the year 2005. Data for the comparison was obtained from `http://avdc.gsfc.nasa.gov/`.

Figure 25: Sonde launch at KNMI at Thursday April 19th 2012, 1 o'clock. The person in the left carries the sonde and the right person is going to launch the balloon. A large distance is maintained between the balloon and the ozone sonde such that the balloon doesn't influence the sonde measurements. In the background the meteorological yard of the KNMI with weather instruments can be seen.

1.10. Conclusions

In this section we have identified the OMI ozone products and the ozone products that are useful to validate the OMDOAO3 effective temperature and the ozone products that can be used to estimate the temperature sensitivity of the OMI ozone products. The temperature sensitivity of the different ozone products have been estimated on a theoretical basis. An overview of what currently is known is listed in table 5. The results are now discussed and it will be concluded how to continue with this study.

For the ground-based measurement, it is has been theoretically estimated that the Dobson standard AD-DSQP observations are sensitive to changes in the effective ozone temperature. The temperature sensitivity for the Dobson AD-DSQP is estimated as 0.125 ± 0.021 % / K. The Brewer instruments are not sensitive to changes in effective ozone temperature, which has been observed with 1998-1999 Toronto measurements in a study of [19, Kerr, J. B., 2002] , which in this study is theoretically confirmed by the new cross sections of Serdyuchenko[10]. The Brewer measurements of vertical ozone column amount are therefore the most obvious choice to validate the OMI ozone products and estimate their temperature sensitivity.

The temperature sensitivity has been estimated for all OMI ozone products. Depending on which cross sections are used and how they are implemented, there may be a temperature dependency of the ozone column amount in all products. For OMO3PR, other dependencies are not expected since the temperatures that are used originate from a medium weather forecasting model (ECMWF). The ozone profile from OMO3PR has been cross-validated with other ozone profiles in a study of [25, M. Kroon et al., 2011] and therefore an ozone effective temperature can be accurately determined with an ozone profile from OMO3PR and a temperature profile from ECMWF. This effective temperature can be used as a reference effective temperature, to validate the OMDOAO3 effective temperature, and to estimate temperature sensitivities of OMI ozone products.

For OMDOAO3 the effective temperature is fitted from the spectrum itself and the effect on the ozone column amount, is part of the further sections. It has theoretically been shown that the slant column amount is not sensitive to changes in effective temperature, which confirms that the DOAS concept is theoretically insensitive to temperature variations. However, the implementation of the cross sections may induce a temperature dependency on the vertical ozone column amount.

For OMTO3, the temperature profiles are used inconsistently with the ozone profiles. The TOMS v8 climatology for temperature profiles depends on month and latitude and therefore errors in temperature depending on latitude or season are not expected. However, other variations in temperature are not captured by the climatology, which are: stratospheric climate change, volcanic eruptions and longitudinal temperature variations.

Balloon borne ozone sondes have been considered to validate the OMI ozone products. However, it turns out that the calculated quantities for ozone column amount and effective ozone temperature are depending on bursting height. Therefore spurious results can be expected if a comparison would be done to validate the OMI ozone products.

It can be concluded that the essential ozone products have been identified to validate the DOAS effective temperature and to determine the temperature sensitivities of OMI ozone products. It the next section the definition of the effective ozone temperature will be investigated in detail. In the sections thereafter ozone products are compared for the year 2005 and in the last chapter improvements for the DOAS method are investigated.

	Temp. sens. [% / K] Theoretical	Errors of temperature dependency of ozone column amount in					
		latitude	season	long-itude	climate	volcanic erup-tions	cross sec-tions
Dobson Brewer	0.125 ± 0.021 0.014 ± 0.003	x	x	x	x	x	x
OMDOAO3 OMTO3 OMO3PR	-0.011 ± 0.002 0.175 ± 0.025 $\sim 0.2\%/\mathrm{K}$	?	?	? x	? x	? x	? ? ?

Table 5: Overview of theoretically estimated temperature sensitivities in this section and errors in temperature dependencies for different ozone products.

2. Ozone effective temperature and ozone temperature spread

In this section definitions of the ozone effective temperature and ozone temperature spread are derived, given the Lambert-Beer law and ozone cross absorption cross sections. The ozone absorption cross sections - which are a critical input to remote sensing retrievals - are dependent on temperature. Before further analysis of the temperature sensitivity of OMI ozone products, first the definitions of ozone effective temperature and ozone temperature spread are introduced. These definitions are essential for the understanding of ozone retrievals and validation studies.

The ozone effective temperature is the average temperature along the average ozone path, and ozone temperature spread is the spread in temperature along the average ozone path. An average ozone path is the average photon path from the sun through the atmosphere and then scattered or reflected by the surface, back through the atmosphere to the satellite detector, that in calculations is expressed an altitude resolved air mass factor. The altitude resolved air mass factor is the average path-lengthening factor, compared to the vertical, for each altitude in the atmosphere and can be calculated with a radiative transfer model. The definitions for ozone effective temperature and ozone temperature spread can be derived by considering the relation between the measured temperature in a controlled laboratory environment, and the reappearance of temperature terms in ozone optical depth. Once the definitions are written down, a simplification can be made to these definition to reduce calculation time. A distinction is made between slant and vertical definitions. For slant definitions the altitude resolved air mass factor is included, accounting for scattering along the ozone path and/or obscuration through clouds. For large data sets, e.g. for a year, the computational cost of calculating the air mass factor profile is too high and in those calculations the altitude resolved air mass factor is neglected. This simplification leads to the vertical definitions. Differences between the two definitions are estimated with calculations from a radiative transfer model as function of the relevant parameters of an ozone retrieval.

2.1. Definitions and observations

In experimental studies [8, 7, 10], it is suggested that the high resolution lab cross sections can be approximated by a second degree polynomial within an error of 1%:

$$\sigma(\lambda,T) = a_0(\lambda) + a_1(\lambda)T + a_2(\lambda)T^2 \tag{12}$$

In subsection 1.2.1, we have seen that the convolution of cross sections is not temperature dependent, and this second degree polynomial relation can also be used for the convoluted cross-sections. Hence the use of convoluted cross sections or lab cross sections is irrelevant for this chapter and therefore we will make no distinction.

The Lambert-Beer law states that for an infinitesimal small non-scattering layer dl, the amount of absorption is equal to

$$dI = -I(\lambda)\sigma(\lambda,T)n(l)dl$$

, from which follows:

$$d\ln I = -\sigma(\lambda,T)n(l)dl$$

Integration over an ozone path and taking the exponent on both side leads to:

$$\frac{I(\lambda)}{F(\lambda)} = \exp - \int \sigma(\lambda,T)n(l)dl$$

where I is the measured radiance at the detector, and F the extraterrestrial solar irradiance. This leads to the definition of the ozone slant optical depth, which can be written as a vertical integral by taking the average over many ozone paths:

$$\tau_s(\lambda) = \overline{\int \sigma(\lambda,T)n(l)dl} = \int n(z)m(\lambda,z)\sigma(\lambda,T)dz \qquad \frac{I(\lambda)}{F(\lambda)} = \exp -\tau(\lambda)$$

Here $n(z)$ is the vertical ozone profile, $m(\lambda,z)$ the altitude resolved air mass factor, which accounts for the different between a vertical light path and the actual light path. The air mass factor therefore accounts for geometry, scattering, clouds, surface albedo and aerosols. And $\sigma(\lambda,T)$ is the temperature and wavelength dependent ozone absorption cross-section.

We can now derive definitions for slant column amount N_s, effective temperature T_{eff}, and effective (temperature squared) $(T)^2_{\text{eff}}$:

$$\begin{aligned}
\tau(\lambda) = & \int n(z)m(\lambda,z)\left[a_0 + a_1 T + a_2 T^2\right] dz && (13)\\
= & N_s a_0 + N_s a_1 \frac{\int n(z)m(\lambda,z)T dz}{N_s} + N_s a_2 \frac{\int n(z)m(\lambda,z)T^2 dz}{N_s} && (14)\\
= & N_s\left[a_0 + a_1 T_{\text{eff}} + a_2 (T^2)_{\text{eff}}\right] && (15)
\end{aligned}$$

Here the definitions for N_s, T_{eff} and $(T)^2_{\text{eff}}$ are:

$$\begin{aligned}
N_s = & \int n(z)m(\lambda,z)dz && (16)\\
T_{\text{eff}} = & \int n(z)m(\lambda,z)T(z)dz \Big/ \int n(z)m(\lambda,z)dz && (17)\\
(T^2)_{\text{eff}} = & \int n(z)m(\lambda,z)T(z)^2 dz \Big/ \int n(z)m(\lambda,z)dz && (18)
\end{aligned}$$

The slant optical depth can be written as:

$$\tau_s(\lambda) = N_s\left[a_0 + a_1 T_{\text{eff}} + a_2\left((T_{\text{eff}})^2 + T^2_{\text{spread}}\right)\right] \qquad (19)$$

$$\text{with } T^2_{\text{spread}} \equiv \text{Var}(T)_{\text{eff}} = (T^2)_{\text{eff}} - (T_{\text{eff}})^2 = \frac{\int n(z)m(\lambda,z)\left[T(z) - T_{\text{eff}}\right]^2 dz}{\int n(z)m(\lambda,z)dz} \qquad (20)$$

Note that relations that were used to obtain these quantities in equation 20, are nothing else than standard rules for calculating the standard deviation and variance of a normal distribution, which can for example be found in [27, John A. Rice, 2007] as $\text{Var}(X) = E(X^2) - [E(X)]^2$. Finally we have written the optical depth τ in formula 19 with variables that are easy to interpret. The slant column amount N_s, which is the ozone amount along the average ozone path; effective temperature T_{eff}, which is the average temperature along the average ozone path and temperature spread T_{spread} which is the standard deviation in temperature along the average ozone path. In this study, we will use these three variables, to calculate the optical depth.

A global occurrence histogram of the ozone effective temperature and temperature spread is plotted in figure 26, where ozone profiles and temperatures profiles from OMO3PR (OMI ozone profile product) and ECMWF (temperature profile from a medium weather forecasting model) have been multiplied, see equation 17. The air mass factor profile is neglected in these calculations, because of the high computational effort. The effect of including or excluding the air mass factor will be discussed in further subsections. The average value of vertical ozone effective temperature for 2005, determined with the profile product and ECMWF temperature

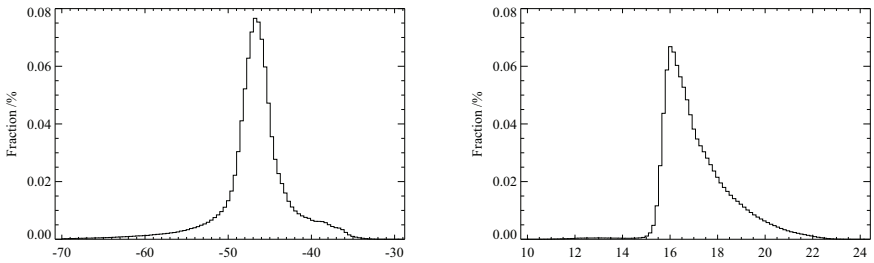

(a) $T_{\text{eff}}(^{\circ}\text{C})$ (b) $T_{\text{spread}}(^{\circ}\text{C})$

Figure 26: Occurrence histogram of the effective temperature [°C], determined with OMI ozone profile product and ECMWF temperature profiles. Data from 2005 is used, and is scaled to produce an equal area histogram. The air mass factor profile is neglected.

profile, is -46.6° C, and is in the range $[-70,-35]^{\circ}$ C. The average value of vertical ozone temperature spread, determined with the profile product and ECMWF temperature profile, is 17.3° C, and is in the range $[11,23]^{\circ}$ C. In figures 27 and 28, global pictures are shown for effective ozone temperature and ozone temperature spread for 2005-10-08. In these pictures it can be seen that the longitudinal variations are much larger in ozone effective temperature and ozone temperature spread toward the higher latitudes.

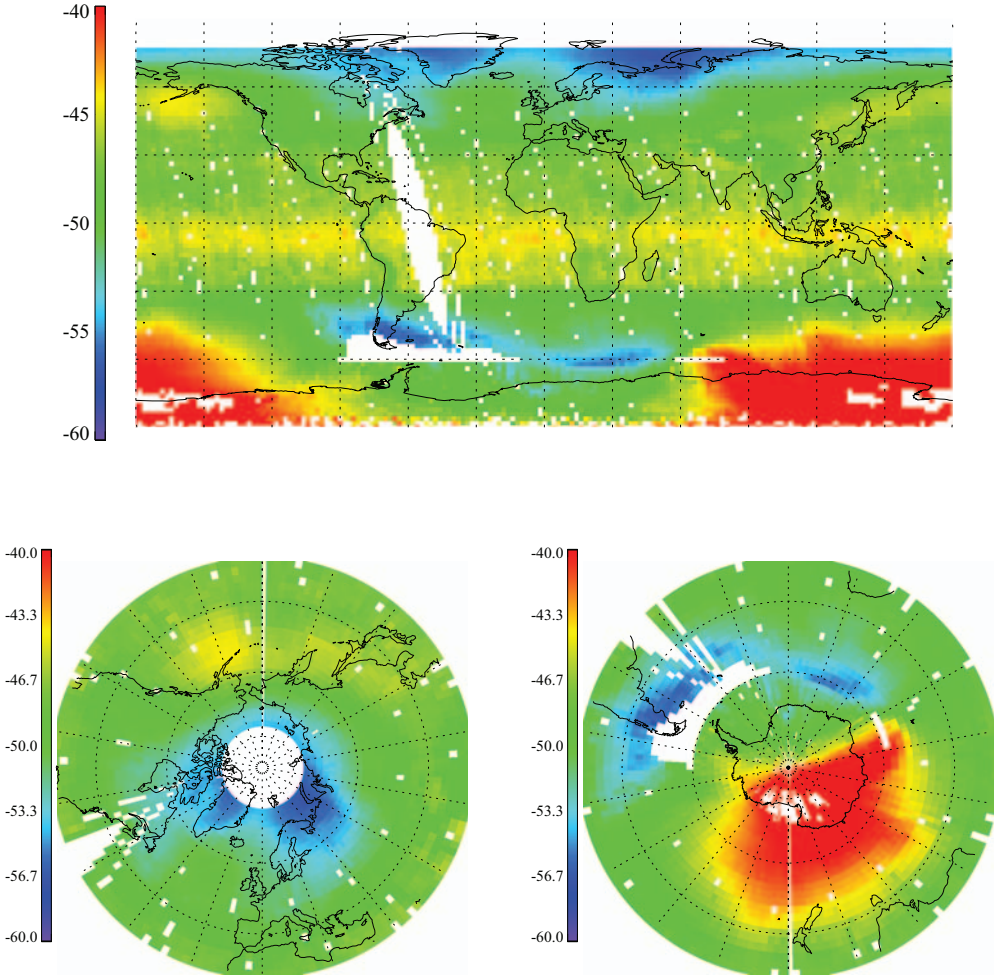

Figure 27: Global distribution of effective ozone temperature [°C] on 2005-10-08 (top) and polar detail plots (bottom). Values are determined with OMI ozone profile product and ECMWF temperature profiles. The air mass factor profile is neglected.

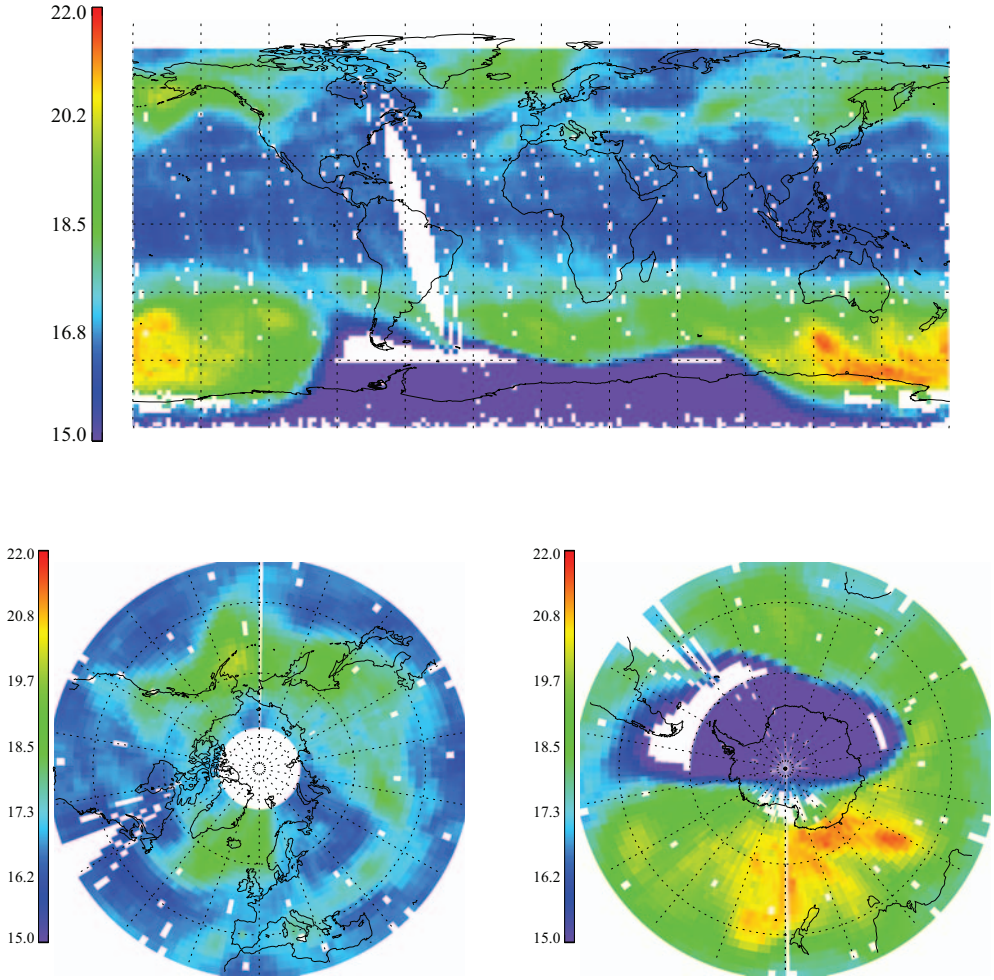

Figure 28: Global distribution of the ozone temperature spread [°C] on 2005-10-08 (top) and polar detail plots (bottom). Values are determined with OMI ozone profile product and ECMWF temperature profiles. The air mass factor profile is neglected.

2.2. Slant and vertical effective ozone temperature

The computational effort of calculating the altitude resolved air mass factor $m(z)$ with a radiative transfer model is high, about 2.5 s per pixel. In calculations with large data sets, the altitude resolved air mass factor is neglected and therefore the effect of this simplification is considered. The two definitions for effective temperature are referred to as slant ($m(z)$ included) and vertical ($m(z)$ excluded) effective temperature:

$$T_{\text{eff},s} = \frac{\int m(z)n(z)T(z)dz}{\int m(z)n(z)dz} \qquad T_{\text{eff},v} = \frac{\int n(z)T(z)dz}{\int n(z)dz} \tag{21}$$

With a radiative transfer model, DISAMAR (Determining Instrument Specifications and Analyzing Methods for Atmospheric Retrieval)[24], the difference between these two definitions is estimated. The results are shown in figure 29 (30) for a clear (cloudy) pixel. An overview of parameters with the largest influence is shown in table 6. From these simulations we can estimate that the air mass factor can cause an offset of -4 to 0 °C. The parameter with the largest influence is the Lambertian cloud pressure, which can cause an offset of -4 °C for a tropical ozone profile. This is mainly caused by the obscuration of the lower extent of the atmosphere. Parameters that have an influence to a lesser extent are surface albedo, Lambertian cloud albedo, ozone profile and solar zenith angle. These parameters influence the vertical temperature weighting, either via the ozone profile or scattering throughout the atmosphere.

parameter	Estimate for offset $T_{\text{eff},s} - T_{\text{eff},v}$ [K]
Lambertian cloud pressure	[-4, 0]
surface albedo	[-2 ,0]
Lambertian cloud albedo	[-2, 0]
ozone profile	[-1, 0]
solar zenith angle	[-1 , +0.5]

Table 6: Estimates for differences in ozone effective temperature, due to including the air mass factor.

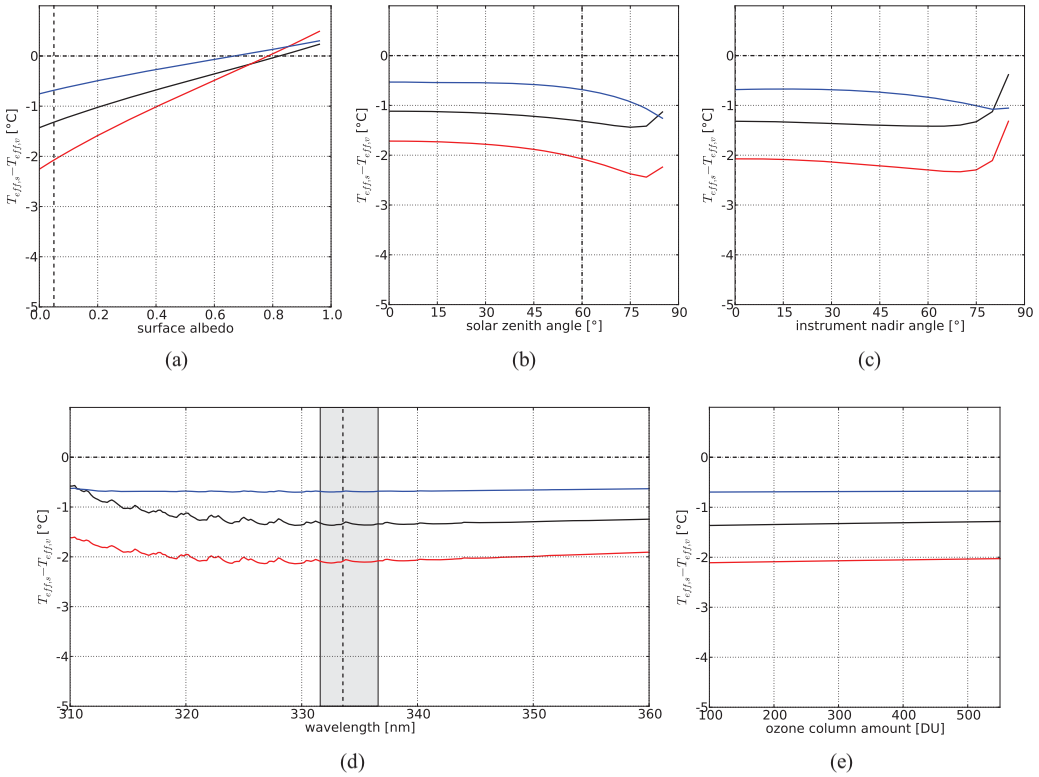

Figure 29: Difference between slant and vertical effective temperature for a clear pixel as function of (a) surface albedo, (b) solar zenith angle, (c) instrument nadir angle, (d) wavelength and (e) ozone column amount. For the slant effective temperature the air mass factor is included in the integral and for the vertical effective temperature not, see equation 21. U.S. Standard Atmospheric ozone and temperature profiles[26] have been used to calculate the effective temperatures for subarctic winter (blue), standard mid latitude (black) and tropics (red). Default parameters are: 1. instrument looking at nadir angle, 2. solar zenith angle of 60 degrees, 3. wavelength 333.56 nm, 4. surface albedo of 0.05. and 5. relative azimuthal angle of 180 degrees. Vertical striped lines indicate the default parameters.

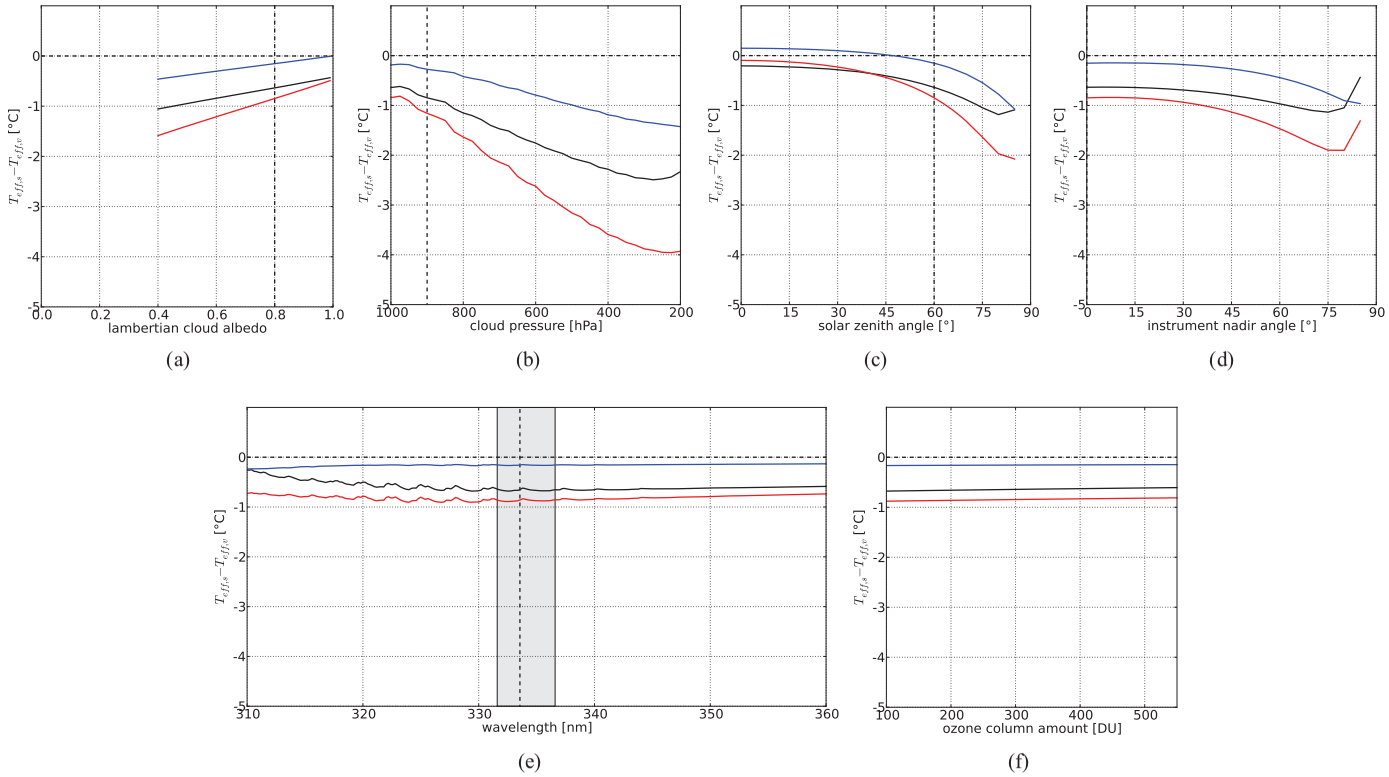

Figure 30: Difference between slant and vertical effective temperature for a cloudy pixel as function of (a) Lambertian cloud albedo, (a) cloud pressure, (c) solar zenith angle, (d) instrument nadir angle, (e) wavelength and (f) ozone column amount. For the slant effective temperature the air mass factor is included in the integral and for the vertical effective temperature not, see equation 21. A Lambertian cloud is placed at the cloud pressure. U.S. Standard Atmospheric ozone and temperature profiles[26] have been used to calculate the effective temperatures for subarctic winter (blue), standard mid latitude (black) and tropics (red). Default parameters are: 1. instrument looking at nadir angle, 2. solar zenith angle of 60 degrees, 3. wavelength 333.56 nm, 4. cloud albedo of 0.8, 5. cloud pressure of 900 hPa and 6. relative azimuthal angle of 180 degrees. Vertical striped lines indicate the default parameters.

2.3. Slant and vertical ozone temperature spread

For completeness, also the difference between ozone temperature spread with and without air mass factor profile is considered. The two definitions for ozone temperature spread are referred to as slant ($m(z)$ included) and vertical ($m(z)$ excluded) ozone temperature spread:

$$T_{\text{spread},s} = \sqrt{\frac{\int n(z)m(\lambda,z)(T(z)-T_{\text{eff}})^2 dz}{\int n(z)m(\lambda,z)dz}} \qquad T_{\text{spread},v} = \sqrt{\frac{\int n(z)(T(z)-T_{\text{eff}})^2 dz}{\int n(z)dz}} \tag{22}$$

With a radiative transfer model, DISAMAR (Determining Instrument Specifications and Analyzing Methods for Atmospheric Retrieval)[24], the difference between the two definitions is estimated. The results are shown in figure 31 (32) for a clear (cloudy) pixel. An overview of parameters with the largest influence is shown in table 7. From these simulations we can estimate that the air mass factor can cause an offset of [-5, +1] °C. The parameter with the largest influence is the Lambertian cloud pressure, that can cause an offset of -5 °C. This is mainly caused by the obscuration of the lower extent of the atmosphere. Parameters that have an influence to a lesser extent are surface albedo, Lambertian cloud albedo, ozone profile and solar zenith angle. These parameters influence the vertical temperature weighting, either via the ozone profile or scattering throughout the atmosphere.

parameter	Estimate for offset $T_{\text{spread},s} - T_{\text{spread},v}$ [K]
Lambertian cloud pressure	[-1, -5]
surface albedo	[-3, +1]
Lambertian cloud albedo	[-2 , -1]
solar zenith angle	[-1, -4]
ozone profile	[-1, -2]

Table 7: Estimates for differences in ozone temperature spread, due to including the air mass factor.

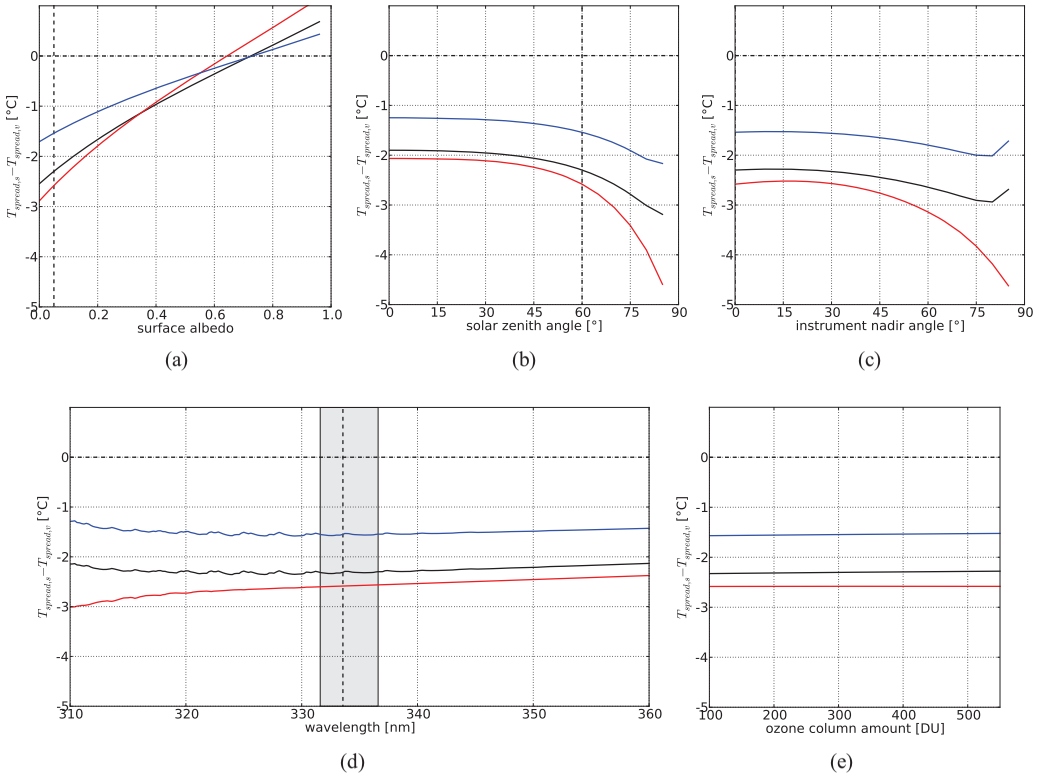

Figure 31: Difference between slant and vertical temperature spread for a clear pixel as function of (a) surface albedo, (b) solar zenith angle, (c) instrument nadir angle, (d) wavelength and (e) ozone column amount. For the slant temperature spread the air mass factor is included in the integral and for the vertical temperature spread not, see equation 22. U.S. Standard Atmospheric ozone and temperature profiles[26] have been used to calculate the temperature spreads for subarctic winter (blue), standard mid latitude (black) and tropics (red). Default parameters are: 1. instrument looking at nadir angle, 2. solar zenith angle of 60 degrees, 3. wavelength 333.56 nm, 4. surface albedo of 0.05. and 5. relative azimuthal angle of 180 degrees. Vertical striped lines indicate the default parameters.

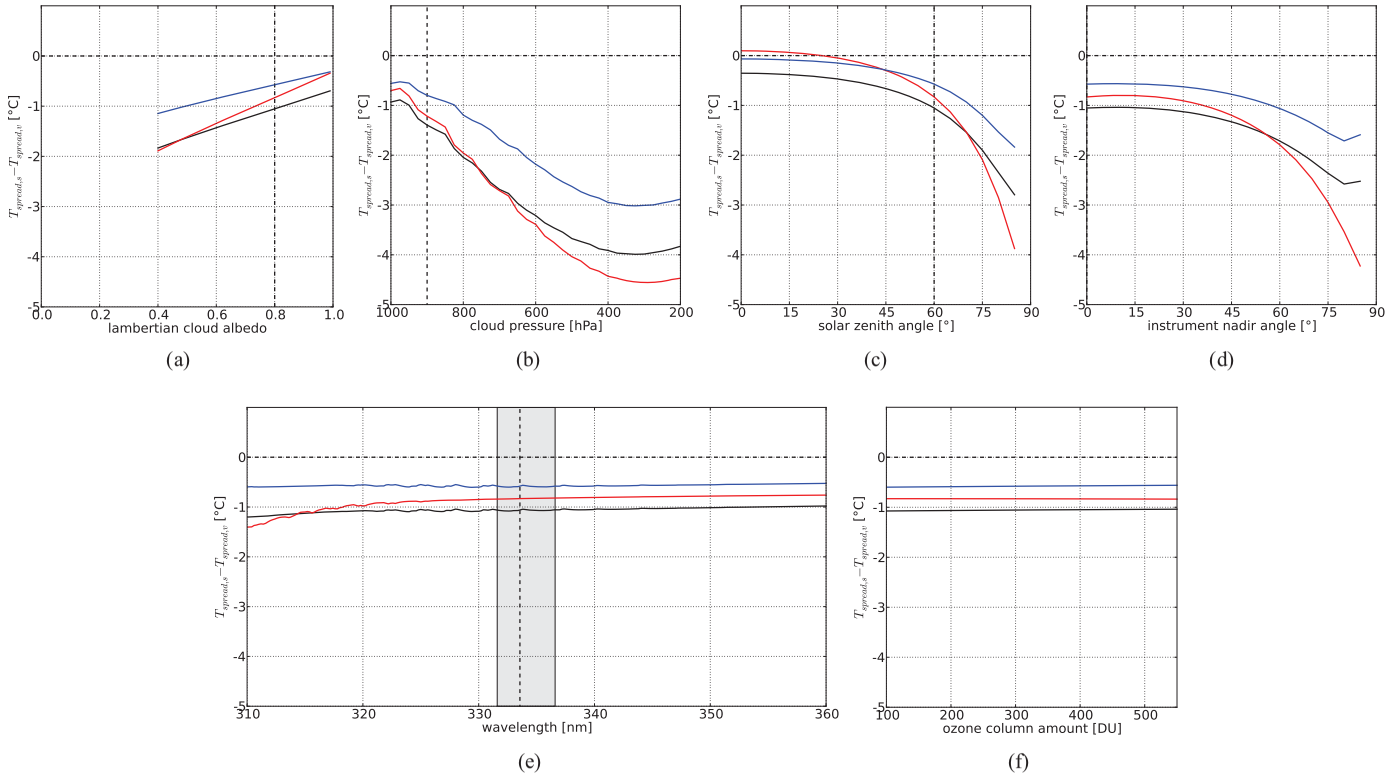

Figure 32: Difference between slant and vertical temperature spread for a cloudy pixel as function of (a) Lambertian cloud albedo, (a) cloud pressure, (c) solar zenith angle, (d) instrument nadir angle, (e) wavelength and (f) ozone column amount. For the slant temperature spread the air mass factor is included in the integral and for the vertical temperature spread not, see equation 22. A Lambertian cloud is placed at the cloud pressure. U.S. Standard Atmospheric ozone and temperature profiles[26] have been used to calculate the temperature spreads for subarctic winter (blue), standard mid latitude (black) and tropics (red). Default parameters are: 1. instrument looking at nadir angle, 2. solar zenith angle of 60 degrees, 3. wavelength 333.56 nm, 4. cloud albedo of 0.8, 5. cloud pressure of 900 hPa and 6. relative azimuthal angle of 180 degrees. Vertical striped lines indicate the default parameters.

2.4. Conclusions

Definitions for the ozone effective temperature and ozone temperature spread have been derived, given the Lambert-Beer law. A distinction is made between vertical and slant definitions, where for the slant definitions the altitude resolved air mass factor is included. For large data sets the, e.g. a year the vertical definitions are used because of the high computational cost to calculate the altitude resolved air mass factor. The relevant parameters for an ozone retrieval that cause a difference with respect to the vertical effective ozone temperature are Lambertian cloud pressure, surface albedo, Lambertian cloud albedo, solar zenith angle and ozone profile. The Lambertian cloud pressure can cause a difference of up to four degrees when the air mass factor is included which is caused by the obscuration of the lower extent of the atmosphere. The other parameters can cause differences of several degrees, that is there due to the vertical temperature weighting via the ozone profile, or scattering throughout the atmosphere. The same parameters have an influence on ozone temperature spread, with approximately the same order of magnitude. The influence of these additional parameters on the effective ozone temperature, underline that a temperature correction, for an ozone product that is sensitive to temperature variations, is not straightforward. A linear temperature correction, which is applied in a study of [4, R. J. van der A et al., 2010] , is neglecting the influence of these additional parameters. When the OMDOAO3 fitted effective temperature, which in principle should equal the slant effective temperature, is compared to the OMO3PR vertical effective temperature, determined with OMO3PR ozone profile and ECMWF temperature profile, the difference is expected to dependent on these parameters.

3. Cross validation of ozone column amount and effective temperature for OMI.

The goal of this chapter is to determine whether the OMI ozone products are sensitive to temperature changes by doing an intercomparison of the OMI ozone products. The three OMI algorithms obtain ozone column amounts and effective temperature all in their own way and use different parts of the UV spectrum, see section 1. OMTO3 uses only two wavelengths in the UV2, OMDOAO3 uses a 5 nm band in the UV2 and OMO3PR uses bands both from UV1 and UV2 to determine an ozone profile. Also the effective temperature is obtained differently in these algorithms. OMTO3 uses the TOMS v8 climatology for ozone, where interpolated temperature profiles are used from a look-up table, with month and latitude as axes. OMDOAO3 fits the effective temperature from the spectrum itself, and OMO3PR uses a temperature profile from a medium-range weather-forecasting model (ECMWF). These choices have advantages and disadvantage for the resulting ozone column amounts. With an inter comparison of all products, we can estimate the order of magnitude for the temperature sensitivities of the products.

In this section first the methods are described how the gridded column amounts, gridded effective temperatures and their gridded differences are obtained. Secondly comparisons are done for ozone column amount, effective temperature and temperature sensitivity respectively. The order of magnitude is estimated for the temperature sensitivity of all OMI ozone products.

3.1. Methods

Column amounts and effective temperatures from OMDOAO3, OMTO3 and OMO3PR are gridded on a $3^\circ \times 2^\circ$ (longitude $\times$ latitude) grid. 14 orbits ($\sim$1 day) are used for each grid that cover about one day, such that ground pixels with a time leap of one day are not overlapping. Only pixels that satisfy quality criteria, as specified in the readme files[28, 29, 30] of the products, are used. Additionally only pixels for which solar zenith angles are smaller than 85° are used. For OMO3PR pixels are skipped if the number of iterations is maximal (20) or if the reflectance-cost-function, a quality measure of the fit, is smaller than 10. Pixels are only used if they are recommended for all three products. Because OMO3PR skips 4/5 ground pixel in the flight-direction, this is also done for OMDOAO3 and OMTO3. Because the cross-track resolution of OMDOAO3 and OMTO3 is twice that of OMO3PR, half the ground pixels are skipped in the cross-track direction for OMDOAO3 and OMTO3. An overview of the versions that are used can be found in table 8.

Product	PGEVersion	Source
OMDOAO3	1.2.3.1	`http://avdc.gsfc.nasa.gov/`
OMO3PR	1.1.0	`http://avdc.gsfc.nasa.gov/`
OMTO3	1.1.2.3	`http://avdc.gsfc.nasa.gov/`

Table 8: Overview of versions and sources that are used in this study.

Gridding, which in principle is taking the average over a grid cell, is done for ozone column amount, effective temperature and their differences for all three OMI ozone products. For differences, first the differences are calculated and after that the average is calculated.

The effective temperature is only directly present in OMDOAO3, which is the fitted effective temperature in the ozone retrieval. For the other two products it has to be calculated. For OMO3PR it is obtained by multiplying the ozone and temperature profile, and hence that the vertical effective temperature is used:

$$T_{\text{eff,OMO3PR}} = \int n_{\text{OMO3PR}}(z) T_{\text{ECMWF}}(z) dz \Big/ \int n_{\text{OMO3PR}}(z) dz$$

Here $n(z)$ is the vertical ozone profile from OMO3PR and $T(z)$ is the vertical temperature profile from a medium-range weather-forecasting model (ECMWF). For the OMTO3 product, the effective temperature is obtained from interpolation from a new look-up table, with month, ozone column amount and latitude as axes. The look-up table can be generated from the existing look up tables for ozone profiles and temperature profiles. The effective temperature for the TOMS V8 climatology is then calculated as:

$$T_{\text{eff,TOMS}}(\text{month}, \text{lat}, \Omega) = \int n_{\text{LUT}}(z) T_{\text{LUT}}(z) dz \Big/ \int n_{\text{LUT}}(z) dz$$

Here $n(z)$ is the ozone profile and $T(z)$ the temperature profile, both from the TOMS v8 climatology, with month, latitude and vertical ozone column amount Ω as axes.

Typical daily values for ozone column amount and effective temperature on 2005-10-08 can be seen in figure 33 and 34. Qualitatively, the ozone column amounts are very similar in these figures. For the effective temperature, qualitative differences can directly be seen from such a figure. For OMTO3, the longitudinal variations in effective temperature are wrong if we compare it to the effective temperature from OMO3PR or OMDOAO3. The most clear example is the difference in the T_{eff} inside and outside the ozone hole. This is not a surprise because the longitudinal variations are not present in a climatology.

For OMDOAO3 the fitted slant ozone effective temperature is plotted. In first instance we may compare the OMDOAO3 fitted effective temperature with the vertical effective temperature of OMTO3 and OMO3PR, although small dependencies on clouds and geometry are expected, see section 2. Qualitatively the OMDOAO3 fitted effective temperature is very similar to the one of OMO3PR, without having spurious spots for low cloud pressure in the ITCZ. The effective temperature from OMDOAO3 however contains some orbital features, which are most clear for the lower latitudes ($< 30\ ^\circ$) in figure (a).

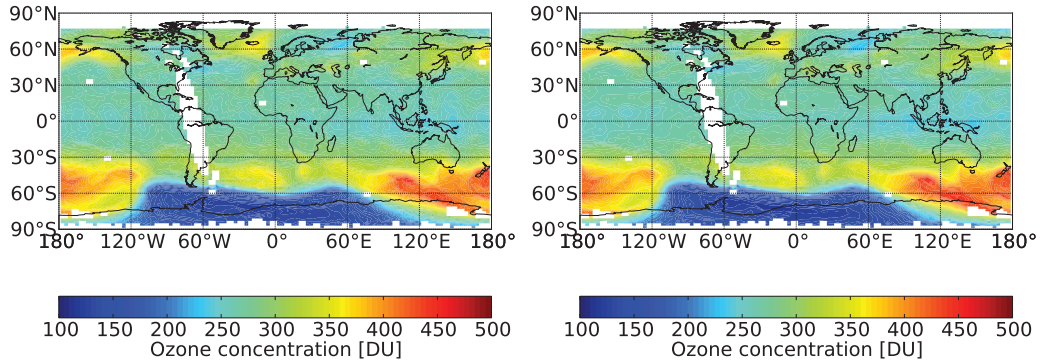

(a) OMDOAO3

(b) OMTO3

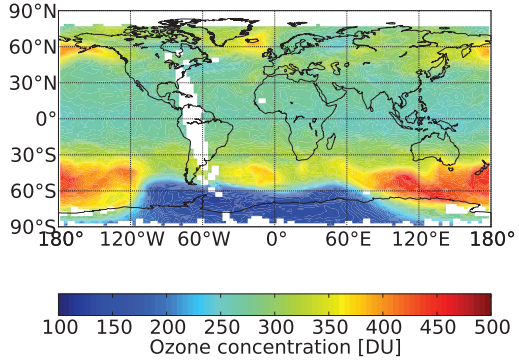

(c) OMO3PR

Figure 33: World plot of typical daily values for gridded ozone column amount on 2005-10-08 for (a) OMDOAO3, (b) OMTO3 and (c) OMO3PR.

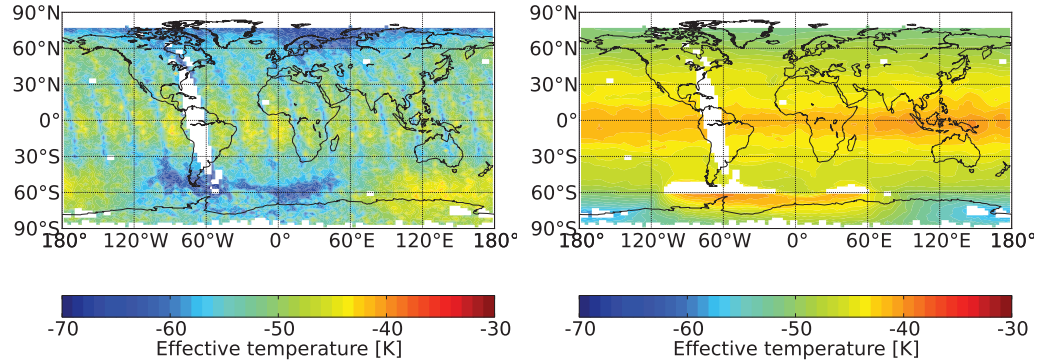

(a) OMDOAO3

(b) OMTO3

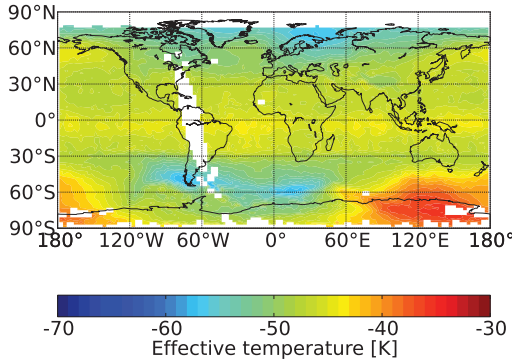

(c) OMO3PR

Figure 34: World plot of typical daily values for gridded effective temperature on 2005-10-08 for (a) OMDOAO3, (b) OMTO3 and (c) OMO3PR.

3.2. Results

3.2.1. Ozone column amount

Correlations are calculated and linear fits are applied for gridded column amounts of OMI ozone products for 2005. An overview of the results is shown in table 9. Scatter density plots can be seen in figure 35. The ozone column amounts for all three products are very similar. The correlations are 1.00 or 0.99 when gridded column amounts are compared. The offset between OMDOAO3 and OMTO3 is smaller than two Dobson Units, which is less than 1% of a 300 DU ozone column. The offset between OMO3PR and OMDOAO3/OMTO3 is about 12 Dobson Units, which is about 4% of a 300 DU ozone column. This difference may be there because a different a priori climatology is used in the radiative transfer calculations. For both OMTO3 and OMDOAO3 the TOMS v8 climatology is used, but for OMO3PR the a priori climatology is used is from Logan, Labow and McPeters. This can result in an offset in the differences, as the ozone column amounts above the clouds are compared for OMO3PR.

	corr.	slope	offset [DU]
OMDOAO3-OMTO3	1.00	0.98 ± 0.00	1.61 ± 0.20
OMDOAO3-OMO3PR	0.99	0.93 ± 0.00	-11.89 ± 0.31
OMTO3-OMO3PR	0.99	0.94 ± 0.00	-12.36 ± 0.06

Table 9: Global slopes and offsets from a linear fit and correlations for ozone column amount for gridded data of 2005. The offset is taken at 300 DU. The uncertainty is estimated as the standard deviation of values of southern and northern hemisphere.

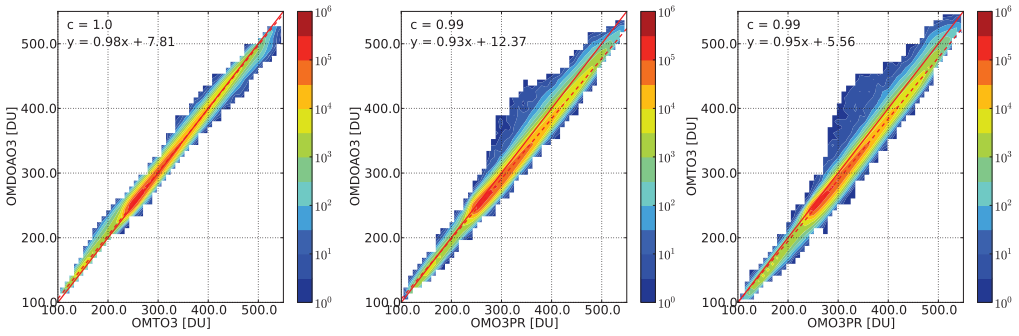

(a) OMDOAO3-OMTO3 (b) OMDOAO3-OMO3PR (c) OMTO3-OMO3PR

Figure 35: Scatter density plots of gridded ozone column amounts for OMI ozone products. Date is used from 2005. Linear fits are drawn as red striped lines.

3.2.2. Effective temperature

Correlations are calculated and linear fits are applied for gridded effective temperatures of OMI ozone products for 2005. An overview of the results is shown in table 10. Scatter density plots can be seen in figure 36. There is an overall good correlation, varying from 0.71 to 0.85, for gridded effective temperatures of OMI ozone products. Hence that the use of climatological temperature profiles for OMTO3 makes sense, and that for OMDOAO3 this can be seen as a confirmation that it is possible to retrieve an ozone effective temperature from a spectrum. The best results, correlation of 0.85 and slope of 0.97, are obtained for the comparison between the OMDOAO3 fitted effective temperature and OMO3PR effective temperature. This makes sense, because both OMDOAO3 and OMO3PR capture the longitudinal variations in effective temperature, which the OMTO3 algorithm lacks. Typical is that OMTO3 has an effective temperature that is on average 3 °C higher than OMO3PR. This may be a consequence of an outdated climatology, as stratospheric temperatures have decreased during the last years (see introduction). The OMDOAO3 fitted effective temperature is on average 5.82°C lower than that of OMO3PR. This difference is consistent for different seasons and regions, which can be seen in table 11. The evolution of the OMDOAO3 fitted effective temperature is also very consistent with the effective temperature obtained with OMO3PR, which can be seen in figure 37. The reason for this difference will be discussed in the next chapter. However, as the difference is consistent for different regions and seasons, the potential of fitting the effective ozone temperature from a spectra is shown with this analysis.

	corr.	slope	offset [K]
OMDOAO3-OMTO3	0.71	0.87 ± 0.11	-7.41 ± 1.02
OMDOAO3-OMO3PR	0.85	0.97 ± 0.02	-5.82 ± 0.04
OMTO3-OMO3PR	0.80	0.74 ± 0.02	3.02 ± 0.40

Table 10: Global slopes and offsets from a linear fit and correlations for effective temperature for gridded data of 2005. The offset is taken at $-50°C$. The uncertainty is estimated as the standard deviation of values of southern and northern hemisphere.

	tropics	mid latitudes	polar regions	global
winter	-5.83 ± 0.05	-5.82 ± 0.31	-5.77 ± 0.24	-5.84 ± 0.18
spring	-5.86 ± 0.53	-5.75 ± 0.45	-5.86 ± 0.57	-5.81 ± 0.48
summer	-5.82 ± 0.04	-5.50 ± 0.02	-5.70 ± 0.23	-5.66 ± 0.06
autumn	-5.94 ± 0.43	-5.79 ± 0.56	-5.67 ± 0.60	-5.85 ± 0.50
2005	-5.87 ± 0.02	-5.78 ± 0.14	-5.82 ± 0.23	-5.82 ± 0.04

Table 11: Offsets from a linear fit in effective temperature for OMDOAO3-OMO3PR for different regions and seasons for gridded data of 2005. The offset is taken at $-50°C$. The uncertainty is estimated as the standard deviation of values of southern and northern hemisphere.

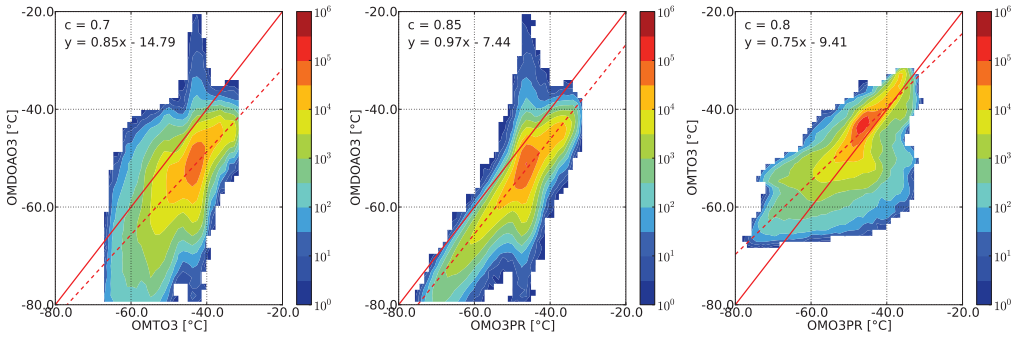

(a) OMDOAO3-OMTO3 (b) OMDOAO3-OMO3PR (c) OMTO3-OMO3PR

Figure 36: Scatter density plots of gridded effective temperature for OMI ozone products. The air mass factor profile is neglected for the effective temperature of OMO3PR and OMTO3, see methods for details. Data is used from 2005. Linear fits are drawn as red striped lines.

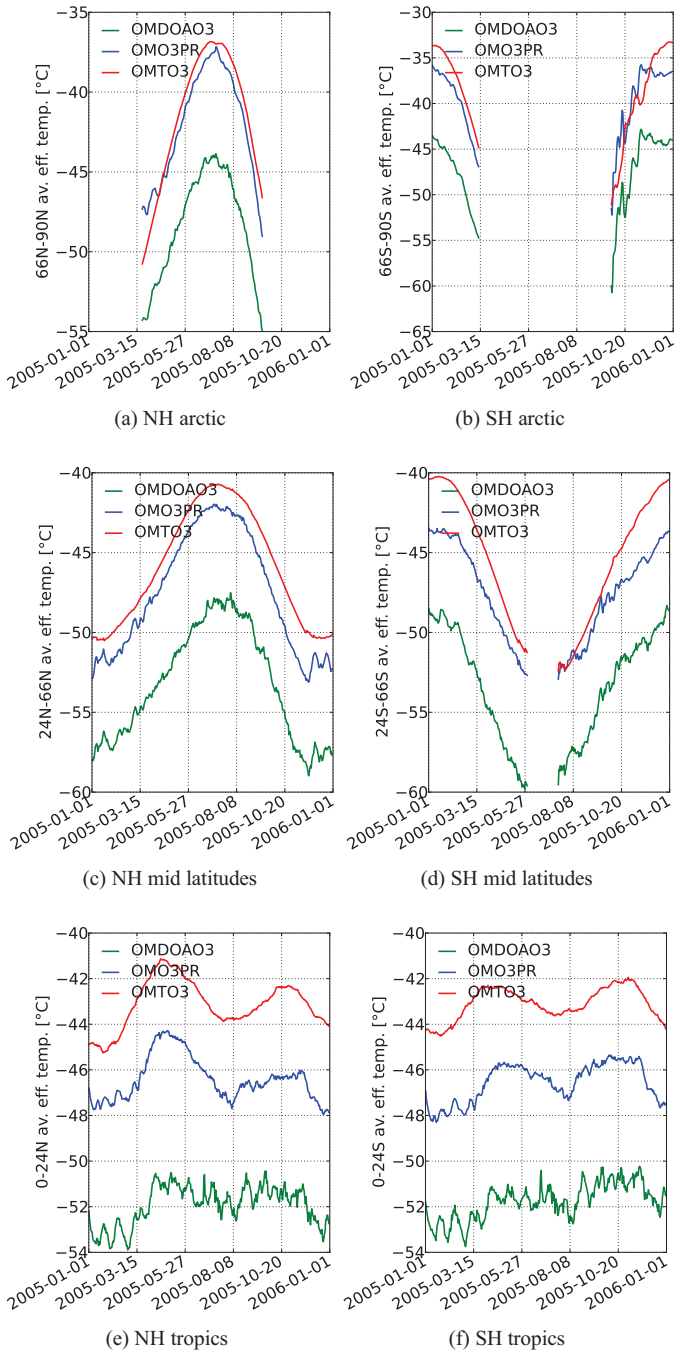

(a) NH arctic (b) SH arctic

(c) NH mid latitudes (d) SH mid latitudes

(e) NH tropics (f) SH tropics

Figure 37: (a) - (f) Evolution of the average effective temperature for OMI ozone products for different regions in 2005. The air mass factor profile is neglected for the effective temperature of OMO3PR and OMTO3, see methods for details. For OMDOAO3 the effective temperature is fitted from the spectrum.

3.2.3. Temperature sensitivity

Correlations are calculated and linear fits are applied for gridded differences in ozone column amount versus gridded differences in effective temperature of OMI ozone products for 2005. The slope of difference in ozone column amount versus difference in effective temperature is a measure for the temperature sensitivity for one of the two ozone products if one is sensitive to temperature variations and the other ozone product is not sensitive to temperature variations. The slope of difference in ozone column amount versus effective temperature is also a measure for the temperature sensitivity for an ozone product, but for in this case the slant column in the ozone product is over- or underestimated as function of ozone effective temperature.

An overview of the results is shown in table 12. Scatter density plots can be seen in figures 38 and 39. The correlations are relatively weak, varying from 0.04 to 0.33 in magnitude. However, from the scatter density plots, and linear fit, it can be seen that there are relations between the difference in ozone column amount and difference in effective temperature. For the comparison of OMDOAO3 and OMTO3, the slopes are consistent for different seasons and regions, see table 13. The difference in temperature sensitivity, OMDOAO3-OMTO3, is -0.13 ± 0.01 % / K, which is much higher than the threshold value of 0.01 %/K that we derived in the introduction for an ozone product that is insensitive for temperature variations. There is no reason to assume that one OMI ozone product is not sensitive to temperature changes. Therefore the only conclusion that can be drawn from such an analysis is that OMI ozone products have temperature sensitivities on the order of 0.10%/K. which is in agreement of a study of [4, R. J. van der A et al., 2010] (see introduction).

Comparison		Temperature sensitivity	
dO_3/O_3	dT	corr.	slope [%/K]
OMDOAO3-OMTO3	OMTO3-OMDOAO3	0.35	0.13± 0.01
OMDOAO3-OMO3PR	OMO3PR-OMDOAO3	0.08	0.06± 0.00
OMTO3-OMO3PR	OMO3PR-OMTO3	0.09	0.07± 0.04
dO_3/O_3	T	corr.	slope [%/K]
OMDOAO3-OMTO3	OMO3PR	-0.23	-0.07± 0.01
OMDOAO3-OMO3PR	OMO3PR	0.00	0.00± 0.02
OMTO3-OMO3PR	OMO3PR	0.12	0.06± 0.03

Table 12: Global slopes from a linear fit and correlations for difference in ozone column amount vs. difference in effective temperature for gridded data of 2005. The uncertainty is estimated as the standard deviation of values of southern and northern hemisphere.

	tropics	mid latitudes	polar regions	global
winter	0.05± 0.03	0.04± 0.00	0.07± 0.01	0.05± 0.01
spring	0.06± 0.00	0.07± 0.00	0.11± 0.00	0.08± 0.00
summer	0.03± 0.02	0.06± 0.01	0.09± 0.04	0.06± 0.02
autumn	0.06± 0.01	0.05± 0.00	0.11± 0.01	0.06± 0.00
2005	0.06± 0.01	0.06± 0.01	0.10± 0.02	0.06± 0.00

Table 13: Slopes [%/K] from a linear fit for difference in ozone column amount, OMDO3PR-OMDOAS, vs. difference in effective temperature, OMDOAO3-OMO3PR for specific regions and seasons for gridded data of 2005. The uncertainty is estimated as the standard deviation of values of southern and northern hemisphere.

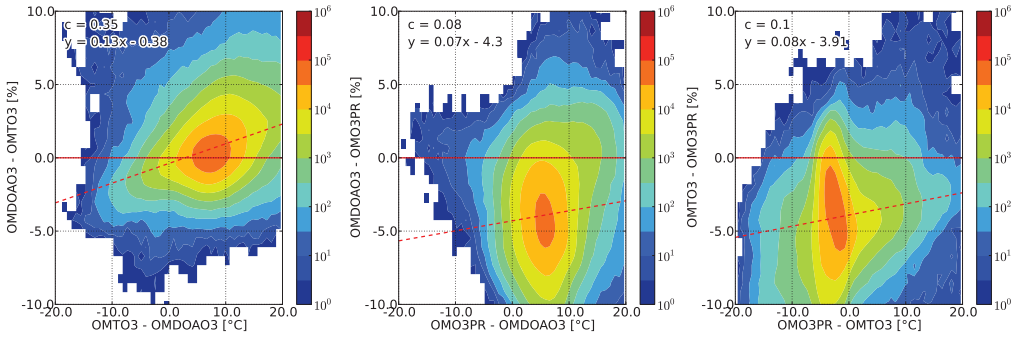

(a) OMDOAO3-OMTO3 (b) OMDOAO3-OMO3PR (c) OMTO3-OMO3PR

Figure 38: Scatter density plots of relative ozone column amount difference plotted against effective temperature difference for OMI ozone products. The air mass factor profile is neglected for the effective temperature of OMO3PR and OMTO3, see methods for details. Data is used from 2005. Linear fits are drawn as red striped lines.

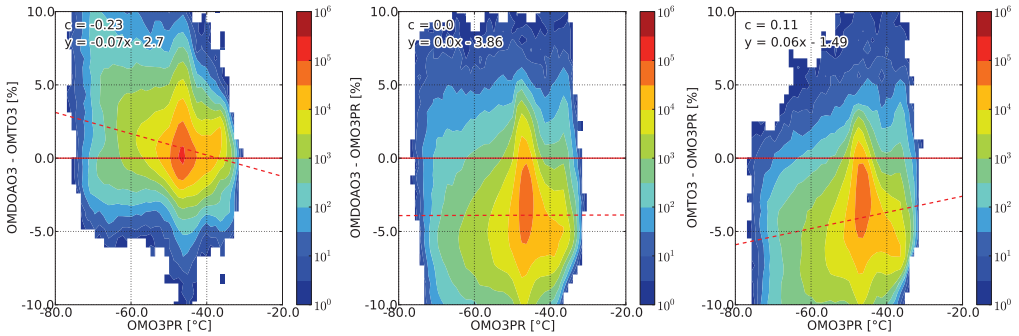

(a) OMDOAO3-OMTO3 (b) OMDOAO3-OMO3PR (c) OMTO3-OMO3PR

Figure 39: Scatter density plots of relative ozone column amount difference against effective temperature from OMO3PR for OMI ozone products. The air mass factor profile is neglected for the effective temperature of OMO3PR and OMTO3, see methods for details. Data is used from 2005. Linear fits are drawn as red striped lines.

3.3. Conclusions

Data from the OMI ozone products from the year 2005 has been gridded and analyzed. Ozone column amounts for the three different OMI ozone products - OMDOAO3, OMTO3 and OMO3PR - are very similar. Correlations for comparison of gridded data for ozone column amount are found of 0.99 or 1.00. The offset between OMDOAO3 and OMTO3 is smaller than two Dobson Units, which is less than 1% of a 300 DU ozone column, which is almost negligible. The offset between OMO3PR and OMDOAO3/OMTO3 is about 12 Dobson Units, which is about 4% of a 300 DU ozone column. A possible explanation for this offset in OMO3PR is the use of a different climatology in the radiative transfer model calculations, but other factors may also be important.

The ozone effective temperature for the ozone products is strongly correlated, but there are differences. OMTO3 uses a climatology for temperature profiles, that does not include temperature changes by: 1. volcanic eruptions, 2. climate change or 3. longitudinal variations. The longitudinal variations can directly be seen from a daily picture of effective temperatures, when it is compared to effective temperatures from OMO3PR or OMDOAO3. OMTO3 has an effective temperature that is 3.02 $\pm$ 0.40 $^{\circ}$C higher than OMO3PR, which may be the consequence of an outdated climatology. The OMDOAO3 fitted effective temperature is on average -5.82 $\pm$ 0.04 $^{\circ}$C lower than that of OMO3PR. This difference is consistent for different seasons and regions, which demonstrates that an ozone effective temperature can be fitted from the radiance spectrum itself.

Difference in ozone column amount are compared against effective temperature or difference in effective temperature. There is no reason to assume that one OMI ozone product is not sensitive to temperature changes. Therefore the only conclusion that can be drawn from such an analysis is that OMI ozone products have temperature sensitivities on the order of 0.10%/K. which is in agreement with a study of [4, R. J. van der A et al., 2010] (see introduction).

4. Validation of OMI ozone products with ground-based observations

The goal of this chapter is to determine whether the OMI ozone products are sensitive to temperature changes by comparing them with ground-based observations. The three OMI algorithms obtain ozone column amounts and effective temperatures all in their own way and use different parts of the UV spectrum, see section 1. OMTO3 uses only two wavelengths in the UV2, OMDOAO3 uses a 5 nm band in the UV2 and OMO3PR use the widest bands both from UV1 and UV2 to determine an ozone profile. Also the effective temperature is obtained differently in these algorithms. OMTO3 uses the TOMS v8 climatology for ozone, where interpolated temperature profiles are used from a look-up table, with month and latitude as axes. OMDOAO3 fits the effective temperature from the spectrum itself, and OMO3PR uses a temperature profile from a medium-range weather-forecasting model (ECMWF). These choices have advantages and disadvantage for the resulting ozone column amounts. In the first section the Brewer direct sun observations have been identified as ozone observations that are not sensitive to temperature variations and therefore they can be used to validate the OMI ozone products and estimate their temperature sensitivities. The effective temperature from the ozone profile product (OMO3PR) in combination with the temperature profile from ECMWF, can be used as a reference effective temperature to estimate the temperature sensitivities of OMI ozone products.

In this section first the methods are described. Secondly OMI ozone column amounts are compared with ground-based measurements and the temperature sensitivities for the OMI ozone products are determined.

4.1. Methods

Column amounts and effective temperatures from OMDOAO3, OMTO3 and OMO3PR have been gridded on a $3^\circ \times 2^\circ$ (longitude $\times$ latitude) grid. The Brewer direct sun and Dobson AD-DSQP observations have been collocated with the OMI ozone products, and artificial satellite files are made. These new "satellite files", wherein the ground-based observations are stored, can be used with the validation toolkit CAMA[31]. Every single Brewer or Dobson observation is used for a grid cell and is compared to the OMI ozone products. Only recommended pixels for the OMI ozone products are used, that are specified in the readme files[28, 29, 30] of the products, and additionally only pixels for which solar zenith angles are smaller than 85°. For OMO3PR pixels are skipped if the number of iterations is maximal (20) or if the reflectance-cost-function, a quality measure of the fit, is smaller than 10. Pixels are only used if they are recommended for all three OMI products. Because OMO3PR skips 4/5 ground pixel in the flight-direction, this is also done for OMDOAO3 and OMTO3. Because the cross-track resolution of OMDOAO3 and OMTO3 is twice that of OMO3PR, also 1/2 ground pixels is skipped in the cross-track direction for OMDOAO3 and OMTO3. An overview of the sources and versions that are used can be found in table 14.

Product	PGEVersion	Source
OMDOAO3	1.2.3.1	`http://avdc.gsfc.nasa.gov/`
OMO3PR	1.1.0	`http://avdc.gsfc.nasa.gov/`
OMTO3	1.1.2.3	`http://avdc.gsfc.nasa.gov/`
Brewer		`http://www.woudc.org/`
Dobson		`http://www.woudc.org/`

Table 14: Overview of versions and sources that are used in this study.

4.2. Results

4.2.1. Ozone column amount

Correlations are calculated and linear fits are applied for the data of 2005 with the CAMA validation toolkit[31]. An overview of the results is shown in table 15. The ozone column amounts from OMI ozone products compare very well with ground-based measurements. The correlations are 0.98 or 0.99. The offsets in ozone column amount are the smallest for the OMDOAO3 ozone product, -.1.80 DU for the Dobson direct sun observations, and -4.09 DU for the Brewer direct sun observations. For OMTO3 and OMO3PR the differences are larger. Typical is that OMTO3 and OMDOAO3 are underestimating the vertical ozone column amount, where OMO3PR is overestimating the vertical ozone when it is compared to the ground-based measurements. The average differences are below 10 DU when OMI ozone products are compared to ground-based measurements, which is 3% of a typical 300 DU vertical ozone column. For OMDOAO3 the average difference is below 4.1 DU, which is about 1% of a typical 300 DU vertical ozone column.

	corr.	slope	offset [DU]
OMDOAO3-Dobson	0.98	0.958	-1.8 $\pm$ 0.1
OMDOAO3-Brewer	0.99	0.97 $\pm$ 0.03	-4.1 $\pm$ 0.6
OMTO3-Dobson	0.98	0.963	-2.1 $\pm$ 0.3
OMTO3-Brewer	0.99	0.96 $\pm$ 0.02	-4.8 $\pm$ 0.1
OMO3PR-Dobson	0.98	1.01	7.07 $\pm$ 0.3
OMO3PR-Brewer	0.98	1.01 $\pm$ 0.01	8.7 $\pm$ 1.7

Table 15: Global slopes and offsets from a linear fit and correlations for ozone column amount for data of 2005. The offset is taken at 300 DU.

4.2.2. Temperature sensitivity

Correlations are calculated and linear fits are applied for differences in ozone column amount versus difference in effective temperature and effective temperature for 2005. The slope of difference in ozone column amount versus difference in effective temperature is a measure for the temperature sensitivity. The slope of difference in ozone column amount versus effective temperature is also a measure for the temperature sensitivity for an ozone product, but in this case the ozone column amount in the ozone product is over- or underestimated as function of ozone effective temperature.

An overview of the results is shown in table 16. Scatter density plots can be seen in figures 40b - 41a. The correlations are weak, varying from 0.04 to 0.33 in magnitude for different comparisons. From the scatter density plots, it can be seen that there are weak relations between the difference in ozone column amount and difference in effective temperature or difference in ozone column amount and effective temperature. There is a lot of noise that complicates the analysis, which are the cause of such low correlations. When the difference in ozone column amount is compared to difference in effective temperature a low correlation and temperature sensitivity for OMDOAO3 is found. This makes sense because for the OMDOAO3 algorithm, the effective temperature is fitted from the spectrum and no dependency is expected. When this comparison is done for OMTO3, a relative high correlation of 0.306 is found, with a temperature sensitivity of 0.255%/K. This is caused by differences in effective temperature that are not captured by the TOMS v8 climatology, which are mainly the longitudinal variations in temperature. For all OMI ozone products a temperature sensitivity is found, when the ozone column amounts are compared to the Brewer direct sun observations as function of temperature. This may be caused by how the temperature dependency of the ozone absorption cross sections is implemented in the algorithm. For OMO3PR a temperature sensitivity of 0.072 ± 0.004 %/K is found, and for OMTO3 a temperature sensitivity of 0.11 ± 0.04 %/K. For OMDOAO3 a temperature sensitivity of 0.028 ± 0.034 %/K is found, which shows that although an effective temperature may be fitted, the ozone product itself can still be sensitive to temperature variations.

Comparison		Temperature sensitivity	
dO_3/O_3	dT	corr.	slope [%/K]
OMDOAO3-Brewer	OMO3PR-OMDOAO3	0.0079	0.008 ± 0.010
OMTO3-Brewer	OMO3PR-OMTO3	0.31	0.26 ± 0.02
dO_3/O_3	T	corr.	slope [%/K]
OMDOAO3-Brewer	OMO3PR	0.068	0.028 ± 0.034
OMTO3-Brewer	OMO3PR	0.28	0.11 ± 0.04
OMO3PR-Brewer	OMO3PR	0.16	0.072 ± 0.004

Table 16: Global slopes from a linear fit and correlations for difference in ozone column amount vs. difference in effective temperature for data of 2005. The uncertainty has been determined by taking the standard deviation on two subsets of the data with the same analysis: west of the prime meridian ([180W, 0]) and east of the prime meridian ([0, 180E]).

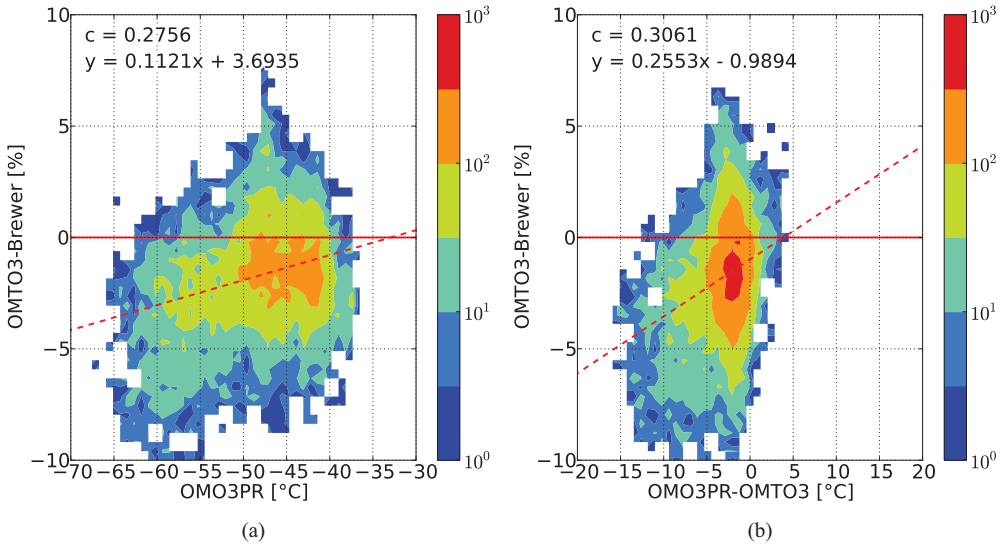

Figure 40: Scatter density plots of (a) relative ozone column amount difference (OMTO3-Brewer) plotted against effective temperature OMO3PR and (b) relative ozone column amount difference (OMTO3-Brewer) plotted against effective temperature difference (OMO3PR-OMTO3) on a logarithmic color scale. The air mass factor profile is neglected for the effective temperature of OMO3PR and OMTO3. Data is used from 2005.

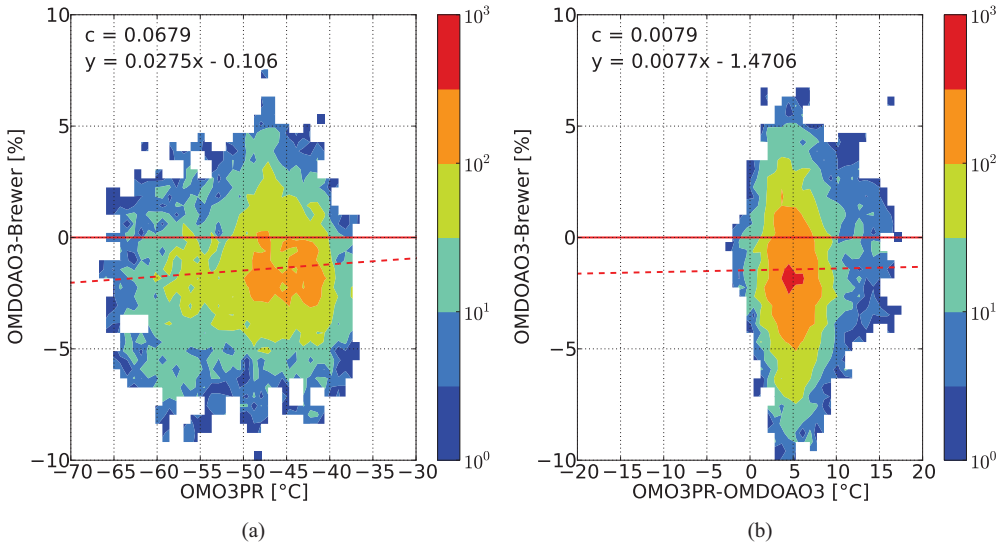

Figure 41: Scatter density plots of (a) relative ozone column amount difference (OMDOAO3-Brewer) plotted against effective temperature OMO3PR and (b) relative ozone column amount difference (OMDOAO3-Brewer) plotted against effective temperature difference (OMO3PR-OMDOAO3) on a logarithmic color scale. The air mass factor profile is neglected for the effective temperature of OMO3PR. Data is used from 2005.

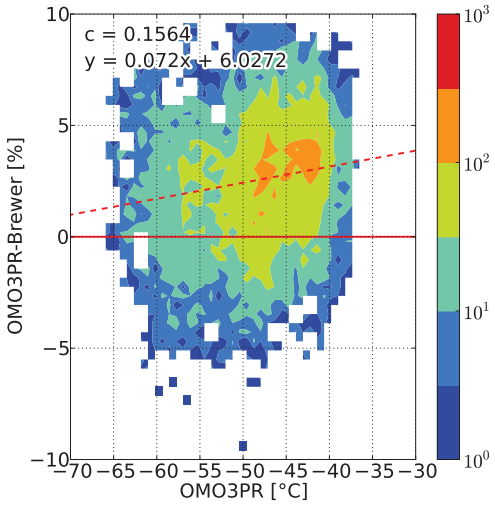

Figure 42: Scatter density plots of relative ozone column amount difference (OMO3PR-Brewer) plotted against effective temperature OMO3PR on a logarithmic color scale. The air mass factor profile is neglected for the effective temperature of OMO3PR. Data is used from 2005.

4.3. Conclusions

The average offsets in ozone column amount, when compared to ground-based observations observations, are the smallest for the OMDOAO3 ozone product and about 1% of a typical ozone column. for OMTO3 and OMO3PR the average differences with ground-based observations are larger, of up to 4% for OMO3PR.

When the temperature sensitivity for OMTO3 is determined, by comparing the difference in column amount to Brewer direct sun observations, against effective temperature difference, a temperature sensitivity of 0.255%/K is found. This is caused by differences in effective temperature that are not captured by the TOMS v8 climatology, which are mainly the longitudinal variations in temperature. For all OMI ozone products a temperature sensitivity is found, when the ozone column amounts are compared to the Brewer direct sun observations as function of temperature. This may be caused by how the temperature dependency of the ozone absorption cross sections is implemented in the algorithm. For OMO3PR a temperature sensitivity of 0.0720 %/K is found, and for OMTO3 a temperature sensitivity of 0.112 %/K. For OMDOAO3 a temperature sensitivity of 0.0275 %/K is found, which shows that although an effective temperature may be fitted from spectrum, the ozone column amount itself can still be sensitive to temperature variations.

5. Considerations for improving the DOAS algorithm

In this section improvements for the OMDOAO3 algorithm are considered. The focus is on new model functions, that can retrieve the slant ozone column amount and effective ozone temperature more accurately. First new model functions are derived based on considerations for improvements. Secondly simulations are done for the improved model functions: Reflectance spectra are calculated with a radiative transfer model and DOAS fits are performed. Results are analyzed, by finding model functions and fit window specifications with the best precisions in slant column amount and effective temperature in combination with a low temperature sensitivity.

5.1. Implementation of ozone optical depth.

In this subsection we will see how the implementation of ozone optical depth can be improved. In chapter 2.1 we have seen that the slant ozone optical depth can be written as:

$$\tau_s(\lambda) = N_s \left[a_0 + a_1 T_{\text{eff}} + a_2 \left((T_{\text{eff}})^2 + T^2_{\text{spread}}\right)\right] \tag{23}$$

Where N_s is the slant ozone column amount, T_{eff} the average temperature along the ozone path, T_{spread} the spread in temperature along the ozone path, and a_i are the temperature expansion coefficients of the ozone absorption cross sections. In the current implementation of OMDOAO3 the absorption coefficients are linearized with respect to temperature at a reference temperature of $T_0 = -73.15°\text{C}$, and temperature spread is ignored. The optical ozone depth is currently approximated by:

$$\tau(\lambda) \approx N_s \left[a_0 + a_1 T_{\text{eff}} + a_2 \left(2T_0 T_{\text{eff}} - T_0^2\right)\right] \tag{24}$$

This approximation is completely unnecessary, and a simple improvement can be achieved by not using this approximation.

The relative errors in the ozone cross-sections, made for an error in T_{eff} or T_{spread} are plotted in figure 43. An error of 10 K in effective temperature leads to an error of 10-20 % in the absorption cross-sections. Note that the percentage error in retrieved ozone column amount is similar to this number, because the optical depth for the measurement stays the same. Neglecting temperature spread, which is on average 17.3 ° C, can lead to an error of about 4% in the absorption cross-sections for the current OMDOAO3 fit window. From these numbers we can state that effective ozone temperature is essential for an accurate ozone retrieval, and the temperature spread may be important. The temperature spread can be implemented in three ways: 1. It can be neglected and assumed to be zero; 2. A climatology can be used or 3. It can be fitted directly from the spectrum. The last option is unlikely since the spectral signal of temperature spread is relatively weak (only 4% of the cross-sections). The choice between neglecting it, or using a climatology has to come from simulations. A simple climatology is obtained in the next subsection.

Note that here absolute errors in the cross sections are discussed, by e.g. neglecting temperature spread. Such estimates for the errors are on the high side for the DOAS retrieval. DOAS is essentially sensitive to the differential optical depth, i.e. the optical depth minus a low order polynomial. Here the absolute cross sections are considered and not the differential ones. In later subsections, different uses of temperature spread will be tested in DOAS simulations, and from there the best conclusions can be drawn.

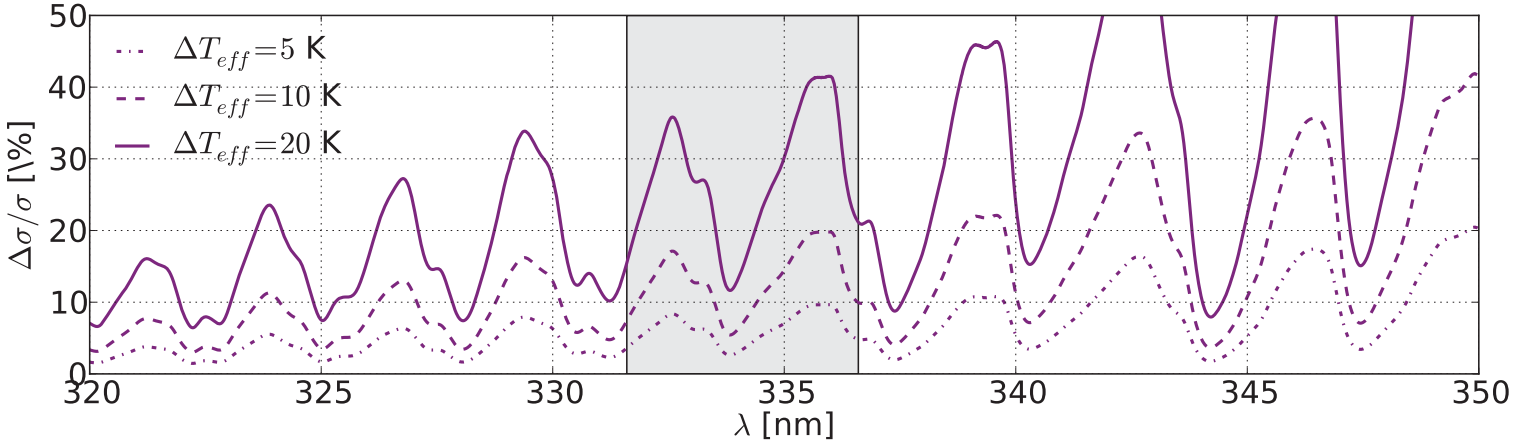

(a) T_{eff}

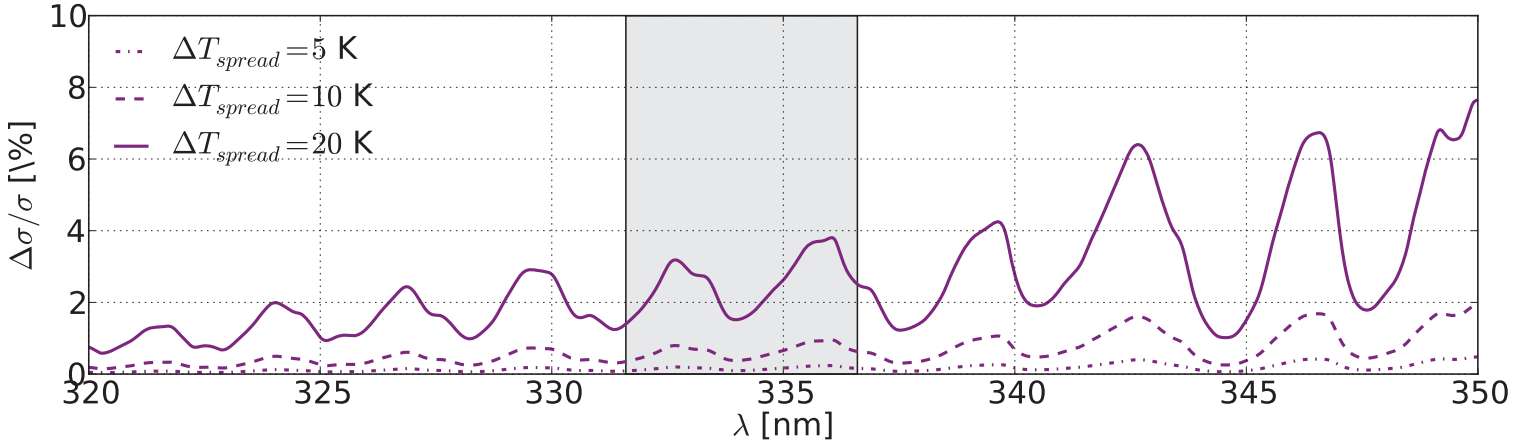

(b) T_{spread}

Figure 43: Plots of relative errors in the ozone absorption cross-sections for the OMI instrument, that are caused by an error in (a) T_{eff} or (b) T_{spread}. Here the cross-sections from Serdyuchenko[10] are used. A reference effective temperature is $-47°$C is taken, which is an average ozone effective temperature.

5.2. Climatology for ozone temperature spread

Analysis of data of 2005 from the OMI ozone profile product and ECMWF temperature profile reveals a strong relation between ozone temperature spread and ozone column amount. A scatter density plot for 2005 is plotted in figure 44. From the ozone profile product, and ECMWF temperature profiles, a climatology is made based on the year 2005:

$$T_{\text{spread,v}} = b_0 + b_1 N_v \approx b_0 + b_1 N_s / M_{\text{geo}} \qquad M_{\text{geo}} = \frac{1}{\cos(\theta)} + \frac{1}{\cos(\theta_0)} \tag{25}$$

Here $T_{\text{spread,v}}$ is the vertical ozone temperature spread (no air mass factor included), b_i are linear expansion coefficients and N_v vertical column amount. An approximation can be made, by assuming that $N_v \approx N_s/M_{\text{geo}}$, where N_s is the slant column amount and M_{geo} a geometrical air mass factor, calculated with solar zenith angle θ_0 an viewing zenith angle θ. A geometrical air mass factor can be calculated before a the slant column is fitted, and hence this relation can be directly used in the DOAS fitting algorithm. The coefficients that were found, based on temperature profiles from ECMWF and ozone profiles from OMO3PR, for the year 2005 are $b_0 = 8.89$ and $b_1 = 0.0279$.

When a climatology is used in the model fit function, essentially two errors are made: 1. There may be errors in the climatology because of the method the climatology was established, or when the climatology is used for a long time span, the climate itself may change, and hence the climatology should be updated. 2. The slant temperature spread is slightly different than the vertical temperature spread because of clouds, geometry or surface albedo, see the discussion in section 2.3, that can cause a difference of up to 5 degrees. If an error in temperature spread is below 10 °C , the error in the cross-sections is still below 1%, see figure 43. However, if the error in temperature spread gets above 20 °C, the errors can be up to 4% in the cross-sections. The nature of this behavior is that the error made in the cross-sections is related quadratically to the error in temperature spread. Both types of errors, that are mentioned here, are very likely to be less than 10 °C, but simply neglecting temperature spread will give larger errors in temperature spread. We can therefore state that the use of a climatology, either with this relation or just a constant, may improve the results of a DOAS fit. In later subsections, different approaches of temperature spread implementations will be tested in DOAS simulations, and from there the best conclusions can be drawn.

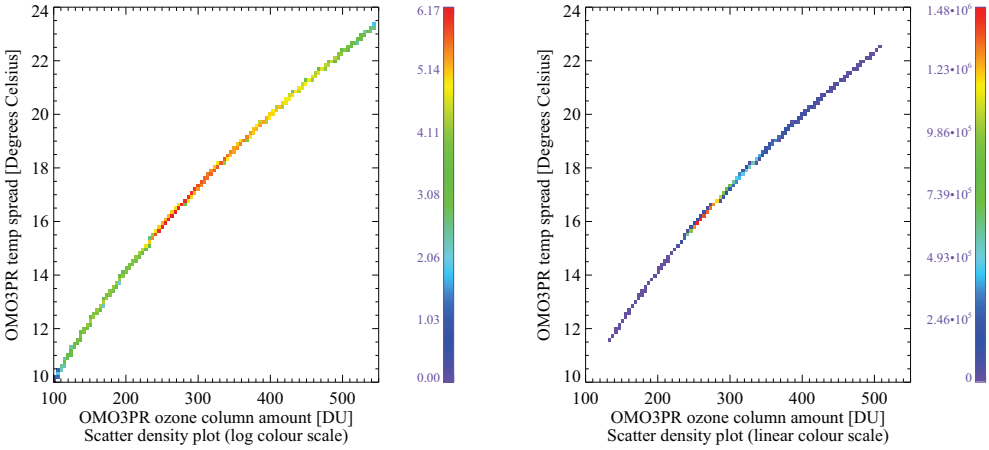

(a) (b)

Figure 44: Scatter density plot of temperature spread [°C] against OMO3PR ozone column amount [DU] on a logarithmic color scale (a) and a linear color scale (b). Data is used from 2005. Temperature spread is determined with OMO3PR ozone profile and ECMWF temperature profile. The altitude resolved air mass factor is neglected.

5.3. Spectral information

When a fit window is chosen, an essential consideration is whether there is enough spectral information in the signal that is measured by the satellite. We can look in multiple ways to the spectral information of ozone slant column amount and effective ozone temperature in a spectral interval: 1. We can look at changes in the relative reflected radiance by removing ozone in a simulation or 2. We can look at the correlation of search directions of fit parameters, which are the derivatives of the model functions to the fit parameters.

The relative changes in reflected radiance are compared to a reference atmosphere for ozone and other atmospheric trace gases, aerosols and a tropospheric cloud. See figure 46. A fit window in the UV1 spectrum is not suitable for a retrieval because the ozone layer is optically so thick that the radiation doesn't penetrate to the surface. In figure 46 it can be seen that the relative change in reflected radiance in the UV2 between ∼310 and ∼345 nm is most suitable. The reflected signal of ozone varies in this band between ∼500% and 1%. and hence that ozone in this band is the dominant absorbing gas, with its own typical structure. Clouds and aerosols may have a much higher impact on the reflected signal but their spectral signatures are smooth. The effects of clouds can be accounted for, by using the OMI Cloud Product (OMCLDO2), in combination with simulations of Lambertian clouds in radiative transfer models. The correlations of derivatives of the fit parameters effective temperature T_{eff} and slant column amount N_s are calculated for 1 nm bands in the UV2, see figure 45. The correlation between different search directions is calculated as ξ. Consequently the maximum is taken of the absolute value of the correlation, for a set of different ξ's for different effective temperatures:

$$
\begin{aligned}
\xi(\lambda_0, T_{\text{eff}}) &= \text{cor}\left(\frac{d\tau}{dN_s}, \frac{d\tau}{dT_{\text{eff}}}\right) \\
\zeta &= \max_{T_{\text{eff}} \in \mathbb{T}} |\xi| \qquad\qquad \mathbb{T} = \{-80, -70, -60, -50, -40, -30, -20\}\ [^\circ\text{C}]
\end{aligned}
$$

The function ζ is plotted as function of wavelength in figure 45. If ζ is high (~ 1.0), we can say that there is not much spectral information in the sense that we can distinguish between N_s and T_{eff} in the signal. If ζ is low (~ 0.0), we might prefer to include such channels, because the spectrum contains information with different spectral structures for T_{eff} and N_s. It can for example be seen that a fit window 320-330 nm contains more spectral information, than a fit window 330-340 nm. It can also be seen that the spectral signatures for the fit parameters slant column amount and slant effective temperature are always more or less correlated. The correlation is never zero and hence that the derivatives are more or less overlapping. This makes the fitting routine less stable, and part of the signal may end up in an arbitrary fit parameter. A quote of John van Neumann illustrates this problem quite well, "With four parameters I can fit an elephant, and with five I can make him wiggle his trunk".

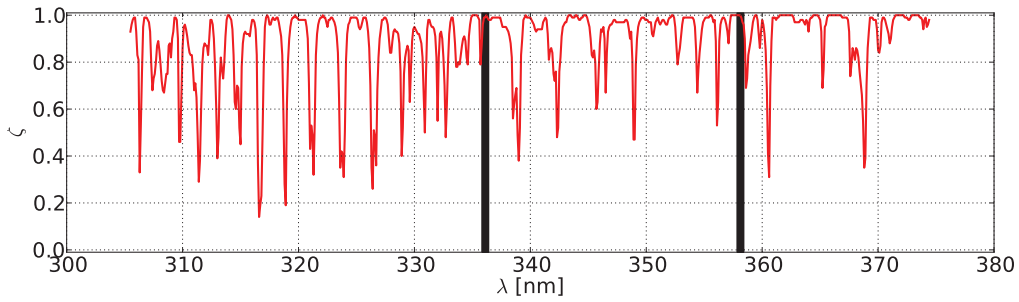

Figure 45: Function ζ plotted as function of wavelength. ζ is a qualitative measure for the correlation of derivatives of fit parameters, see text. For a lower value of ζ, the search direction of the fit parameters are less correlated and hence the fitting routine is expected to converge more easily. In this plot, Fraunhofer lines of (Ti+, 336.112 nm) and (Fe, 358.121 nm) are indicate with a black line. [32]

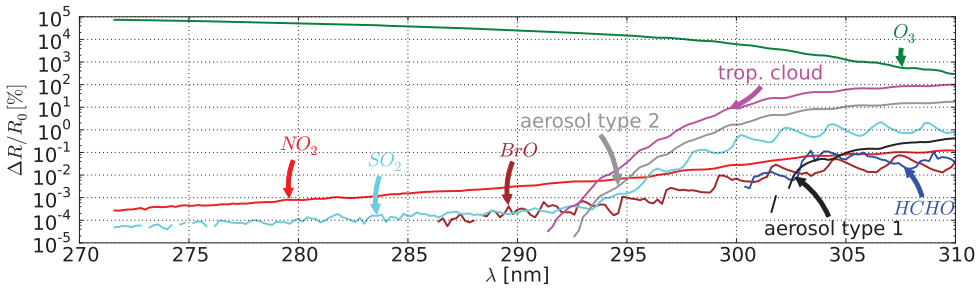

(a) UV1, logarithmic plot

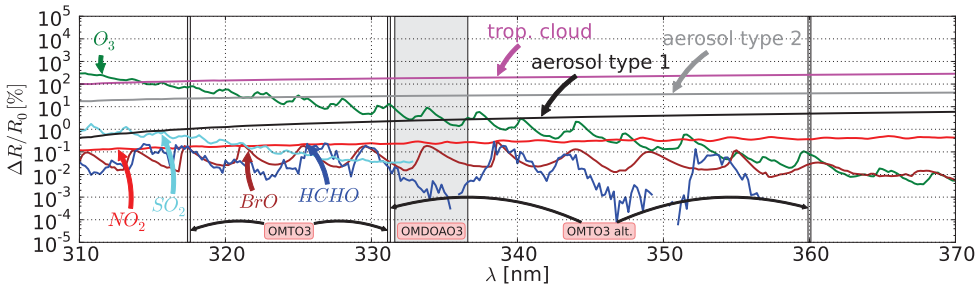

(b) UV2, logarithmic plot

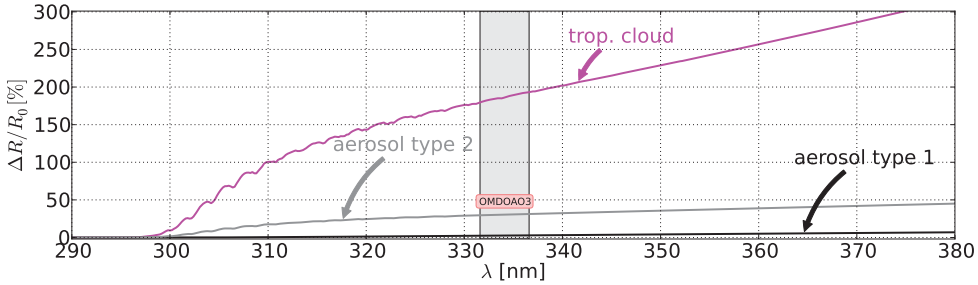

(c) aerosols, linear plot

Figure 46: Relative changes in reflected radiance compared with a reference atmosphere for several relevant trace gases, aerosols and a tropospheric cloud in the (a) UV1 and (b) UV2 wavelength range on a logarithmic scale. (c) For aerosols also on a logarithmic scale. The atmosphere is subject to Rayleigh scattering. Clouds and aerosols are placed in a layer at $\sim$1 km height. The aerosol layer has an optical depth of 2, with type 1 being a strong absorber and type 2 a weak absorber (scattering effect is dominant). The cloud is a Lambertian reflector with an albedo of 0.8. Standard profiles are used for trace gases, for which concentrations are: 300 DU for ozone, $5.0 * 10^{15}$molecules/cm^2 for NO_2, $2.0 * 10^{16}$molecules/cm^2 for HCHO, 2 DU for SO_2 and $5 * 10^{13}$molecules/cm^2 for BrO. Viewing geometry specifications are: solar zenith angle of 25° and the instrument looking in nadir direction. The simulations are made with a radiative transfer model, DISAMAR[24].

5.4. Wavelength dependency of fit parameters

In a DOAS fit, a certain wavelength band is used, e.g. the band of the current OMDOAO3 window 331.6 - 336.6 nm, to obtain fitted parameters such as slant column amount and effective temperature. Simulations are done with a radiative transfer model, to estimate the wavelength dependency of these two fit parameters. Currently a constant slant column amount is fitted. In this subsection we will present simple functions, that can capture the wavelength dependency of slant column amount, that can be used for a DOAS fit.

With a radiative transfer model, DISAMAR[24], altitude resolved air mass factor profiles are calculated for different geometries, ozone profiles and temperature profiles. With these altitude resolved air mass factor profiles slant effective temperature and effective air mass factor can be calculated. The effective air mass factor for the fit window is defined as the ratio between slant ozone column amount and vertical ozone column amount. The geometrical air mass factor is the ratio between slant and vertical ozone column amount, where only the path-lengthening effect of geometry is taken into account. Definitions of effective temperature, effective air mass factor and geometrical air mass factor are:

$$T_{\mathrm{eff},s} = \frac{\int m(z,\lambda)n(z)T(z)dz}{\int m(z,\lambda)n(z)dz} \qquad M(\lambda) = \frac{\int m(z,\lambda)n(z)dz}{\int n(z)dz} \qquad {M_{\mathrm{geo}}}^2 = \frac{1}{\cos(\theta)} + \frac{1}{\cos(\theta_0)}$$

Here $m(z)$ is the altitude resolved air mass factor determined by scattering and surface reflection, $n(z)$ ozone profile, $T(z)$ temperature profile, θ viewing zenith angle and θ_0 solar zenith angle.

The results from the simulation can be seen in figure 47. In figure 47a, the effective temperature is plotted against wavelength for different ozone and temperature profiles. We can see that the effective temperature is practically constant - deviations are less than 0.5 K - for wavelengths higher than 320 nm. For this reason, we might say that we want to choose a fit window above 320 nm, because for those wavelengths, the effective temperature is well defined.

In figure 47b, the effective air mass factor is plotted against wavelength for different ozone and temperature profiles. We can see that a constant effective air mass factor is not well-defined because the air mass factor is depending on wavelength. The air mass factor is related to the penetration depth or cross-sections and Rayleigh scattering. Several simple functions have been tested, for which the ones with lowest average errors are listed in table 17. Three function are listed, with different numbers of fit parameters γ_i, varying from one for a constant air mass factor to three. The fit parameters γ_i depend on geometry, ozone column amount, ozone profile and effective temperature. In these functions, τ is the optical depth, λ wavelength, and $\sigma(\lambda)$ the ozone absorption cross-section. The advantage of using such simple functions, is that a wider fit window may be used. Potentially, the wavelength dependency of slant column amount, via scattering and penetration depth, can be fitted, and the precision of slant column amount and effective temperature may become better, and the temperature sensitivity of the ozone retrieval may decrease.

[2] For convenience the formula given here is only valid for a plane-parallel atmosphere. For a spherical shell atmosphere corrections have to be made on this equation.

Function	Average absolute error [%]	
	330 - 335 nm	320 - 340 nm
$M(\lambda) = \gamma_1$	1.06	4.10
$M(\lambda) = \gamma_1 + \gamma_2 \tau(\lambda)/\lambda^4$	0.22	0.56
$M(\lambda) = \gamma_1 + \gamma_2 1/\lambda^4 + \gamma_3 \sigma(\lambda)$	0.02	0.04

Table 17: Average absolute errors for a 5 nm and 20 nm band for fits of simple functions of a wavelength dependent air mass factor. The simulated wavelength dependent air mass factors are calculated with a radiative transfer model, DISAMAR[24]. The simulated air mass factor depends on wavelength via scattering and penetration depth. U.S. Standard Atmospheric ozone and temperature profiles[26] have been used to calculate the air mass factor for subarctic winter and standard mid latitude ozone profiles. The tested pixel is cloud free. The viewing angle of the instrument is 60 degrees and the solar zenith angle is 80 degrees. The surface albedo is set to 0.05 for the mid latitude profile, and to 0.95 for the subarctic winter profile. The relative azimuthal angle is 180 degrees.

5.5. Simulations for new model functions.

In this subsection, new model functions for the DOAS fit are introduced and tested, under different atmospheric and geometrical configurations, and with different specifications of the fit window. Reflectance spectra for different configurations (e.g. specific combination of clouds, surface albedo and geometry), are calculated with a radiative transfer model. Model functions are programmed in Python, and the resulting fitted variables, slant column amount and slant effective temperature, are compared to the true variables from the modeled atmosphere. Next to that, the temperature sensitivity can be calculated, by varying the effective temperature in the modeled atmosphere, and see what the resulting change in fitted slant ozone column amount is.

Several model functions have been tested. For all new model functions all three temperature expansion coefficients of the newest cross sections from Serdyuchenko[10] have been used. Temperature spread is neglected, inserted as a constant value, a climatology is used, or is tried to fit from the spectra itself. The air mass factor is a constant, or a simple function with two or three fit parameters is used. The list and figures of all results is very long and only the most interesting results are discussed. The complete result set can be retrieved from the author.

It turns out that adding T_{spread} as additional parameter is not giving any physical results, probably because the search directions of the essential parameters (N_s, T_{eff}, T_{spread}) are strongly correlated. The use of three parameters for a wavelength dependent effective air mass factor gives diverging results. The results can therefore be summarized by two new model functions, H and I, that actually give physical realistic results:

$$
\begin{aligned}
\text{H,I}: \quad Y_{\text{sim}} = \quad & \frac{I(\lambda,\theta,\theta_0,\phi-\phi_0)}{F(\lambda)} = Y_A + Y_B \\
Y_A = \quad & P(\lambda)\exp\left[-N_s(\lambda,\gamma_1,\gamma_2)\sigma(\lambda,T_{\text{eff}},T_{\text{spread}})\right] \\
Y_B = \quad & c_{\text{ring}}\frac{I_{\text{Ring,nl}}}{F(\lambda)}\exp\left[-N_s(\lambda,\gamma_1,\gamma_2)\sigma^R(\lambda,T_{\text{eff}},T_{\text{spread}})\right] \qquad (26) \\
& \qquad (27)
\end{aligned}
$$

Here is I measured radiance at the top of the atmosphere, F the extraterrestrial solar irradiance,

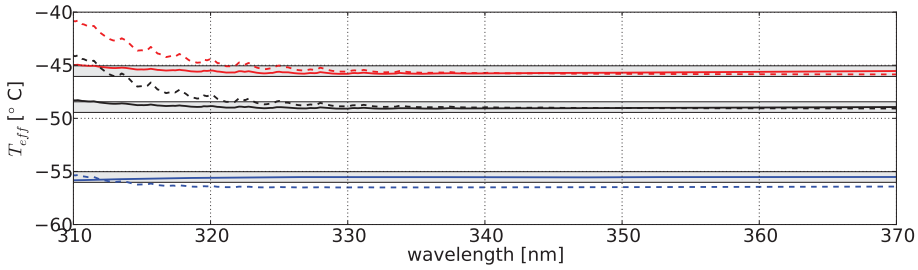

(a) Slant effective temperature

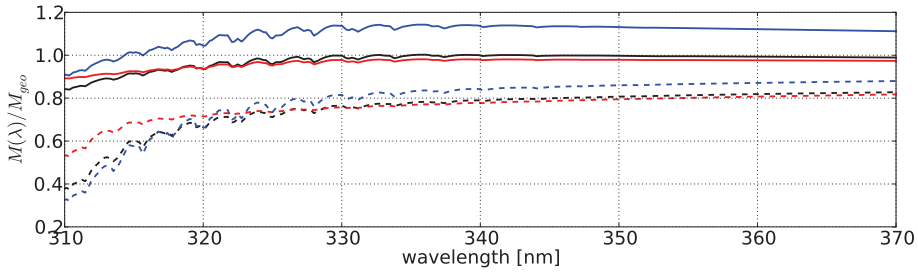

(b) Effective air mass factor

Figure 47: Simulations for wavelength dependency of slant effective temperature and air mass factor, simulated with a radiative transfer model, DISAMAR[24]. (a) Slant effective temperature. The effective temperature is dependent on wavelength via the air mass factor profile. 1-degree wide temperature bands have been plotted, to indicate the variation of effective temperature. (b) Ratio of effective air mass factor and geometrical air mass factor. The air mass factor is dependent on wavelength via scattering and penetration depth. U.S. Standard Atmospheric ozone and temperature profiles [26] have been used to calculate the air mass factor profile for subarctic winter (blue), standard mid latitude (black) and tropics (red). The pixel is cloud free. For the solid lines, the instrument is looking in nadir direction and the solar zenith angle is 60 degrees. For the dashed lines, the viewing angle of the instrument is 60 degrees and the solar zenith angle is 80 degrees. The surface albedo is set to 0.05 for mid latitude and tropical profiles, and to 0.95 for subarctic winter profile. The relative azimuthal angle is 180 degrees.

P a low-order polynomial, N_s ozone slant column density, σ convoluted ozone absorption cross section, λ wavelength, T_{eff} effective temperature and T_{spread} ozone temperature spread. The implementation of the ring effect, which is described in section 1.7, is left unchanged. The essential changes in these new model functions are that the all temperature expansion coefficients of the cross sections are maintained, temperature spread can be implemented and a wavelength dependent air mass factor can be used. The cross-sections are calculated as:

$$\begin{aligned}\sigma(\lambda, T_{\text{eff}}, T_{\text{spread}}) = &\quad a_0 + a_1 T_{\text{eff}} + a_2 (T_{\text{eff}}^2 + T_{\text{spread}}^2) \\ \sigma^R(\lambda, T_{\text{eff}}, T_{\text{spread}}) = &\quad a_0^R + a_1^R T_{\text{eff}} + a_2^R (T_{\text{eff}}^2 + T_{\text{spread}}^2)\end{aligned}$$

and the Raman scrambled ozone absorption cross sections are then:

$$a_0^R = \frac{m(\theta)a_0 + m(\theta_0)a_{0,s}}{m(\theta) + m(\theta_0)} \qquad a_1^R = \frac{m(\theta)a_1 + m(\theta_0)a_{1,s}}{m(\theta) + m(\theta_0)} \qquad a_2^R = \frac{m(\theta)a_2 + m(\theta_0)a_{2,s}}{m(\theta) + m(\theta_0)}$$

In model function H, the slant column is fitted itself, and for model function I, two fit parameters are used for a wavelength dependent slant column amount:

$$H : N_s(\lambda, \gamma_1, \gamma_2) = N_s \qquad I : N_s(\lambda, \gamma_1, \gamma_2) = \quad \gamma_1 \Big/ \left(1 - \gamma_2 \tfrac{\sigma(\lambda, T_{\text{eff}})}{\lambda^4}\right) \tag{28}$$

(29)

5.6. Results

Reflectance spectra for different configurations are calculated with a radiative transfer model, DISAMAR[24]. The U.S. standard atmospheric mid latitude ozone and temperature profiles[26] have been used to calculated the spectra. In total eight reflectance spectra have been used for the simulations, for which the configurations are listed in table 18. The resulting geometrical air mass factor is either 3.0 or 7.6, which is a realistic sample of air mass factors. Only eight reflectance spectra have been used, to be able to test many different model functions and fit window specifications.

Variable	Value(s)
Solar Zenith Angle	0 , 80 °
Viewing Zenith Angle	60 °
Relative azimuthal angle	180 °
Effective temperature	-60 °C , -40 °C
Cloud pressure	900 hPa
Cloud fraction	0.0 , 1.0
Surface albedo	0.05

Table 18: Configurations of the relevant parameters that are used in the simulations. In total eight reflectance spectra have been used.

Consequently, the reflectance spectra have been used, to perform DOAS fits, with different model functions and different specifications of the fit window. The polynomial degree has been varied between 0 and 3. For temperature spread, a climatology is used, a constant value or it is neglected. Fit windows specifications have been tested with the central wavelength between 315 and 350 nm, and fit window width between 2.5 and 60 nm. The resulting fit values for slant column amount and effective temperature, are compared to values from the radiative transfer model at the central wavelength of the fit window. The precision for the fit parameters, slant column amount and effective temperature, is then estimated by the standard deviation of the bias, the difference between fitted and true value, e.g.

$$\text{“Slant column amount precision”} = \text{std}(\Delta N_{s,1}, \cdots, \Delta N_{s,8}) \text{ [DU]}$$

where $\Delta N_{s,i}$ is the difference between fitted slant column amount and slant column amount at the central wavelength in the model, for configuration i. The temperature sensitivity is calculated by taking the average temperature sensitivity of all configurations. For two configurations, e.g. configuration 1 and 2, where the temperature changes, ceteris paribus, the temperature sensitivity is calculated as:

$$\text{“Temperature sensitivity for configuration 1 and 2”} = (N_{s,1} - N_{s,2}) \big/ [N_{s,1} * (T_{s,1} - T_{s,2})] \text{ [\%/K]}$$

Where $N_{s,i}$ are the fitted slant column amounts, and $T_{s,i}$ are the modeled effective temperatures.

An overview of the results is given in table 19. Contour plots of the average differences, precision and temperature sensitivity are plotted in figures 48 - 50. It turns out that the choice for a combination of a model function and fit window specifications is an optimal estimation problem. By this we mean that there is no perfect fit window, and offsets in fitted slant effective temperature and slant ozone column amount always exists. For this reason it does not matter if a

parametrization for temperature spread, in whatever form, is used. There is no perfect fit window for which there are no offsets in fitted slant effective temperature and slant ozone column amount. However, an educated best guess can be made based on simulations for which model function and fit window specifications have the best performance. Also small offsets in effective temperature and slant ozone column amount don't have to be seen as a problem, since we have identified the relevant parameters for an ozone retrieval and corrections can be stored in a look up table.

For the current OMDOAO3 model function and fit window, the fitted effective temperature, compared to the modeled slant effective temperature, has an offset of -5.8 ± 1.7 °C in the simulations. See figure 48. This is in good agreement with the offset that has been found with observations for the OMDOAO3 fitted effective temperature of -5.82 $\pm$ 0.04 °C in section 3. Hence that the found offset in effective ozone temperature can be explained by the DOAS fitting method itself.

In the simulations, we can see that it is possible to reduce the temperature sensitivity by a factor ten, by using model function H or I, which is the use of all temperature expansion coefficients in the cross-sections. See an overview of the results in table 19. In table 19 standard fit windows are shown as a reference, and selected fit windows which have a good precision in the fitted parameters, and a low temperature sensitivity. The current temperature sensitivity is estimated as 0.033 %/K, which goes to -0.0049 %/K for model function H, and to -0.0061 %/K for model function I. Both temperature sensitivities of the new model functions are much lower than the threshold sensitivity of 0.01 %/K, which is a threshold temperature sensitivity for an ozone retrieval that is able to determine ozone trends with an accuracy of 1%. Model function I can be used for noise reduction, because this model function is able to fit the wavelength dependent air mass factor. A fit window of 17.5 nm can be used, which is about four times the size of the current OMDOAO3 fit window can be used, with similar results for precision in fitted parameters and temperature sensitivity in the simulation.

Model function			Fit window		Slant column amount precision	Slant effective temperature precision	Temperature sensitivity
Letter	T_{spread} [°C]	Polynomial degree	Center [nm]	Width [nm]	[DU]	[°C]	[%/K]
G	0.0	2	325.0	5.0	28.6	2.3	-0.084 ± 0.009
G	0.0	2	335.0	5.0	13.1	1.7	0.036 ± 0.006
G	0.0	2	334.0	5.0	7.0	1.8	0.033 ± 0.006
H	0.0	2	325.0	5.0	23.4	0.28	-0.031 ± 0.011
H	0.0	2	335.0	5.0	9.2	0.84	0.005 ± 0.008
H	0.0	2	334.2	5.0	4.1	0.35	-0.005 ± 0.007
H	17.3	2	334.2	5.0	3.0	0.33	-0.010 ± 0.007
I	0.0	2	331.0	17.5	4.7	0.46	-0.006 ± 0.006
I	17.3	3	329.8	20.0	5.0	0.46	-0.008 ± 0.006

Table 19: Short result list of new model functions and fit window specifications. Model function G is currently used in for OMDOAO3. For H and I all temperature expansion coefficients of the second-degree polynomial of ozone absorption cross sections are used. For I, additionally a wavelength-dependent slant ozone column amount is fitted. The precision is a measure for how good the DOAS implementation is able to retrieve the parameters. The temperature sensitivity is a measure for how much the slant column amount depends on effective ozone temperature. See text for details.

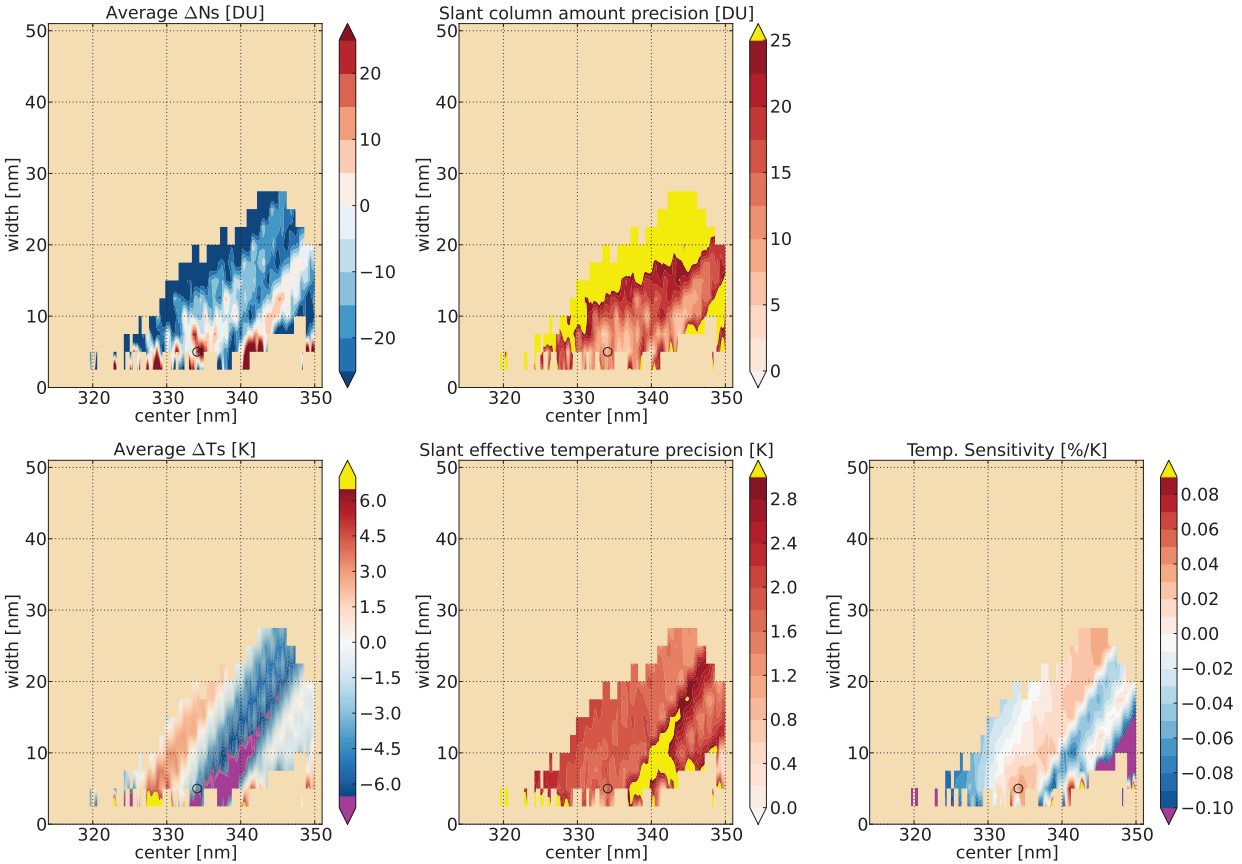

Figure 48: Results for the relevant fit parameters and temperature sensitivity for model function with a second degree polynomial. No climatology for temperature spread is used. On the vertical axes fit window width is shown and on the horizontal axes the central wavelength of the fit window. See text for more details. The current OMDOAO3 fit window is encircled.

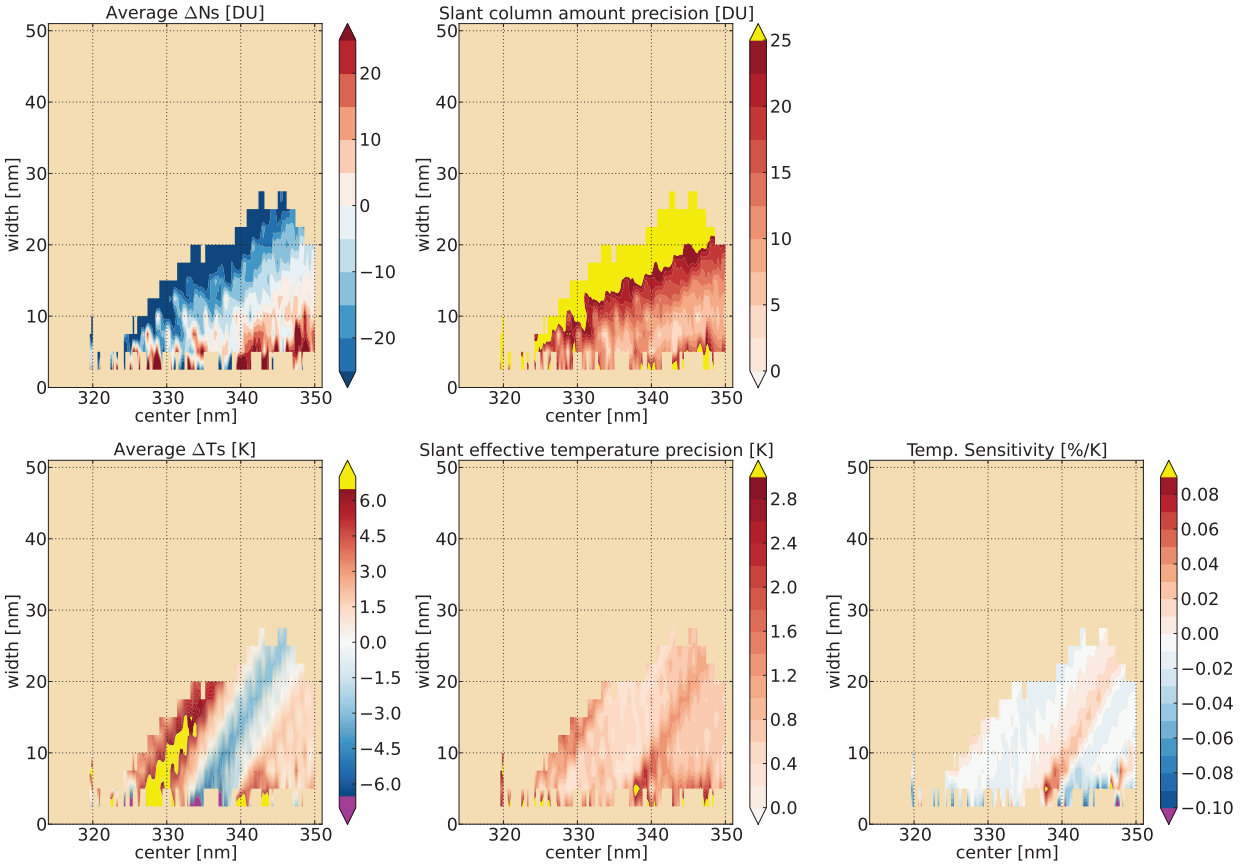

Figure 49: Results for the relevant fit parameters and temperature sensitivity for model function H with a second degree polynomial. No climatology for temperature spread is used. On the vertical axes fit window width is shown and on the horizontal axes the central wavelength of the fit window. See text for more details.

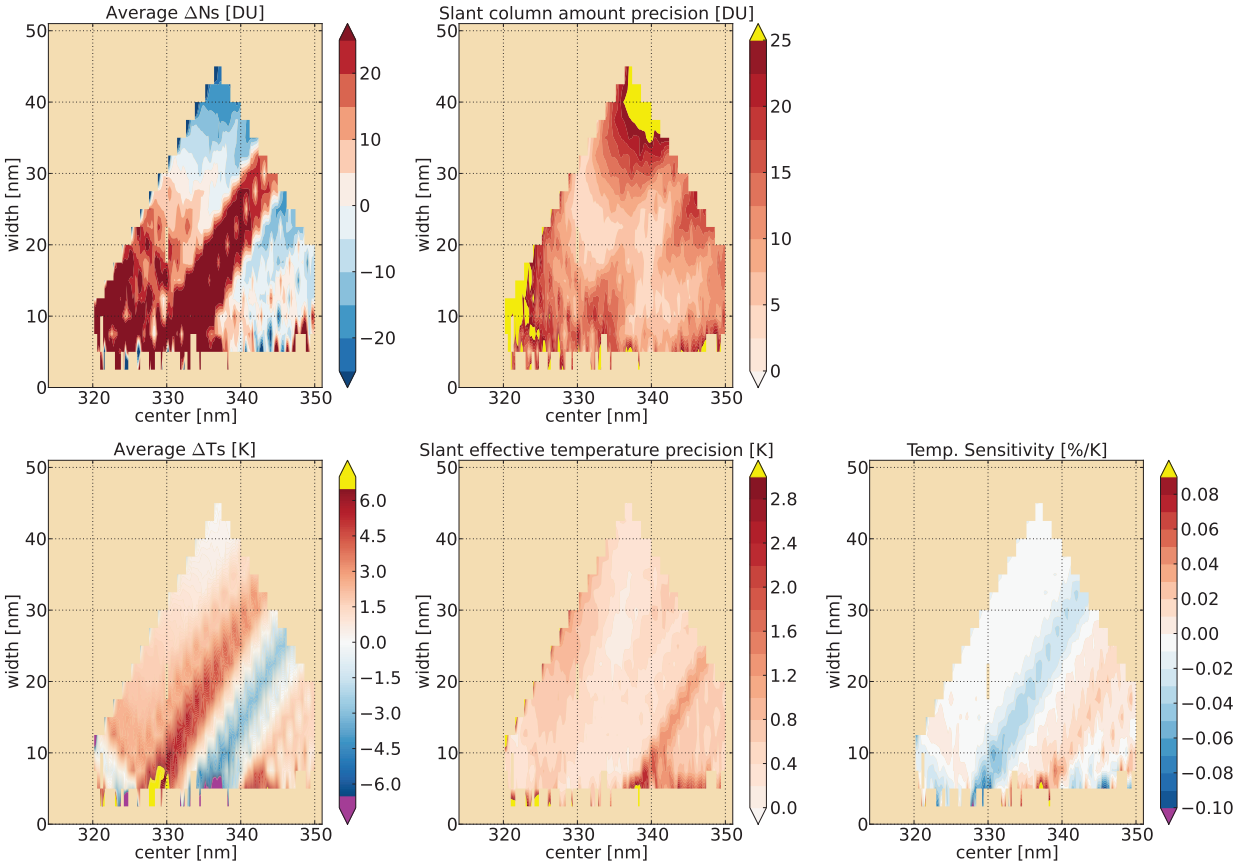

Figure 50: Results for the relevant fit parameters and temperature sensitivity for model function I with a second degree polynomial. No climatology for temperature spread is used. On the vertical axes fit window width is shown and on the horizontal axes the central wavelength of the fit window. See text for more details.

5.7. Application of proposed model function on OMI measurements

The proposed model functions, with fit window specification, in the previous subsection have been implemented and applied to measured reflectance spectra. In figure 51 the fitted parameters can be seen for one orbit. The results are as expected: The slant column amounts are very similar. The noise in the fitted effective temperature has been reduced substantially with model function I, that use a wide fit window, because more data is used and hence noise is reduced. World plots are made for the new model functions, where it also can be seen that model function I has less noise in the resulting fitted effective temperature. A further analysis is proposed, but for this step two essential major things have to be done: 1. New look-up tables have to be made for the empirical air mass factor for the new model functions to convert the slant column amount into vertical column amount (see subsection 1.7. 2. Large data sets (e.g. a year) have to be reprocessed such that again a validation of the ozone column amount, effective temperature and temperature sensitivity can be done.

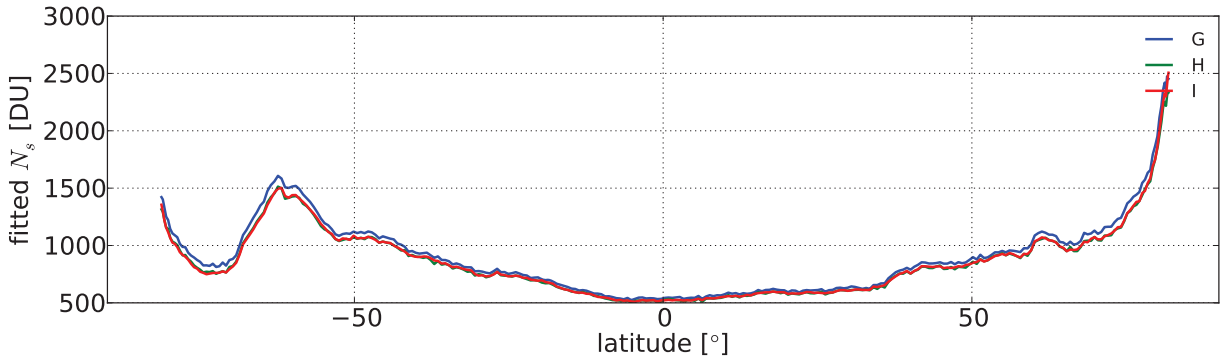

(a) ozone slant column amount

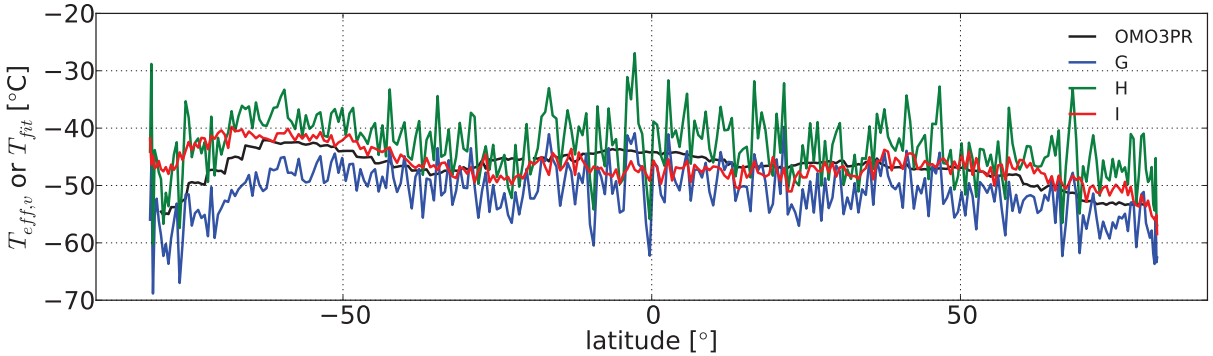

(b) effective temperature

Figure 51: (a) Ozone slant column amounts and (b) effective temperatures resulting from fits that are applied to OMI measured reflectance spectra on 2005-10-10, orbit 6448, row 30. G is the model function used in the current operational OMDOAO3 implementation. For functions H and I all temperature expansion coefficients in the ozone absorption cross sections have been maintained. For model function I, a 17.5 nm wide fit window has been used. See text for details.

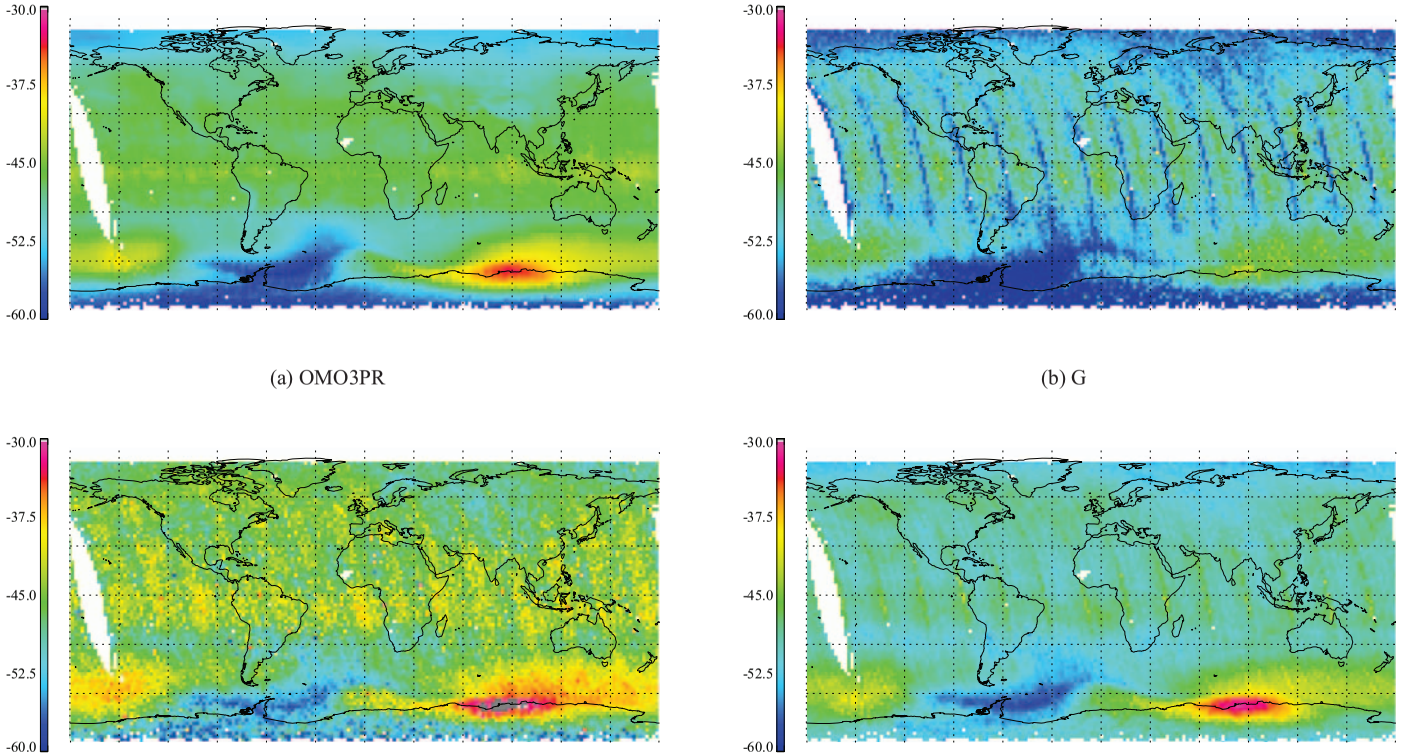

(a) OMO3PR

(b) G

(c) H

(d) I

Figure 52: World plots of fitted effective temperature for OMO3PR (ozone profile product and ECMWF temperature profile), and for three model functions of OMDOAO3 on 2005-10-10. G is the model function used in the current operational OMDOAO3 implementation. For functions H and I all temperature expansion coefficients in the ozone absorption cross sections have been maintained. For model function I, a 17.5 nm wide fit window has been used. See text for details.

5.8. Conclusions

Improvements for the OMDOAO3 algorithm are considered. In the current implementation of OMDOAO3 the ozone absorption coefficients are linearized at a temperature of 200 Kelvin. It is unnecessary to linearize the cross sections with respect to temperature. A second degree polynomial is suggested by the laboratory measurements [7, 8, 9, 10]. In the new model functions all the temperature expansion coefficients of the second degree polynomial are implemented of the ozone absorption cross sections. A climatology for temperature spread is obtained with ozone profiles from OMO3PR and temperature profiles from ECMWF, but it turns out that the use of temperature spread is not important for the ozone retrieval. Correlations of derivatives of the fit parameters were calculated as function of wavelength. It turns out that the derivatives of slant column amount and effective temperature are always more or less correlated, which essentially may make the fitting routine unstable. Simple functions are found, that are able to capture the wavelength dependent slant column amount, with one, two or three fit parameters. New model function have been implemented in the OMDOAO3 algorithm, where the essential changes are that all temperature expansion coefficients of the cross sections are maintained, temperature spread can be implemented and a wavelength dependent air mass factor can be used.

From simulated reflectance spectra and DOAS fits, it has been observed that it is possible to reduce the temperature sensitivity with a factor five. The current OMDOAO3 implementation has a temperature sensitivity of 0.033 %/K in the simulation. For the proposed implementations, this is -0.0049 %/K for model function H and 0.0061 %/K for model function I. The temperature sensitivities for the new model functions are lower than 0.01%/K, which is a threshold temperature sensitivity for an ozone retrieval that is able to determine ozone trends with an accuracy of 1%. Model function I can be used for noise reduction, because this model function is able to fit the wavelength dependent slant column amount. A wider fit window of 17.5 nm can be used, which is about four times the size of the current OMDOAO3 fit window, with similar results in the fitted parameters and temperature sensitivity in the simulation.

A further analysis is proposed, but for this step two major things have to be done: 1. New look-up tables have to be made for the empirical air mass factor for the new model functions to convert the slant column amount into a vertical column amount (see subsection 1.7) and 2. Large data sets (e.g. a year) have to be reprocessed for the new model functions such that again the ozone column amounts, effective temperatures and temperature sensitivities can be validated.

Summary

The objectives of this study are 1. to validate the OMDOAO3 fitted effective temperature; 2. to estimate the temperature sensitivity of OMI ozone products and 3. to improve the DOAS concept such that an ozone trend can accurately be determined with DOAS obtained vertical ozone column amounts.

In section 1 the OMI ozone products, and other relevant ozone products for this validation study, are identified. It has been determined that an ozone retrieval that is able to capture ozone trends with an accuracy of 1%, needs to have a temperature sensitivity of approximately 0.01%/K or less. The temperature sensitivities for ground-based measurement are estimated. The temperature sensitivity for the Dobson AD-DSQP is estimated as 0.125 ± 0.021 %/K. The Brewer instruments are not sensitive to changes in effective ozone temperature, which is observed with 1998-1999 Toronto measurements in a study of [19, Kerr, J. B., 2002] , and is in this study theoretically confirmed by the new cross sections of Serdyuchenko[10]. The Brewer measurements of vertical ozone column amount are therefore the most obvious choice to validate the OMI ozone products and estimate their temperature sensitivity. The temperature sensitivity has been estimated for all OMI ozone products. Depending on which cross sections are used, and how they are implemented, there may be a temperature dependency of the ozone column amount in all products. For OMO3PR, other temperature dependencies are not expected since the temperatures that are used originate from a medium weather forecasting model (ECMWF). The ozone profile from OMO3PR has been cross-validated with other ozone profiles in a study of [25, M. Kroon et al., 2011] and therefore an ozone effective temperature can be determined accurately with an ozone profile from OMO3PR and a temperature profile from ECMWF. This effective temperature can be used as a reference effective temperature to validate the OMDOAO3 effective temperature and to estimate temperature sensitivities of OMI ozone products. For OMDOAO3 the effective temperature is fitted from the spectrum itself. It has been shown with simulations that the slant column amount is not sensitive to changes in effective temperature, ceteris paribus, which confirms that the DOAS concept is theoretically insensitive to temperature variations. However, the implementation of the cross sections may induce a temperature dependency on the fitted slant ozone column amount. For OMTO3, the other OMI ozone column amount product, temperature profiles are based on the TOMS v8 climatology instead of actual temperature data. The TOMS v8 climatology for temperature profiles depends on month and latitude and therefore errors in temperature depending on latitude or season are not expected. However, other variations in temperature are not captured by the climatology, which are: stratospheric climate change, volcanic eruptions and longitudinal temperature variations. Balloon borne ozone sondes are considered to validate the OMI ozone products. Simple assumption are made for the ozone column above the bursting height. It turns out that the calculated quantities for ozone column amount and effective ozone temperature are depending on bursting height. Therefore spurious results can be expected if a comparison would be done to validate the OMI ozone products. There may however be a more advanced method to estimate the upper missing part above the bursting height that gives realistic values for the key ozone variables.

In section 2 definitions for the ozone effective temperature and ozone temperature spread are derived, given the Lambert-Beer law. A distinction is made between vertical and slant definitions, where for the slant definitions the altitude resolved air mass factor is included. For large data sets, e.g. a year, the vertical definition is used because of the high computational cost to calculate the altitude resolved air mass factor. The relevant parameters for an ozone retrieval that cause a difference with respect to the vertical effective ozone temperature are Lambertian

cloud pressure, surface albedo, Lambertian cloud albedo, solar zenith angle and ozone profile. The Lambertian cloud pressure can cause a difference of up to four degrees when the air mass factor is included which is caused by the obscuration of the lower extent of the atmosphere. The other parameters can cause differences of several degrees, which are there due to the vertical temperature weighting via the ozone profile, or scattering throughout the atmosphere. The same parameters have an influence on ozone temperature spread, with approximately the same order of magnitude. The influence of these additional parameters on the effective ozone temperature underline that a temperature correction, for an ozone product that is sensitive to temperature variations, is not straightforward. When the OMDOAO3 fitted effective temperature, which should equal the slant effective ozone temperature, is compared to the OMO3PR vertical effective temperature, determined with OMO3PR ozone profile and ECMWF temperature profile, differences are expected to be dependent on these parameters.

In section 3 data from the OMI ozone products from the year 2005 are gridded. Ozone column amounts for the three different OMI ozone products - OMDOAO3, OMTO3 and OMO3PR - are very similar. Correlations for comparison of gridded data for ozone column amount are 0.99 or 1.00. The offset between OMDOAO3 and OMTO3 is smaller than 2 DU, which is less than 1% of a 300 DU ozone column, which is almost negligible. The offset between OMO3PR and OMDOAO3/OMTO3 is about 12 DU, which is about 4% of a 300 DU ozone column. Possible explanations for this offset in OMO3PR are the use of a different climatology in the radiative transfer model calculations or other factors.

The ozone effective temperature for the ozone products is strongly correlated but there are differences. OMTO3 uses a climatology for temperature profiles, that does not include temperature changes by: 1. volcanic eruptions, 2. climate change or 3. longitudinal variations. The longitudinal variations can directly be seen from a daily picture of effective temperatures, when it is compared to effective temperatures from OMO3PR or OMDOAO3. OMTO3 has an effective temperature that is 3.02 ± 0.40 °C higher than OMO3PR, which may be the consequence of an outdated climatology. The OMDOAO3 fitted effective temperature has an offset of -5.82 ± 0.04 °C, compared to the reference effective temperature (from OMO3PR/ECMWF). This difference is consistent for different seasons and regions, which proofs that an ozone effective temperature can be fitted from the radiance spectrum itself. Differences in ozone column amount are compared with effective temperatures or differences in effective temperature. There is no reason to assume that one OMI ozone product is not sensitive to temperature changes. Therefore the only conclusion that can be drawn from the cross validation is that OMI ozone products have temperature sensitivities on the order of 0.10%/K. which is in agreement with a study of [4, R. J. van der A et al., 2010] .

In section 4, ground-based measurements are used to validate the OMI ozone products. The average offsets in ozone column amount, when compared to ground-based observations observations, are the smallest for the OMDOAO3 ozone product and about 1% of a typical ozone column. For OMTO3 and OMO3PR the average differences with ground-based observations are larger, of up to 4% for OMO3PR. When the temperature sensitivity for OMTO3 is determined, by comparing the difference in column amount to Brewer direct sun observations, against effective temperature difference, a temperature sensitivity of 0.26 ± 0.02 %/K is found. This is caused by differences in effective temperature that are not captured by the TOMS v8 climatology, which are mainly the longitudinal variations in temperature. For all OMI ozone products a temperature sensitivity is found, when the ozone column amounts are compared to the Brewer direct sun observations as function of temperature. This may be caused by how the temperature dependency of the ozone absorption cross sections is implemented in the algorithm. For

the OMO3PR total column amounts a temperature sensitivity of 0.072 $\pm$ 0.004 %/K is found, and for OMTO3 a temperature sensitivity of 0.11 $\pm$ 0.04 %/K. For OMDOAO3 a temperature sensitivity of 0.028 $\pm$ 0.034 %/K is found, which shows that although an effective temperature may be fitted from spectrum, the ozone column amount itself can still be sensitive to temperature variations.

Improvements for the OMDOAO3 algorithm are considered in section 5. In the current implementation of OMDOAO3 the ozone absorption coefficients are linearized with respect to temperature, which is unnecessary. In the new model functions all the temperature expansion coefficients are used of the second degree polynomial for the ozone absorption cross sections. A climatology for temperature spread is obtained with ozone profiles from OMO3PR and temperature profiles from ECMWF but it turns out that the use of temperature spread is not important for the ozone retrieval. Correlations of derivatives of the fit parameters were calculated as function of wavelength. It turns out that the derivatives of slant column amount and effective temperature are always more or less correlated. Simple functions are found, that are able to capture the wavelength dependent slant column amount, with one, two or three fit parameters. New model functions are implemented in the OMDOAO3 algorithm, where the essential changes are that all temperature expansion coefficients of the cross sections are maintained, temperature spread can be implemented and a wavelength dependent air mass factor can be used. For the current OMDOAO3 retrieval algorithm, the fitted effective temperature, compared to the modeled slant effective temperature, has an offset of $-5.8 \pm 1.7\,^{\circ}$C in the simulations. This is in good agreement with the offset that has been found with observations for the OMDOAO3 fitted effective temperature of -5.82 $\pm$ 0.04 $^{\circ}$C. Hence, the found offset in effective ozone temperature can be explained by the DOAS fitting method itself. From simulated reflectance spectra and DOAS fits, it has been observed that it is possible to reduce the temperature sensitivity with a factor five. The current OMDOAO3 implementation has a temperature sensitivity of 0.033 $\pm$ 0.006 %/K in the simulation. For the proposed implementations, this is -0.005 $\pm$ 0.007 %/K for model function H and -0.006 $\pm$ 0.006 %/K for model function I. The temperature sensitivities for the new model functions are lower than 0.01%/K, which is a threshold temperature sensitivity for an ozone retrieval that is able to determine ozone trends with an accuracy of 1%. Model function I can be used for noise reduction, because this model function is able to fit the wavelength dependent slant column amount. A wider fit window of 17.5 nm can be used, which is about four times the size of the current OMDOAO3 fit window, with similar results in the fitted parameters and temperature sensitivity in the simulation.

A further analysis is proposed, but for this step two major things have to be done: 1. New look-up tables have to be made for the empirical air mass factor for the new model functions to convert the slant column amount into a vertical column amount. 2. Large data sets, e.g. a year, have to be reprocessed for the new model functions. The resulting ozone column amounts, effective temperatures and temperature sensitivities can be validated again.

Recommendations

The latest cross sections of Serdyuchenko[10] are recommended for all ozone products. This study shows that they are consistent with other ozone absorption cross sections and are able to capture the temperature dependency better than other ozone cross sections, as they are measured at 11 temperatures. For OMTO3 and the Dobson measurements, a linear combination of wavelengths may be taken for the radiances, instead of just subtracting them, in such a way that the temperature sensitivity becomes negligible. This is an enormous task, because all the measurements should be reprocessed. Otherwise, ozone trends determined from those measurements are sensitive to stratospheric temperature variations, and a bias on the order of 10% in the determined ozone trends is likely.

For OMDOAO3, and generally for all DOAS algorithms, the use of all temperature expansion coefficients of the second degree polynomial for the ozone absorption cross sections is recommended. This may improve the accuracy of the resulting fitted parameters and reduce the temperature sensitivity of the resulting vertical ozone column amount. New look-up tables for the empirical air mass factor have to be calculated for OMDOAO3 when the new model functions are implemented. It is recommended that a year of data, e.g. 2005, is reprocessed, so that a validation can be done for the resulting ozone column amounts, fitted effective temperatures and temperature sensitivities.

References

[1] Fahey, D.W., and M.I. Hegglin, Twenty questions and answers about the ozone layer: 2010 update, scientific assessment of ozone depletion: 2010, 2011. 72 pp., World Meteorological Organization, Geneva, Switzerland.

[2] WMO guide to meteorological instruments and methods of observation, 2008. WMO-No. 8 (Seventh edition), www.wmo.int/pages/prog/www/IMOP/publications/CIMO-Guide/CIMO_Guide-7th_Edition-2008.html.

[3] G. Manney et al., Unprecedented arctic ozone loss in 2011, Nature (2011).

[4] R. J. van der A et al., Multi sensor reanalysis of total ozone, Atmos. Chem. Phys. vol. 10 (2010) pp.11277 – 11294.

[5] J.P. Veefkind et al., Total ozone from the Ozone Monitoring Instrument OMI using the DOAS technique, IEEE Transactions on geoscience and remote sensing vol. 44 (2006) pp.1239 – 1244.

[6] Andreas Richter and Thomas Wagner, The Remote Sensing of Troposhperic Composition from Space: Chapter 2 Solar Backscatterd Radiation: UV, Visible and Near IR-Trace Gases., 2011.

[7] A. M. Bass et al., The ultraviolet cross-sections of ozone: I: the measurements, II: results and temperature dependence, 1984. Ozone Symposium, Greece.

[8] J. Brion et al., High-resolution laboratory absorption cross section of O3. temperature effect, Chemical Physics Letters (1993). Vol. 213, No. 5,6.

[9] S. Voigt et al., The temperature dependence (203-293K) of the absorption cross sections of O3 in the 230-850 nm region measured by Fourier-transform spectroscopy, Journal of Photochemistry and Photobiology (2001). A: Chemistry Vol. 143.

[10] Serdyuchenko et al., New broadband high-resolution ozone absorption cross-sections., 2011.

[11] J. Orphal, A critical review of the absorption cross-sections of O3 and NO2 in the ultraviolet and visible, Journal of Photochemistry and Photobiology (2003). A: Chemistry Vol. 157.

[12] J.F. de Haan, Accounting for Raman Scattering in DOAS, version 1.0, KNMI, De Bilt, The Netherlands, 2003. Note SN-OMI-KNMI-409.

[13] SCI-TEC Instruments Inc., BREWER MKII Spectrophotometer Operator's Manual, 1999. OM-BA-C231 REV B, August 15, 1999.

[14] Dobber et al., Ozone monitoring instrument calibration, IEEE Transactions on geoscience and remote sensing vol. 44 (2006) pp.1209 – 1238.

[15] M. Dobber, R. Voors, R. Dirksen, Q. Kleipool, P. Levelt, The high-resolution solar reference spectrum between 250 and 550 nm and its application to measurements with the ozone monitoring instrument., Journal of Solar Physics (2008). Volume 249, no. 2, 281-291, June 2008, DOI 10.1007/s11207-008-9187-7.

[16] Randel et al., An update of observed stratospheric temperature trends., J. Geophys. Res. (2009). VOL. 114, D02107, doi:10.1029/2008JD010421.

[17] Solomon, S., D. Qin, M. Manning, Z. Chen, M. Marquis, K.B. Averyt, M. Tignor and H.L. Miller (eds.), IPCC, 2007: The Physical Science Basis. Contribution of Working Group I to the Fourth Assessment Report of the Intergovernmental Panel on Climate Change (2007). Cambridge University Press, Cambridge, United Kingdom and New York, NY, USA, 996 pp.

[18] W. D. Komhur, Operations handbook - ozone observations with a dobson spectrophotometer, 1980. NOAA/ESRL Global Monitoring Division.

[19] Kerr, J. B., New methodology for deriving total ozone and other atmospheric variables from brewer spectrophotometer direct sun spectra., J. Geophys. Res. (2002). 107(D23), 4731, doi:10.1029/2001JD001227.

[20] Redondas et al., Brewer algorithm sensitivity analysis, 2006. SAUNA workshop, Puerto de la Cruz, Tenerife, November.

[21] Produced by OMI Team, Edited by Pawan K Bhartia, OMI algorithm theoretical nasis document volume II OMI Ozone Products, 2002. ATBD-OMI-02, Version 2.0, eospso.gsfc.nasa.gov/eos_homepage/for_scientists/atbd/docs/OMI/ATBD-OMI-02.pdf.

[22] D. Balis et al., Validation of ozone monitoring instrument total ozone column measurements using brewer and dobson spectrophotometer ground-based observations., Journal of Geophysical Research (2007). Vol. 112, D24S46, doi:10.1029/2007JD008796.

[23] Kelly V. Chance and Robert J.D. Spurr, Ring effect studies: Rayleigh scattering, including molecular parameters for rotational Raman scattering, and the Fraunhofer spectrum., Journal of Applied Optics (1997). Vol. 36, No. 21, 20 July 1997.

[24] Johan F de Haan, Determining instrument specifications and analyzing methods for atmospheric retrieval., 2011. RP-TROPOMI-KNMI-066 DISAMAR V2.2.1 documentation.

[25] M. Kroon et al., Validation of operational ozone profiles from the ozone monitoring instrument., Journal of Geophysical Research (2011). Vol. 116, D18305, doi:10.1029/2010JD015100.

[26] U.S. Standard Atmosphere, 1976, National Oceanic And Atmospheric Administration, National Aeronautics And Space Administration, United States Air Force, Washington D.C., 1976.

[27] John A. Rice, Mathematical Statistics and Data Analysis, Third Edition, 2007.

[28] Pepijn Veefkind and Maarten Sneep, OMDOAO3 readme file, 2009. KNMI, disc.sci.gsfc.nasa.gov/.
[29] OMTO3 readme file, 2005. toms.gsfc.nasa.gov/omi/.
[30] J.F. de Haan and J.P. Veefkind, OMO3PR readme file, 2009. KNMI, disc.sci.gsfc.nasa.gov/.
[31] M. Sneep et al., Documentation for the 'CAMA' verification and validation toolkit, 2010. MA-OMIE-KNMI-832.
[32] Fraunhofer lines, 2007. en.wikipedia.org/wiki/Fraunhofer_lines.

Acknowledgment

This research was supported by the *Ministry of Infrastructure and the Environment* in the form of a research internship at the *Royal Netherlands Meteorological Institute* (KNMI). I would like to thank Pepijn Veefkind, Maarten Sneep and Johan de Haan for initiating and supporting this work. Next to that, I would like to thank Geert-Jan Roelofs, Bhartia Pawan, David Haffner, Mark Kroon, Piet Stammes, Marc Allaard, Tim Vlemmix, Olaf Tuinder, Anna Serdyuchenko, Jacqueline Baas, Albert-Jan Swart, Jan Oude Nijhuis and Culan Oude Nijhuis for supporting this work in other forms such as helpful discussions, mental support and support for writing skills. I am also grateful for the provision of the new cross-sections of Serdyuchenko[10] prior to publication by the Bremen group.

The Author,
Albert Oude Nijhuis

A complete list of all KNMI-publications (1854 – present) can be found on our website

www.knmi.nl/knmi-library/knmipub_en.html

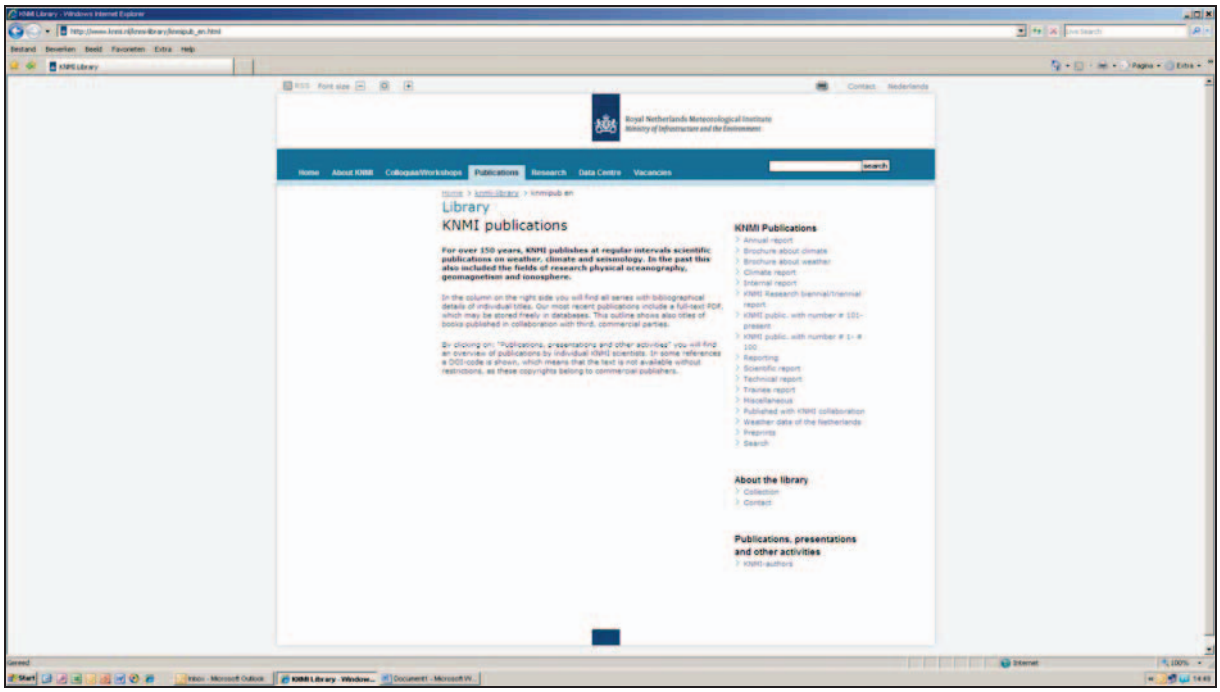

The most recent reports are available as a PDF on this site.